Ingvild Kinn Ekroll

Ultrasound imaging of blood flow based on high frame rate acquisition and adaptive signal processing

Thesis for the degree of Philosophiae Doctor (PhD)

Trondheim, March 2013

Norwegian University of Science and Technology
Faculty of Medicine
Department of Circulation and Medical Imaging

NTNU
Innovation and Creativity

Abstract

Ultrasound imaging of blood flow is in widespread use for assessment of atherosclerotic disease. Imaging of the carotid arteries is of special interest, as blood clots from atherosclerotic plaques may follow the blood stream to the brain with fatal consequences. Color flow imaging and PW Doppler are important tools during patient examination, providing a map of the mean velocities in an image region and the full velocity spectrum in a small region of interest respectively. However they both suffer from limitations which may hamper patient diagnostics.

Recent technological advances have enabled an increased acquisition rate of ultrasound images, providing possibilities for further improvement in robustness and accuracy of color flow and PW Doppler imaging. Based on these advances, we aimed to utilize the high acquisition rate to enable robust vector Doppler imaging, where both velocity magnitude and direction is estimated. Additionally, we wanted to incorporate information from several parallel receive beams in spectral Doppler, which is currently limited to velocity estimation in a limited region of a single beam.

Two limitations in conventional PW Doppler are especially considered, namely the trade-off between temporal and spectral resolution, and the increased spectral broadening in situations of high velocity or large beam-to-flow angles. By utilizing information from several parallel receive beams, we show that by applying adaptive spectral estimation techniques, it is possible to obtain high quality PW Doppler spectra from ensembles similar to those found in conventional color flow imaging. A new method to limit spectral broadening is also presented, and we show spectra with improved resolution and signal-to-noise ratio for a large span in beam-to-flow angles.

Plane wave vector Doppler imaging was investigated using both realistic simulations of flow in a (diseased) carotid artery bifurcation, and *in vivo* studies. It was found that the plane wave approach could provide robust vector velocity estimates at frame rates significantly higher than what is found in conventional blood flow imaging. The technique was implemented in a research ultrasound system, and a feasibility study was performed in patients with carotid artery disease. Promising results were found, showing an increased velocity span and the successful capture of complex flow patterns. All together, the proposed techniques may provide more efficient clinical tools for vascular imaging, as well as quantitative information for research into new markers for cardiovascular disease.

Preface

This thesis is submitted in partial fulfillment of the requirements for the degree of *Philosophiae Doctor* (Ph.D.) at the Faculty of Medicine of the Norwegian University of Science and Technology (NTNU). The research was funded by *Medical Imaging Laboratory* (MI-Lab), and was carried out at the Department of Circulation and Medical Imaging. The main supervisor has been PhD Lasse Løvstakken from Department of Circulation and Medical Imaging, NTNU. Co-supervisors have been MD,PhD Torbjørn Dahl and Professor Hans Torp.

Acknowledgements

Several people should be thanked for their support during my years as a PhD student. First of all, I would like to thank my main supervisor Lasse for his kind guidance, and for always providing new and fruitful ideas. That you manage to keep a positive attitude when I feel progression is slow, is also much appreciated. I would also like to express my gratitude to my co-supervisors: Torbjørn, for being of invaluable help with clinical studies and for pointing out what is important during patient examinations, and Hans, for being a profound source of knowledge in ultrasound in general, and Doppler imaging in particular.

Many of my colleagues deserve a sincere thank you, especially Thor Andreas, Jochen and Saeed for their invaluable help with the research scanner, and Tonje and Solveig for being fellow "Doppler girls", with whom I have shared many problems, Doppler related and others. The rest of my workmates should also be thanked for creating a great working atmosphere and many entertaining lunch discussions.

Finally, Jørgen, I thank you for your never-ending patience in enduring times of work related frustration and for being, simply, the best.

Table of Contents

Abbreviations

APES	Amplitude and phase estimation
AR	Autoregressive
BAPES	Blood spectral amplitude and phase estimation
BMI	Body mass index
B-mode	Brightness mode
BPC	Blood spectral power Capon
CCA	Common carotid artery
CFD	Computational fluid dynamics
CFI	Color flow imaging
CT	Computed tomography
CVD	Cardiovascular disease
CW	Continuous wave
DOA	Direction of arrival
ECA	External carotid artery
EDV	End diastolic velocity
$F_{\#}$	F-number
FDA	Food and drug administration
FIR	Finite impulse response
FFT	Fast Fourier transform
fps	frames per second
FWHM	Full width half maximum
Ham-FFT	Hamming weighted FFT

ICA	Internal carotid artery
IIR	Infinite impulse response
IMT	Intima-Media thickness
Ispta	Attenuated spatial peak time average intensity
IVUS	Intravascular ultrasound
IQ	In-phase Quadrature
LDL	Low density lipoprotein
MI	Mechanical index
M-mode	Motion mode
MRI	Magnetic resonance imaging
MUSIC	Multiple signal classification
MV	Minimum variance
OW	Observation window
PRB	Parallel receive beams
PRF	Pulse repetition frequency
PRT	Pulse repetition time
PSC	Power spectral Capon
PSD	Power spectral density
PSV	Peak systolic velocity
PW	Pulsed wave
PWE	Plane wave emission
PWI	Plane wave imaging
PWV	Pulse wave velocity
REC	Regional committee for medical and health research ethics
RF	Radio frequency
RMS	Root mean square
ROI	Region of interest
rx	receive
SAD	Sum of absolute differences
SNR	Signal-to-noise ratio
SSD	Sum of square differences
T_{PRF}	1/PRF = PRT
tx	transmit
US	Ultrasound
VD	Vector Doppler
WSS	Wall shear stress

Chapter 1

Introduction

Ultrasound for the purpose of measuring distance was developed in an advanced form already 50 million years ago, when bats began using pulses of sound to guide their flight through darkness. This was however not known until the 1940s, when Pierce and Griffin[1] discovered that bats started colliding with even large obstacles when their ears and mouth were covered. It has later been found that other animals, such as the dolphin, also use this form of echolocation or *pulse-echo* technique. Researchers started experimenting with ultrasound, which is sound with frequencies over the human hearing range, in the early 1900s, and the work of the French physicist Paul Langevin is often regarded as the inception of modern ultrasound. Today, ultrasound is used in a variety of medical disciplines, including obstetrics and gynecology, radiology, pediatrics, ophthalmology, neurology and in the cardiovascular field[2]. The popularity and widespread use of the technique is due to it being a non-invasive and relatively low cost technique which has no harmful effects on the body when appropriate guidelines are followed[3].

To be able to detect small objects it is necessary to use sound with short wavelengths, which is why sound in the audible range (20 Hz–20 kHz) is neither utilized by the bat or for diagnostic purposes. The bat emits pulses of ultrasound in the frequency range from 25–200 kHz, which in air results in wavelengths from 1.3–0.15 cm. In medical diagnostics, frequencies in the range of 2–10 MHz are commonly used when imaging through the skin[4], and with an approximate velocity of sound equal to 1500 m/s in human tissues, the wavelengths are in the range of 750–150 µm.

Imaging of moving structures within the body was first performed in 1953–54 by Inge Edler and Hellmuth Hertz in Lund, Sweden, when they used the pulse-echo technique to record the movement of heart valves[5]. A short time later, Satomura in Japan found that it was possible to measure heart movement using the Doppler shift in the frequency of backscattered ultrasound[6], a method which was soon further investigated for measurements of blood velocity[7, 8]. The first flowmeters appeared in the 1960s[9, 10], and evaluation of Doppler ultrasound as an important clinical tool for medical diagnostics was performed by many researchers in the seventies and eighties[11–16]. Today, Doppler techniques are important and widely used diagnostic tools, implemented in most commercial ultrasound scanners. The techniques are mainly used to measure blood flow in the cardiovascular system, but are also used in other areas, for instance to measure deformation of the heart muscle[17].

There are two common ways to display Doppler velocity measurements. One provides the full spectrum of blood velocities in a small region of interest as a function of time, and is often called *spectral Doppler*. This modality is based on Pulsed Wave (PW) or Continuous Wave (CW) Doppler techniques, which are further explained in the following chapters. The second modality is called *color flow imaging* (CFI), which gives an overview of the mean velocity in a 2D or 3D region of interest. In this modality, the mean velocities are color coded and overlaid the grayscale pulse-echo image. As it enabled visualization of leaking heart valves and other flow abnormalities which were previously easy to overlook, it became a clinical success story and a breakthrough for diagnostic ultrasound imaging. The technique which is still used to estimate the mean velocity in commercial ultrasound systems today, was introduced by Namekawa *et al.*[18] and Kasai *et al.*[19] in the 1980s. Examples of both spectral Doppler and CFI can be found in Fig. 2.4, in Section 2.2.

One area where color flow and spectral Doppler imaging is widely used, is in assessment of carotid artery stenosis. Stenoses in the carotid arteries of the neck may cause regions in the brain to infarct due to the shedding of emboli. These emboli will follow the blood stream to smaller arteries in the brain, where they cause a stroke by blocking the blood flow. Historically, X-ray angiography was the gold standard for detecting and grading of stenoses, whereas today MRI, CT and ultrasound are all used for this purpose. Ultrasound color flow imaging in combination with pulse-echo imaging and spectral Doppler is the most commonly used technique, probably due to the lack of side-effects, widespread availability, low cost and a relatively short examination time[21]. Using ultrasound, the degree of stenosis is typically based on measurements of the maximum velocity in the region, as given by the spectral Doppler technique.

Although greatly successful, Doppler ultrasound is hampered by a fundamental limitation: it is one-dimensional. Only the velocity component in the direction of the ultrasound beam can be measured, whereas the true blood flow is three-dimensional. As a consequence, the measured velocity is dependent on the beam-to-flow angle. To obtain an estimate of the true velocity magnitude, it is assumed that the blood flow is parallel to the vessel axis, and angle correction of the 1D velocity estimate is performed. As blood flow through stenoses may differ from the vessel course, assumptions on the flow angle may cause considerable spread in velocity measurements and large interobserver variability[22–24].

To overcome the angle dependency, several techniques for estimating two or all three vector velocity components have been investigated from the early 1970s until today[25–30]. However, because of their own limitations, addressed in the following chapters, vector velocity estimation has not yet reached clinical practice. When it does, however, the potential benefits are many; including increased understanding of blood flow in healthy and diseased arteries, improved quantitative measurements of blood flow, and reduced intra- and interobserver variability in velocity measurements during patient examinations.

Recent technical advances have enabled storage and processing of large quantities of raw ultrasound data, which in turn enables formation of several image lines in parallel. By transmitting broad ultrasound beams and forming multiple image lines on receive,

it is therefore possible to increase the image acquisition rate. As further explained in Section 2.1.2, utilizing plane wave transmission, a full image may be generated for every ultrasound pulse, although with a more limited penetration depth compared to focused transmission, in addition to loss in resolution and contrast.

The increased acquisition rate may have many positive implications for Doppler imaging, especially color flow imaging. In conventional color flow imaging, mean velocity estimates are built line-by-line, requiring several transmissions each. In result, there is a trade-off between frame rate, image quality and size of the color flow image region. As the number of transmissions per line is kept as low as possible to obtain acceptable frame rates, also the measurable velocity span is affected, for instance resulting in missing velocity estimates in regions of low flow, typically close to the vessel wall or in complex flow regions.

By utilizing plane wave imaging and parallel receive beamforming, new possibilities arise, both for development of new processing techniques and improvement of already existing techniques. In this work we aim to utilize the high acquisition rate to enable robust vector Doppler imaging, with the ability to capture slow and complex flow. Additionally, we want to incorporate information from several parallel receive beams in spectral Doppler, which is currently limited to velocity estimation in a limited region of a single beam.

1.1 Aims of study

The overall aim of this study has been to investigate techniques which may enable a more quantitative ultrasound imaging modality for blood flow in the carotid arteries. All of the contributions focus on developing methods which take advantage of the opportunities provided by acquiring data in large spatial regions simultaneously. A prerequisite for all of the investigated techniques is therefore the possibility to use unfocused transmit beams and parallel receive beamforming. To clarify the aims in more detail, the following questions are stated:

Can the velocity resolution in short ensemble PW Doppler be increased?
Color flow imaging is a powerful tool for detecting flow presence and flow abnormalities. However, limitations in conventional acquisition make the modality more qualitative than quantitative which hampers patient diagnostics. Fundamental limitations include the 1D velocity measurements, a limited velocity span and the conflicting interests of high frame rate and image quality. In combined modalities, the latter also creates a trade-off between temporal and spectral resolution in PW Doppler, currently the most important tool for ultrasound based grading of stenoses. This compromise would be less severe if the required number of transmissions for spectral estimation is reduced. However, this is not feasible using conventional spectral estimation techniques. One aim is therefore *to investigate whether the velocity resolution in short ensemble PW Doppler can be improved by utilizing parallel receive beams and adaptive spectral estimation techniques.*

Could velocity delineation in near transverse flow situations be improved?
Another limitation in PW Doppler is spectral broadening, where single velocities appear as a range of velocities in the Doppler spectrum. Spectral broadening may originate from a short observation time of the blood scatterers, and is then termed the transit time effect. This effect may lead to severe errors in velocity measurements. Spectral broadening due to the transit time effect is frequently present in carotid artery imaging, with large beam-to-flow angles being the rule rather than the exception, and as the presence of stenoses leads to high blood velocities. A second aim is therefore *to investigate whether unfocused transmission and parallel receive beams could be utilized to improve delineation of PW Doppler in situations with high velocities or near transversal flow.*

Can plane wave vector Doppler provide robust velocity estimates?
High quality PW Doppler is important since it is the only really quantitative blood velocity measurement available. Measurements based on the resulting velocity spectra are also used as selection criteria when forwarding patients to carotid endarterectomy[1]. However, the outcome of these velocity measurements relies heavily on the user to provide the necessary directional information for calibration. Due to the disturbed flow present in stenotic regions, different examiners may measure a wide variety of velocities, and patients might therefore benefit from a more automated measurement protocol. However, automation requires estimates of the flow direction and spectral Doppler *simultaneously*, and therefore a third aim is *to investigate whether automated calibration of velocity spectra could be achieved using plane wave vector Doppler imaging.*

Plane wave blood flow imaging. A feasible approach in patients?
Due to expected loss of penetration, resolution and contrast, it was unknown whether plane wave imaging could work in real-life imaging conditions. A final aim is therefore *to investigate whether the plane wave approach is feasible in patients with carotid artery disease.*

1.2 Thesis outline

The following section provides a presentation of the contributions included in this thesis, their motivation and findings. A general discussion of the results can be found in Section 1.4, towards the end of this chapter. To make the thesis more self-contained, a more extensive background for the techniques applied in this work is included in Chapter 2. The chapter is mainly aimed for readers who are not too familiar with ultrasound imaging, and emphasizes Doppler imaging in particular. The term *blood flow imaging* will be used as a collective term for all techniques which visualize blood flow. Chapter 2 also provides some background on atherosclerosis, in addition to ultrasound imaging and assessment of this disease. Finally, Chapters 3–6 present studies performed during the course of this work, a period of time stretching from August 2009 to December 2012.

[1] A surgical procedure where plaque is removed from the artery to prevent stroke

1.3 Summary of contributions

In the following, the motivations for the different contributions are elaborated, and a summary of the results is given for each of the four studies.

1.3.1 Retrospective PW Doppler utilizing adaptive signal processing (Chapter 3)

Pulsed Wave (PW) Doppler is an essential component of cardiovascular ultrasound diagnostics, as it is currently the main modality for providing quantitative information on the blood velocities present in a certain spatial region. However, for navigation purposes it is often combined with B-mode or Color Flow Imaging (CFI). PW Doppler acquisition in the combined modality is interrupted for B-mode and color flow imaging, resulting in a trade-off between temporal and spectral resolution in the Doppler spectrum and the image quality and frame rate of the combined modalities. The trade-off arises due to the high number of ultrasound pulses (≈ 60) needed to form an estimate of the velocity spectrum using conventional spectral estimation techniques. To obtain high velocity resolution with the commonly used Welch estimator[2], a large number of pulse transmissions is needed, occupying time which could be spent building a B-mode or color flow image. The velocity resolution of the Welch estimator is inversely proportional to the number of temporal samples in a given observation window. Thus, if the number of transmissions is reduced, the velocity resolution decreases. To avoid large interruptions in the CFI or B-mode acquisition, techniques which reduce the required observation window while retaining spectral resolution are of interest.

This work investigates how the required observation window can be reduced by adaptive spectral estimation techniques, utilizing 2D spatial information available due to unfocused transmission and parallel receive beamforming. Four adaptive estimation techniques were investigated, whereof one, the projection-based Capon estimator, has not before been considered for spectral Doppler estimation. The other techniques have been explored for PW Doppler previously, however not for observation windows comparable to those found in color flow imaging (8–16).

Velocity spectra of high resolution and contrast (signal-to-noise ratio) could be generated from observation windows down to 10 temporal samples, making retrospective PW Doppler from regular color flow imaging a real option. As a result, a 4–6 times increase in temporal resolution could be obtained in *in vivo* examples, while keeping a spectral resolution equal to or increased compared to the conventional approach. Alternatively, for a given observation window, the frequency resolution could be increased compared to the conventional approach. However, the transit time of the scatterers through the sample volume presents a fundamental limitation to the obtainable spectral resolution, and at high velocities the resolution of the adaptive methods approached the resolution of the conventional technique.

[2] A periodogram approach to spectral estimation

This work is described in the paper "Spectral Doppler Estimation Utilizing 2-D Spatial Information and Adaptive Signal Processing"*, accepted for publication in IEEE Transactions on Ultrasonics, Ferroelectrics and Frequency Control, Vol. 59, No. 6, 2012, and presented here in its original form. The candidate was the main contributor to all aspects of the work.*

1.3.2 A new method to limit spectral broadening in PW Doppler (Chapter 4)

As addressed in the previous contribution, spectral broadening due to the transit time effect is a major limitation in PW Doppler. At high velocities or when the angle between the flow direction and the ultrasound beam is close to 90 degrees, the effect gives a limited spectral resolution, making delineation of the true maximum velocities challenging. There have been many attempts to improve spectrum and mean frequency estimation of Doppler signals, but most techniques base the spectral estimation on samples originating from one spatial position. However, to obtain improved delineation both in high and low velocity regions, ways to increase the observation time of the scatterers should be investigated. A new method called 2D Tracking Doppler is proposed in this work, based on an algorithm first described by Torp and Kristoffersen[31]. Instead of increasing the observation window and keeping the sample volume stationary, the scatterers are tracked from pulse to pulse in space and time. When correctly tracking the blood scatterer movement, an increased observation time is achieved, and a velocity spectrum with reduced spectral broadening can be constructed.

In the initial version of the technique[31], tracking of the scatterers could only be performed in the radial direction. Improved spectral resolution was therefore dependent on a small beam-to-flow angle. In this work, plane wave transmission and parallel beamforming is utilized, which provides the opportunity to do tracking both in the radial and lateral direction. By following the movement of the scatterers both radially and between parallel beams, the method is suited for a wide range of beam-to-flow angles. Computer simulations and *in vitro* and *in vivo* ultrasound recordings were used to investigate the performance of the technique, and improved spectral resolution was shown for beam-to-flow angles between 40°and 82°.

This project was a joint effort with PhD student Tonje Dobrowen Fredriksen. She did most of the algorithm implementation both for the experimental work and the simulations. The candidate gave major contributions to algorithm development, data acquisition, pre-processing and writing. The work is described in the paper "2D Tracking Doppler: A New Method to Limit Spectral Broadening in Pulsed Wave Doppler"*, submitted to IEEE Transactions on Ultrasonics, Ferroelectrics and Frequency Control, and presented here in its current form.*

1.3.3 Quantification of flow and tissue velocities using multi-angle plane wave imaging (Chapter 5)

PW Doppler can only provide velocity information from a small region of interest, however, in that region a detailed look at the velocity distribution is given. Using manual angle correction of the velocity spectrum, quantitative measurements of e.g. peak systolic velocity is possible. Color flow imaging on the other hand, provides an overview of the *spatial* velocity distribution by displaying the mean velocity of blood in a 2D or 3D region. As a consequence of shortcomings in conventional color flow imaging such as the limited measurable velocity span, time consuming line-by-line acquisition and angle dependent velocity estimates, CFI is only of limited quantitative use. In relation to carotid artery disease, a 2D or 3D quantitative imaging modality is desired, as improved visualization of blood flow patterns and robustness in peak systolic velocity measurements may benefit the patient by providing more detailed and accurate diagnostic information.

In this work, such a modality was approached using plane wave transmissions and parallel receive beamforming. This allows larger Doppler ensembles to be acquired at reasonable frame rates, providing near instantaneous images of blood flow in a large image region. More specifically, a quantitative, angle independent, 2D modality for flow and tissue imaging based on multi-angle plane wave acquisition is evaluated. Simulations of realistic flow in a carotid artery bifurcation were used to assess the accuracy of the Vector Doppler (VD) technique, showing both a clear increase in accuracy when the ensemble length was extended from 8 to 50 samples and good ability to depict the actual flow conditions.

A comparison to velocity estimates from focused imaging was done using simulations of stationary parabolic flow in a straight tube. Stationary flow was chosen as focused acquisition using large ensembles is time consuming and would lead to significant time-lag artifacts if the time-varying flow in the carotid bifurcation model was utilized. Even though the increased sidelobe level resulted in poor B-mode image contrast, the accuracy in velocity estimates from single plane wave transmission was comparable to that of focused Doppler imaging with similar ensemble lengths.

A packet acquisition scheme based on the simulation results was implemented on a research scanner, and software was developed for offline beamforming, enabling the technique to be evaluated also *in vivo*. Promising results for the plane wave vector Doppler technique were found using healthy volunteers, for both flow and tissue imaging, as vector velocities could be estimated both in the vessel wall and the blood simultaneously.

This work is described in the paper "Simultaneous Quantification of Flow and Tissue Velocities Based on Multi-Angle Plane Wave Imaging"*, accepted for publication in IEEE Transactions on Ultrasonics, Ferroelectrics and Frequency Control (In Press). The candidate was the main contributor to all aspects of the work. However, simulations were performed utilizing the CFD-ultrasound coupling code developed by second author Dr. Abigail Swillens.*

1.3.4 Combined vector velocity and spectral Doppler imaging of complex flow in the carotid arteries (Chapter 6)

Given the opportunities enabled by plane wave imaging techniques, we developed an all-in-one modality for imaging of blood flow in the carotid arteries. An imaging scheme was applied, providing 2D vector velocity blood flow images and PW-Doppler spectra, in addition to separate B-mode images of sufficient quality. Due to limitations in sensitivity, it was not clear whether the plane wave techniques would work robustly in a broad range of patients. Both carotid depth and surrounding tissue calcifications will vary from patient to patient, potentially providing an insufficient signal-to-noise ratio (SNR). One of the aims of this study was therefore to investigate whether this would represent a disadvantage which makes plane wave imaging of patients with carotid artery disease unfeasible in practice.

The modality was evaluated by applying it in a study including 12 patients from the outpatient vascular clinic. Patient examinations were performed using a research ultrasound scanner where the all-in-one modality was implemented. Channel RF data was beamformed and further processed offline. Successful vector velocity images could be formed in all 12 patients, whose body mass index (BMI) ranged from 21 to 31 (carotid depths from 16–28 mm). The modality could provide an increased velocity span compared to regular color flow imaging and an increased frame rate (63–66 fps) compared to conventional duplex imaging (≈20 fps). PW spectra of comparable quality to that of a high end system could be obtained, and by using adaptive spectral estimation techniques as described in Chapter 3, the contrast and resolution of the spectra could be increased.

Automation of the clinical protocol with respect to measurements of the peak systolic velocity was demonstrated, utilizing directional estimates from vector Doppler to calibrate the velocity spectra for all image points simultaneously. Based on traces of the maximum velocity and automatic detection of the peak systolic velocity, a spatial map of the peak systolic velocity could be generated. This represents a new way of presenting velocity data, and may be beneficial in carotid artery diagnostics by highlighting regions of high velocity and the extension of the stenotic region, guiding the examiner to an appropriate placement of the sample volume.

This work is described in the paper "Combined vector velocity and spectral Doppler imaging for improved imaging of complex blood flow in the carotid arteries", *submitted to Ultrasound in Medicine and Biology, and presented here in its current form. The candidate was the main contributor to all aspects of this work except the important part of patient examinations, for which Dr. Torbjørn Dahl is gratefully acknowledged.*

1.4 Discussion of results

1.4.1 Alternative spectral Doppler techniques

Two aspects of spectral Doppler estimation were addressed in the first two contributions: i) improving spectral resolution in short ensembles suitable for retrospective PW Doppler from CFI and ii) improving spectral resolution in regions of high velocity or near transversal flow by increasing the observation time.

Adaptive spectral estimation techniques

In contribution 1, we investigated how the required observation window in spectral Doppler could be substantially reduced by utilizing spatial information provided by parallel receive beamforming in adaptive spectral estimation techniques. One of the incentives was seeing whether spectra of sufficient spectral resolution could be generated from ensembles with lengths similar to those found in conventional color flow imaging (typically 8–16 samples), implicating a packet acquisition scheme with limited options for temporal averaging. Nonparametric spectral estimators compared to the conventional periodogram approach were the power spectral Capon method (PSC) and the Amplitude and phase estimation (APES) technique, due to previous works showing their robustness in general[32] and in the setting of spectral Doppler ultrasound[33–35]. Additionally, two parametric approaches were included, both based on eigendecomposition of the signal covariance matrix. The latter techniques are parametric in the sense that the number of signal components (signal eigenvectors) needs to be estimated from the signal covariance matrix before spectral locations are found, adding some complexity to the techniques. Whereas Multiple signal classification (MUSIC) has been considered for use in spectral Doppler estimation earlier, the projection based Capon technique has not.

It was shown that ensemble lengths shorter than 20 samples could be utilized for all of the alternative spectral estimation techniques. In fact, ensembles as short as 10 samples could be used for spectral estimation of relatively high spectral resolution and contrast. Further, due to the high spectral resolution at low velocities, the need for wall filtering is reduced. At such small ensembles, the PSC method displayed a higher resolution than the APES method with equal averaging area, and was therefore the preferred estimator of the two. The difference in resolution follows from the estimator formulation; the APES estimator requires temporal averaging in the estimation of a noise-and-covariance matrix, reducing the effective observation window further, whereas the full data window may be utilized for spectral estimation in the Capon formulation. The possibility of formulating the Capon spectral estimate with no temporal averaging provides an advantage in packet acquisition schemes such as CFI, where the number of available samples is very limited. On the other hand, some averaging is needed to support an invertible estimate of the signal covariance matrix in both estimators, and the lack of temporal averaging in the applied Capon formulation makes the estimator less robust than APES with respect to averaging area.

The parametric approaches, here represented by the signal subspace projection based Capon technique and the noise subspace based MUSIC, were able to provide

spectrograms of a resolution only matched by the PSC technique. The contrast found in the spectral estimates of the projection based Capon technique was unmatched by any other estimator. The main disadvantage of the parametric approaches is that the dimensions of the signal and noise subspaces must be estimated for every new time instant in the periodogram, as the blood signal varies throughout the cardiac cycle, leading to higher computational load. MUSIC has the additional disadvantage that only the *pseudospectrum* is estimated. The dimensions of the signal subspace were estimated using a cross spectral metric[36], however, other techniques might be more efficient or more robust. If the estimated number of signal components is incorrect, the spectra can be obscured by spurious peaks (too many components) or contain only the clutter signal (too few components), a challenge which here manifests itself most clearly in the time of highest flow acceleration (highest bandwidth). This represents the more severe drawback of using the projection based Capon technique over the PSC approach, and one should be aware that while noise is effectively blocked, the same could be the case for the signal if the eigenvector inclusion criterion is too strict.

The 2D Tracking Doppler technique

In contribution 2 the aim was no longer to reduce the required observation window, but rather to increase the observation time of the moving scatterers. By increasing the observation time, the effects of spectral broadening due to the transit time effect may be reduced, providing increased velocity resolution in high velocity regions. Similar to two of the adaptive spectral estimation techniques, the 2D Tracking Doppler algorithm can also be regarded as parametric, as it requires the flow angle as an input for the estimation procedure. The assumed flow angle is used to resample the Doppler signal along an oblique line in space, using both radial and lateral samples (several parallel receive beams). Several slow-time[3] instances of the resampled signal are further summed along straight lines in a domain spanned by space and slow-time, where summation along different angles contribute to the power in different velocity cells of the power spectrum. A similar approach was taken by Alam and Parker in the "butterfly search" technique[37], but the approach was limited to track along the direction of the beam, which will only improve the performance in situations with small beam-to-flow angles.

The 2D Tracking Doppler technique could produce an increased velocity resolution for a wide range of beam-to flow angles (40°–82°), and also to increase the SNR, both *in vitro* and *in vivo*. The increase in SNR can be explained by the inherent properties of noise and the tracking Doppler technique. Along trajectories where the velocity is constant, the signal will match in phase when summed, whereas the contribution from noise will not.

Simulations of the expected Doppler power spectra were performed using an extended version of the signal model used in[31]. The extended model included thermal noise and clutter filtering. Out-of-plane movement was not taken into account. The simulated spectra therefore describe an ideal situation where the flow direction is in the imaging plane and the beam-to-flow angle is measured precisely. Any out-of-plane

[3]Explanation of the expression *slow-time* is found in Section 2.1.3

movement or incorrect positioning of the tracking line would broaden the main lobe of the power spectrum. However, the simulated spectra corresponded well with the spectra generated from the *in vitro* recordings, in a relevant case both showing 4 times increase in spectral resolution, and 7 dB increase in spectral SNR.

An important challenge for the practical implementation of the 2D Tracking Doppler method is to extract data along the correct trajectory through a 3D (2D tracking + time) domain, following the movement of the blood scatterers. The trajectory was in this study determined from a B-mode image of the geometry and chosen as a straight line. Curved flow fields, accelerated flow and turbulent flow were not considered in this work, and steady-state flow conditions were assumed. The latter is, however, justified for the observation times used, which were $\leq 10\,\text{ms}$. To avoid broadening of the velocity spectrum, the flow has to be constant for a length corresponding to the tracking length. In this work the tracking length was 1.5 cm (at the highest velocities), which could be too long in the more complex situations described above.

1.4.2 Plane wave vector Doppler imaging of the carotid arteries

In contribution 3 and 4, we address the angle dependency in blood flow imaging. More specifically we investigate how plane wave imaging can be utilized to obtain robust vector Doppler estimates of flow in the carotid arteries at sufficient frame rates to capture complex flow patterns. It is also shown that calibrated PW Doppler spectra can be obtained retrospectively at all points in the image simultaneously, providing an opportunity to display the velocity information as a spatial map of the peak systolic velocities.

Simultaneous quantification of flow and tissue velocities

In contribution 3, the robustness of plane wave vector Doppler imaging was investigated using both simulations and *in vivo* recordings. Based on the simulations, it was found that by increasing the ensemble length from 8 to 50 samples, the robustness of the vector Doppler technique was significantly increased. The root-mean-square (RMS) deviation in the z-component (normal to the transducer surface) of the velocity was reduced by approximately 70 %, while the RMS deviation in the x-component (parallel to the transducer surface) was reduced by approximately 80 %, resulting in a good depiction of even complex flow fields. The increased robustness obtained by using an increased ensemble length can partly be attributed to the properties of the clutter filter, as they, depending on how much signal is removed, may introduce bias in the autocorrelation estimates and signal dropouts due to segmentation algorithms. By using large ensemble lengths, desirable filter properties can be obtained by most common clutter filter designs, but an additional variance reduction is achievable when using polynomial regression filters, as more temporal samples are available for averaging.

The main advantage of using plane wave imaging is the high acquisition rate, enabling extremely high frame rates, or alternatively, relatively high frame rates

and increased image quality. The packet acquisition approach investigated in this work aimed for the latter category, allowing large ensembles for velocity estimation, and B-mode images to be built during an interruption of the Doppler sequences. We demonstrated that robust vector Doppler estimates in a large region of interest could be achieved in a duplex context *in vivo*, with a frame rate of 63 Hz, which is acceptable for quantitative analysis. The frame rate was limited due to the number of B-mode compound angles and the pulse repetition frequency causing heating of the transducer surface. The maximum angle of $\pm$ 7.2° and 43 compound angles resulted in a spatial resolution and contrast corresponding to that of focused imaging with a transmit F-number of 4[38]. However, if 30 transmissions were used for B-mode at 12 kHz, and 30 transmissions were used for Doppler at 4 kHz, a modality including both B-mode, vector Doppler and retrospective PW Doppler at a frame rate of 100 Hz is achievable, where the B-mode image contrast only needs to be slightly compromised[38]. Another option is to interleave focused B-mode transmissions with plane wave Doppler transmissions on the expense of a reduced B-mode frame rate. This could provide good temporal resolution for PW- and vector Doppler imaging in addition to good spatial resolution and contrast in the B-mode image, and was investigated further in contribution 4. As the movements in tissue are of a slower nature than blood flow, a lower B-mode frame rate can usually be accepted.

An additional aim of this study was to see whether both flow and tissue velocities could be extracted from the same vector Doppler acquisition scheme. Simulations of slowly rotating flow and recordings in healthy volunteers indicated that tissue vector Doppler was indeed possible. However, when the accuracy found from simulations was compared to velocity estimates found *in vivo*, the diastolic velocities seemed to be comparable to the RMS error. On the other hand, the presented tissue velocity spectra and autocorrelation estimates were convincing in their correspondence, and indicated that the velocity magnitude was correctly identified. One explanation of the seeming discrepancy could be that the obtained accuracy from simulations includes velocities from all possible angles with the transmit/receive beam direction. This will give a lower accuracy than a situation with smaller beam-to-velocity angles. Another, and probably more important, difference, is the more uniform velocity found in the vessel wall compared to the cylindrical phantom used in simulations. Due to the large side lobes of the plane wave point spread function, neighbouring voxels will have a larger influence on the RMS error in the cylindrical phantom where a velocity gradient is present, than in the more uniform movement of the tissue *in vivo*. However, further investigations in the accuracy of tissue velocity imaging should be done using more realistic simulations of vessel wall movement through the cardiac cycle, similar to what was done for flow in the carotid bifurcation.

Combined vector velocity and spectral Doppler imaging of complex flow

Contribution 4 presented results from an all-in-one modality utilizing plane wave vector Doppler imaging. The modality was tested in a population of patients with carotid artery disease, and could provide successful vector Doppler images and retrospective velocity spectra from patients within a BMI range of 21 to 31. Although successful

in the small group of patients, a limitation of the study was that none of the patients had a large degree of calcifications, another that only the carotid arteries were imaged. Calcifications and the increased depth of the vertebral arteries would increase the imaging challenge, and it is still unknown whether the plane wave approach would be successful under such circumstances.

To avoid excessive transducer surface heating, a compromise between penetration depth and pulse repetition frequency was encountered, limiting the maximum measurable velocity. However, superficial vessels generally lie parallel to the skin surface, giving relatively large beam-to-flow angles. In result, most of the patients imaged had Doppler shifts supported by the given velocity range. Still, in severely stenosed regions and in branches, aliasing could appear.

Both focused and unfocused transmissions could be used to build the B-mode images. Advantages of using focused B-mode imaging include increased penetration, resolution and contrast. By utilizing an interleaved acquisition scheme, these advantages can be obtained without compromising the Doppler frame rate, although at the cost of a reduced B-mode frame rate. However, when applied to carotid imaging, where the tissue movement is small compared to blood flow or myocardial contractions, an interleaved approach is justified. The plane wave scheme, where unfocused transmissions were used both for flow and tissue imaging had a common frame rate for the B-mode and flow images. However, further investigation should be done to find an optimal number of imaging angles for the coherent compounding, as the span in angles chosen in our application corresponds to a transmit F number of 4, providing lower lateral resolution than the focused approach. Fewer transmitted plane waves and a larger angle span would give an increase in the frame rate and the lateral resolution respectively, however with a reduction in contrast and SNR.

The modality could provide spectra of sufficient temporal resolution and contrast for quantitative analysis. Both conventional and adaptive spectral estimation techniques could be used to generate maps of peak systolic velocities, and examples of spectra generated by both techniques were given. Increased computational time is a disadvantage of the adaptive techniques, but as the PW spectral estimation is retrospective in our application, the slight increase in computational complexity is tolerable when higher spectral resolution and contrast are obtained.

Calibration of the spectra at all points in the image was done using the flow direction estimates from vector Doppler. Further, automatic baselineshift and traces of the peak velocities could be used to form a spatial map of the peak systolic velocities. In such a map, regions of high velocities are highlighted, aiding the patient examiner in placement of the sample volume. Assessing the peak systolic velocity is an important part of the clinical protocol when a patient with carotid artery disease is examined, and the measured value is one of the selection criteria for carotid endarterectomy. In that respect, automatic angle correction of the velocities would be beneficial, as this may reduce both intra- and interobserver variability[39]. The extent of the stenotic region is also important, and because the velocities displayed in a regular color flow image is dependent on a beam-to-flow angle which is changing during the course of the stenosis, the extent of the region may be visualized better in a map of the peak systolic velocities.

Further work should focus on developing more robust techniques for estimation of the peak velocity, and also compare estimates of peak systolic velocities found using the different spectral estimation techniques, including the 2D tracking Doppler technique described in Chapter 4. Comparison of the different techniques in a situation of known maximal velocity is important as the increased velocity resolution in alternative spectral Doppler techniques may reduce the peak systolic velocity estimate as compared to regular PW Doppler. As overestimation of the peak systolic velocity is a known phenomenon in the literature[23, 40, 41], reduced spectral broadening may be beneficial. However, new techniques may introduce measurements which are not consistent with current criteria for grading of stenoses, and a thorough investigation of the accuracy of the alternative spectral estimation techniques and the automated calibration is needed.

1.5 Concluding remarks

This work has focused on pulsed Doppler applications, and is a contribution to the continuously developing field of blood flow imaging. We have shown that by using adaptive estimation techniques, exceptionally short ensembles may be used for spectral estimation, and that retrospective PW Doppler from ensembles used in conventional color flow imaging is feasible. However, the methods are more computationally demanding than the regular periodogram approach. Additionally, care should be taken when applying parametric methods which require estimation of the number of signal components. Signal space estimators provide effective reduction of noise, but if the inclusion criteria are too strict, they may also lead to signal suppression.

We have shown that by tracking in 2D, reduced spectral broadening may be obtained by increasing the effective observation time of the scatterers, improving spectral resolution in high velocity regions and in regions with near transversal flow. However, regions of accelerated or disturbed flow still present a challenge, and further work should investigate whether it is possible to improve velocity delineation also under such conditions.

On the topic of vector velocity estimation, we have shown that plane wave imaging is a feasible approach, where the high acquisition rate enables large ensemble lengths and thereby less drop-outs in color flow imaging, in addition to high robustness in the vector Doppler estimates. A combined acquisition providing spectral and vector Doppler information in a packet scheme with B-mode imaging was implemented on a research ultrasound system, and tested in a group of patients with carotid artery disease. The results gave promising results for plane wave vector Doppler *in vivo*. By combining spectral and vector Doppler estimates, an alternative way of presenting velocity information was demonstrated, which may aid in measurements during the examination protocol. However, it is still unknown whether the plane wave imaging approach will be a success in patients with a large degree of calcifications, as such cases were not present in the investigated patient population.

Further work

Hopefully, this thesis work may be continued, as there is room for further development in all of the investigated techniques. Some suggestions of further work have already been mentioned in Section 1.4, and some are discussed in the chapters containing the different contributions. However, short descriptions of possible continuations are also given here.

As the projection based Capon technique gave very promising results for short ensemble spectral estimation, more robust techniques for estimation of the number of signal components should be developed and evaluated using known velocity fields. It would also be interesting to compare the adaptive spectral estimation techniques to the 2D Tracking Doppler technique and whether it is possible (and desirable) to combine them.

A controlled study of stenosis grading utilizing the alternative spectral estimation techniques and the conventional techniques should be performed. The grading should preferably be done by experienced clinicians and in a controllable environment. Whether additional reduction in measurement variability is obtained by utilizing automatic calibration of the velocity spectra should also be looked into.

In this work we focused on blood flow imaging. However, since it was found that also tissue velocity estimates could be extracted from the same acquisition, further work should focus on development on more sensitive motion detection algorithms and the extension to wall strain estimation. Simulations of similar complexity as applied here for flow imaging should be used, and feasibility studies could be performed using the current patient material. A small feasibility study for imaging plaques before and during carotid endarterectomy has been approved by the Regional committee for medical and health research ethics, and will be used to see whether these techniques are sensitive enough to quantify plaque deformation.

Vector Doppler estimation techniques have low computational complexity, and should therefore be suited for real-time implementation on a high end ultrasound system. Until now, the possibility to do fully parallel beamforming has been limited, but due to the continuous increase in memory and computational power of commercial ultrasound systems, real-time vector Doppler in a large imaging region could be realized in a not too distant future. These technological advances may also support the real-time implementation of alternative spectral estimation techniques.

1.6 List of publications

In addition to published and unpublished manuscripts included in this thesis, written and oral contributions have been made to national and international conferences. A list of the material to which the candidate has been a contributor is included in the following.

Papers included in the thesis

1. **Ingvild Kinn Ekroll**, Hans Torp and Lasse Løvstakken, "Spectral Doppler Estimation Utilizing 2D Spatial Information and Adaptive Signal Processing", *IEEE Transactions on Ultrasonics, Ferroelectrics and Frequency Control, Volume 59, Number 6, pages 1182-1192.*

2. Tonje Dobrowen Fredriksen, **Ingvild Kinn Ekroll**, Lasse Løvstakken and Hans Torp, "2D Tracking Doppler: A New Method to Limit Spectral Broadening in Pulsed Wave Doppler", submitted for review to *IEEE Transactions on Ultrasonics, Ferroelectrics and Frequency Control*

3. **Ingvild Kinn Ekroll**, Abigail Swillens, Patrick Segers, Torbjørn Dahl, Hans Torp and Lasse Løvstakken, "Simultaneous quantification of flow and tissue velocities based on multi-angle plane wave imaging", accepted for publication in *IEEE Transactions on Ultrasonics, Ferroelectrics and Frequency Control.*

4. **Ingvild Kinn Ekroll**, Torbjørn Dahl, Hans Torp and Lasse Løvstakken, "Combined vector velocity and spectral Doppler imaging of complex blood flow in the carotid arteries", submitted to *Ultrasound in Medicine and Biology*

Conference proceedings

1. **Ingvild Kinn Ekroll**, Hans Torp and Lasse Løvstakken, "Retrospective PW-Doppler based on spatiotemporal adaptive signal processing", *IEEE International Ultrasonics Symposium Proceedings 2010*

2. **Ingvild Kinn Ekroll**, Abigail Swillens, Patrick Segers, Hans Torp and Lasse Løvstakken, "Simultaneous quantification of flow and tissue velocities based on multi-angle plane wave imaging with extended velocity range", *IEEE International Ultrasonics Symposium Proceedings 2011*

3. Tonje Dobrowen Fredriksen, **Ingvild Kinn Ekroll**, Lasse Løvstakken and Hans Torp, "2D Tracking Doppler: A New Method to Limit Spectral Broadening in Pulsed Wave Doppler", *IEEE International Ultrasonics Symposium Proceedings 2012*

4. **Ingvild Kinn Ekroll**, Hans Torp and Lasse Løvstakken, "In vivo Vector Flow Imaging With Retrospective Pulsed Wave Doppler", *IEEE International Ultrasonics Symposium Proceedings 2012*

Presentations and abstracts

1. **Ingvild Kinn Ekroll**, Hans Torp and Lasse Løvstakken, "Retrospective PW-Doppler based on spatiotemporal adaptive signal processing", *2010 IEEE International Ultrasonics Symposium*

2. **Ingvild Kinn Ekroll**, Hans Torp and Lasse Løvstakken, "Improving PW-Doppler ultrasound using adaptive signal processing", *22nd international conference of Society of Medical Innovation and Technology (SMIT), 2010*

3. **Ingvild Kinn Ekroll**, Hans Torp and Lasse Løvstakken, "Improved spectral Doppler in medical ultrasound based on spatiotemporal adaptive signal processing", *Joint National PhD conference in Medical Imaging and the Annual MedViz conference, 2011*

4. **Ingvild Kinn Ekroll**, "US imaging of cardiovascular disease – Improved screening and diagnostics of the carotid artery",*The Artimino Conference on Medical Ultrasound Technology, 2011*

5. **Ingvild Kinn Ekroll**, Abigail Swillens, Patrick Segers, Hans Torp and Lasse Løvstakken, "Simultaneous quantification of flow and tissue velocities based on multi-angle plane wave imaging with extended velocity range", *2011 IEEE International Ultrasonics Symposium*

6. **Ingvild Kinn Ekroll**, Torbjørn Dahl, Hans Torp and Lasse Løvstakken, "In vivo Vector Flow Imaging With Retrospective Pulsed Wave Doppler", *2012 IEEE International Ultrasonics Symposium*

7. Thor Andreas Tangen, Ragnhild Øvland, **Ingvild Kinn Ekroll**, Natale Rolim and Lasse Løvstakken, "Coherent plane wave compounding and motion artifacts in small-animal cardiac imaging", *2012 IEEE International Ultrasonics Symposium*

Patent applications

1. Lasse Løvstakken, **Ingvild Kinn Ekroll** and Hans Torp, "Multi-dimensional Doppler Imaging for Automated Quantitative Analysis", *US provisional patent application, submitted 7. December 2012.*

References

[1] D. Griffin, "Audible and Ultrasonic Sounds of Bats," *Experientia*, vol. 7, no. 12, pp. 448–453, 1951.

[2] W. McDicken, *Diagnostic Ultrasonics*. Edinburgh: Churchill Livingstone, 1991.

[3] S. Barnett, G. Ter Haar, M. Ziskin, H. Rott, F. Duck, and K. Maeda, "International recommendations and guidelines for the safe use of diagnostic ultrasound in medicine," *Ultrasound Med. Biol.*, vol. 26, no. 3, pp. 355–366, 2000.

[4] B. Angelsen, *Ultrasound Imaging. Waves, Signals and Signal Processing*. Trondheim, Norway: Emantec, 2000.

[5] I. Edler and H. C.H., "The use of the ultrasonic reflectoscope for the continuous recording of movements of heart walls," *Kungl fysiogr sällsk*, vol. 24, no. 5, 1954.

[6] S. Satomura, "Ultrasonic Doppler method for the inspection of cardiac functions," *J. Acoust. Soc. Am.*, vol. 29, no. 11, pp. 1181–, 1957.

[7] S. Satomura, "Study of the Flow Patterns in Peripheral Arteries by Ultrasonics," *J. Acoust. Soc. Jpn*, 1959.

[8] D. Franklin, W. Schlegal, and R. Rushmer, "Blood flow measured by Doppler frequency shift of backscattered ultrasound," *Science*, vol. 132, no. 3478, pp. 564–565, 1961.

[9] D. Baker, H. Stegall, and W. Schlegel, "A sonic transcutaneous blood flowmeter," *Proc., 17th Ann. Conf. Eng. Med. Biol.*, vol. 6, 1964.

[10] P. P. and F. Leger, "Doppler ultrasonic pulsed blood flowmeter," *Proc. (th Int. Conf. Med. Biol. Eng.*, pp. 10–11, 1969.

[11] S. Johnson, D. Baker, R. Lute, and H. Dodge, "Doppler echocardiography, the localization of cardiac murmurs," *Circulation*, vol. 48, pp. 810–822, 1973.

[12] J. Holen, R. Aaslid, K. landmark, and S. Simonsen, "Determination of pressure gradient in mitral stenosis with a non-invasive ultrasound doppler technique," *Acta Med. Scand.*, vol. 199, pp. 455–460, 1976.

[13] A. Brubakk, B. Angelsen, and L. Hatle, "Diagnosis of valvular heart disease using transcutaneous doppler ultrasound," *Cardiovasc. Res.*, vol. 11, pp. 461–469, 1977.

[14] D. Fitzgerald and J. Drumm, "Non-invasive measurement of human fetal circulation using ultrasound: a new method," *Br. Med. J.*, vol. 2, pp. 1450–1451, 1977.

[15] L. Hatle, A. Brubakk, A. Tromsdal, and B. Angelsen, "Non-invasive assessment of pressure drop in mitral stenosis by doppler ultrasound," *Br. Heart. J.*, vol. 40, pp. 131–140, 1978.

[16] M. Spencer and J. Reid, "Quantitation of carotid stenosis with continuous-wave (C-W) Doppler ultrasound," *Stroke*, vol. 10, pp. 326–330, 1979.

[17] W. McDicken, G. Sutherland, C. Moran, and L. Gordon, "Colour doppler velocity imaging of the myocardium," *Ultrasound in Medicine & Biology*, vol. 18, no. 6-7, pp. 651 – 654, 1992.

[18] K. Namekawa, C. Kasai, M. Tsukamoto, and A. Koyano, "Realtime bloodflow imaging system utilizing auto-correlation techniques," *Ultrasound in Medicine & Biology*, vol. Suppl. 2, pp. 203–208, 1983.

[19] C. Kasai, K., A. Koyano, and R. Omoto, "Real-time two-dimensional blood flow imaging using an autocorrelation technique," *IEEE Transactions on Sonics and Ultrasonics*, vol. 32, pp. 458–464, 1985.

[20] T. L. Szabo, *Diagnostic Ultrasound Imaging.* Saint Louis, MO, USA: Elsevier Academic Press, 2004.

[21] J. Kips, P. Segers, and L. M. van Bortel, "Identifying the vulnerable plaque: A review of invasive and non-invasive imaging modalities," *Artery Research*, vol. 2, pp. 21–34, 2008.

[22] A. Alexandrov, D. Vital, D. Brodie, P. Hamilton, and J. Grotta, "Grading Carotid Stenosis With Ultrasound. An interlaboratory comparison," *Stroke*, vol. 28, pp. 1208–1210, 1997.

[23] E. Y. Lui, A. H. Steinman, R. S. Cobbold, and K. W. Johnston, "Human factors as a source of error in peak doppler velocity measurement," *Journal of Vascular Surgery*, vol. 42, no. 5, pp. 972.e1 – 972.e10, 2005.

[24] G.-M. von Reutern, M.-W. Goertler, N. M. Bornstein, M. D. Sette, D. H. Evans, A. Hetzel, M. kaps, F. Perren, A. Razumovky, T. Shiogai, E. Titianova, P. Traubner, N. Venketasubramanian, L. Wong, and M. Yasaka, "Grading Carotid Stenosis Using Ultrasonic Methods," *Stroke*, vol. 43, no. 3, pp. 916–921, 2012.

[25] B. Dunmire, K. Beach, K.-H. Labs, M. Plett, and D. S. Jr., "Cross-beam vector doppler ultrasound for angle-independent velocity measurements," *Ultrasound in Medicine & Biology*, vol. 26, no. 8, pp. 1213 – 1235, 2000.

[26] L. Bohs, B. Geiman, M. Anderson, S. Gebhart, and G. Trahey, "Speckle tracking for multi-dimensional flow estimation," *Ultrasonics*, vol. 38, no. 1-8, pp. 369 – 375, 2000.

[27] J. Jensen and P. Munk, "A new method for estimation of velocity vectors," *Ultrasonics, Ferroelectrics and Frequency Control, IEEE Transactions on*, vol. 45, pp. 837 – 851, 1998.

[28] M. Aderson, "Multi-dimensional velocity estimation with ultrasound using spatial quadrature," *Ultrasonics, Ferroelectrics and Frequency Control, IEEE Transactions on*, vol. 45, no. 3, pp. 852 –861, 1998.

[29] V. L. Newhouse, D. Censor, T. Vontz, J. A. Cisneros, and B. B. Goldberg, "Ultrasound doppler probing of flows transverse with respect to beam axis," *Biomedical Engineering, IEEE Transactions on*, vol. BME-34, no. 10, pp. 779 –789, 1987.

[30] K.-W. Yeung, "Angle-insensitive flow measurement using doppler bandwidth," *Ultrasonics, Ferroelectrics and Frequency Control, IEEE Transactions on*, vol. 45, no. 3, pp. 574 –580, 1998.

[31] H. Torp and K. Kristoffersen, "Velocity matched spectrum analysis: A new method for suppressing velocity ambiguity in pulsed-wave Doppler," *Ultrasound in medicine & biology*, vol. 21, no. 7, pp. 937–944, 1995.

[32] P. Stoica and R. Moses, *Spectral Analysis of Signals*. Upper Saddle River, NJ: Prentice Hall, 2005.

[33] M. Allam and J. Greenleaf, "Isomorphism Between Pulsed-Wave Doppler Ultrasound and Direction-of-Arrival Estimation-Part II: Experimental Results," *IEEE Transactions on Ultrasonics, Ferroelectrics and Frequency Control*, vol. 43, pp. 923–935, 1996.

[34] F. Gran, A. Jakobsson, and J. Jensen, "Adaptive spectral doppler estimation.," *IEEE transactions on ultrasonics, ferroelectrics, and frequency control*, vol. 56, no. 4, p. 700, 2009.

[35] K. Hansen, F. Gran, M. Pedersen, I. Holfort, J. Jensen, and M. Nielsen, "In-vivo validation of fast spectral velocity estimation techniques," *Ultrasonics*, 2009.

[36] J. Goldstein and S. Reed, "Reduced-Rank Adaptive Filtering," *IEEE Transactions on Signal Processing*, vol. 45, no. 2, pp. 492–496, 1997.

[37] S. Alam and K. Parker, "The butterfly search technique for estimation of blood velocity," *Ultrasound in medicine & biology*, vol. 21, no. 5, pp. 657–670, 1995.

[38] G. Montaldo, M. Tanter, J. Bercoff, N. Benech, and M. Fink, "Coherent plane-wave compounding for very high frame rate ultrasonography and transient elastography," *Ultrasonics, Ferroelectrics and Frequency Control, IEEE Transactions on*, vol. 56, pp. 489 –506, march 2009.

[39] R. Steel, K. V. Ramnarine, F. Davidson, P. J. Fish, and P. R. Hoskins, "Angle-independent estimation of maximum velocity through stenoses using vector doppler ultrasound," *Ultrasound in Medicine & Biology*, vol. 29, no. 4, pp. 575 – 584, 2003.

[40] A. H. Steinman, J. Tavakkoli, J. G. M. Jr., R. S. Cobbold, and K. Johnston, "Sources of error in maximum velocity estimation using linear phased-array doppler systems with steady flow," *Ultrasound in Medicine & Biology*, vol. 27, no. 5, pp. 655 – 664, 2001.

[41] A. H. Steinman, A. C. Yu, K. W. Johnston, and R. S. Cobbold, "Effects of beam steering in pulsed-wave ultrasound velocity estimation," *Ultrasound in Medicine& Biology*, vol. 31, no. 8, pp. 1073 – 1082, 2005.

Chapter 2

Background

In the following sections, a brief introduction to diagnostic ultrasound in general and blood flow imaging in particular is given. The purpose is to give the unfamiliar reader a more comprehensive background for techniques applied throughout this work. The text is inspired by many textbooks on diagnostic ultrasound imaging, and for a more extensive description of the topics, please refer to [1–6]. At the end of the chapter, some background on ultrasound imaging of atherosclerotic disease will also be provided.

2.1 Diagnostic ultrasound imaging

The origin of image formation in ultrasound is the difference in compressibility and density between materials in the body, causing reflection and scattering of the ultrasound beam. By assuming constant speed of sound c, it is possible to determine the distance z to different objects in the body, using the relation

$$z = \frac{c\,t}{2}, \tag{2.1}$$

where t is the time from transmission of the ultrasound wave to reception of the backscattered echoes.

Transmission of ultrasound in medical diagnostics is most often performed using a transducer with piezoelectric elements. When a voltage of changing polarity is applied, the elements expand and contract, causing tissue in contact with the transducer surface to vibrate and ultrasound waves to radiate into the tissue. The other way around, a transducer can also convert acoustic vibrations into an electric voltage, and thus may also be used to receive backscattered ultrasonic waves.

The transmitted ultrasound field is attenuated during its progression through tissue, by approximately 0.5 dB/cm MHz[2]. This means that although the resolution of ultrasound imaging is proportional to the frequency of the transmitted pulse, a compromise between penetration depth and resolution is encountered: the attenuation increases with increasing frequency. Diagnostic ultrasound usually operates in the range of 2–10 MHz when imaging through the skin, but frequencies up to 40 MHz have been used intraoperatively and when ultrasound catheters are used for imaging from the inside of blood vessels.

2.1.1 Focused imaging

Conventional ultrasound imaging is based on transmission of focused ultrasound beams. Different parts of the transducer referred to as (sub-)apertures are used to generate ultrasound beams with reduced beam width and increased pressure at certain depths. Focusing may be obtained by using an acoustic lens, a curved aperture, or by delaying the different transducer elements to form a curved wavefront. An image is built by steering the transmit beam in different directions or moving the aperture by switching the transducer elements on and off. One image line is formed for every transmit beam by delaying and summing the received signal from each element in the active aperture. The resulting grayscale depiction of the insonified region is commonly called brightness mode or B-mode imaging.

Whereas the axial resolution in ultrasound imaging is determined by the pulse length and the frequency of the transmitted ultrasound field, the lateral resolution is determined by the transmit and receive beam width. Defined by the distance from the beam axis to a -3 dB drop in the pressure amplitude, the beam width D_f at focus depth is given by

$$D_f = \frac{\lambda z_f}{D} = F_{\#}\lambda, \tag{2.2}$$

where λ is the wavelength, z_f is the focus depth and D is the size of the aperture. Similar to imaging with a regular camera, the ratio between the focus depth and the active aperture is called the F-number, $F_{\#}$. When focusing both on transmit (tx) and receive (rx), the two-way $F_{\#}$ is given by

$$F_{\#tr} = \left(\frac{1}{F_{\#tx}} + \frac{1}{F_{\#rx}} \right)^{-1}. \tag{2.3}$$

2.1.2 Plane wave imaging

In plane wave imaging, an *unfocused* ultrasound beam is emitted using the full aperture to insonify a broad region of interest. Parallel beamforming is used on receive[7, 8], which means that multiple image lines are formed from every pulse transmission. An illustration of the wavefronts originating from focused and unfocused transmission can be found in the left panel of Fig. 2.1, where the dashed lines illustrate the number of image lines per transmitted pulse. Parallel receive beamforming can also be utilized in conjunction with focused transmission, however the number of receive beams is limited by the transmit beam width, and image artifacts may be generated due to misalignment of transmit and receive beams[9].

The concept of plane wave imaging was introduced for B-mode imaging by Delannoy[10], and has later been applied to both elastography[11] and blood flow imaging[12–14]. The broad imaging region enables fast acquisition of ultrasound images, which is why plane wave imaging is sometimes referred to as *ultrafast ultrasound imaging*. A related approach which also allows high acquisition rates, is synthetic transmit aperture imaging, where defocused pulses are emitted using small subapertures, and several low-resolution images are added to obtain retrospective transmit focusing[15, 16].

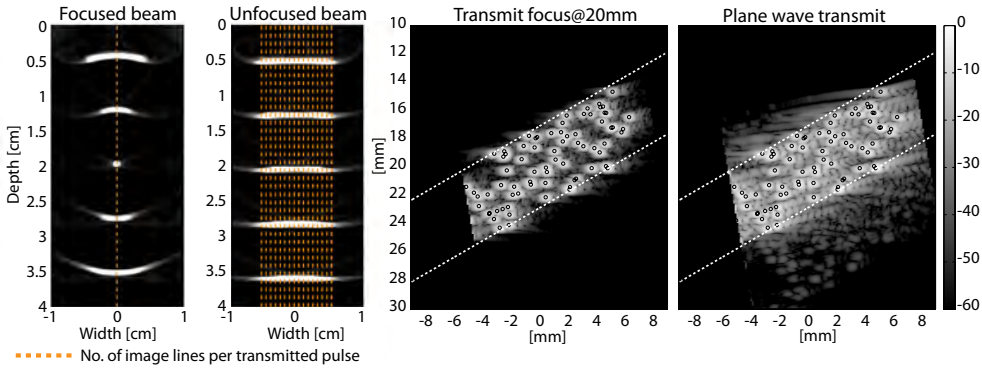

Figure 2.1: Simulations of focused and plane wave transmission (left) and imaging (right). The left panel illustrates that by using plane instead of focused transmissions, a large number of parallel receive beams may be generated per pulse. The right panels show simulated images of point scatterers using focused and single plane wave imaging.

The main limitation of plane wave transmission is the reduced penetration due to lack of transmit focusing, as well as decreased contrast and lateral resolution ($F_{\#tr} = F_{\#rx}$ when $z_f \to \infty$). This is illustrated in the right panels of Fig. 2.1, where true point scatterer locations are indicated by black circles overlaid simulated images from both focused and single plane wave imaging. However, it has recently been shown that by coherently adding the low resolution images from several transmit angles, retrospective transmit focusing may be achieved also in the case of plane wave transmission[17]. A comparison of images constructed from single and multiple plane wave transmissions, in addition to conventional focused imaging, can be found in Fig. 2.2.

2.1.3 Doppler imaging

Ultrasound imaging of moving objects is often called Doppler imaging. The term Doppler is used because an ultrasound wave reflected by a moving scatterer will experience a shift in frequency, similar to that observed by Christian Doppler in light from stars approaching or receding from us. It can be shown[5] that the shift in frequency is equal to

$$f_d = 2f_0 \frac{v \cos\theta}{c}, \tag{2.4}$$

where the transmitted frequency is f_0, the scatterer velocity is v, the speed of sound is c and θ is the angle between the ultrasound beam and the velocity direction of the scatterer. The equation is valid when $v \cos\theta \ll c$. Typical velocities for blood flow in the healthy carotid arteries are up to 1 m/s, while it in stenotic regions may reach as high as 2–3 m/s. When using a transmit frequency of 5 MHz, the possible Doppler shifts are in the audible range; from 0 to 20 kHz.

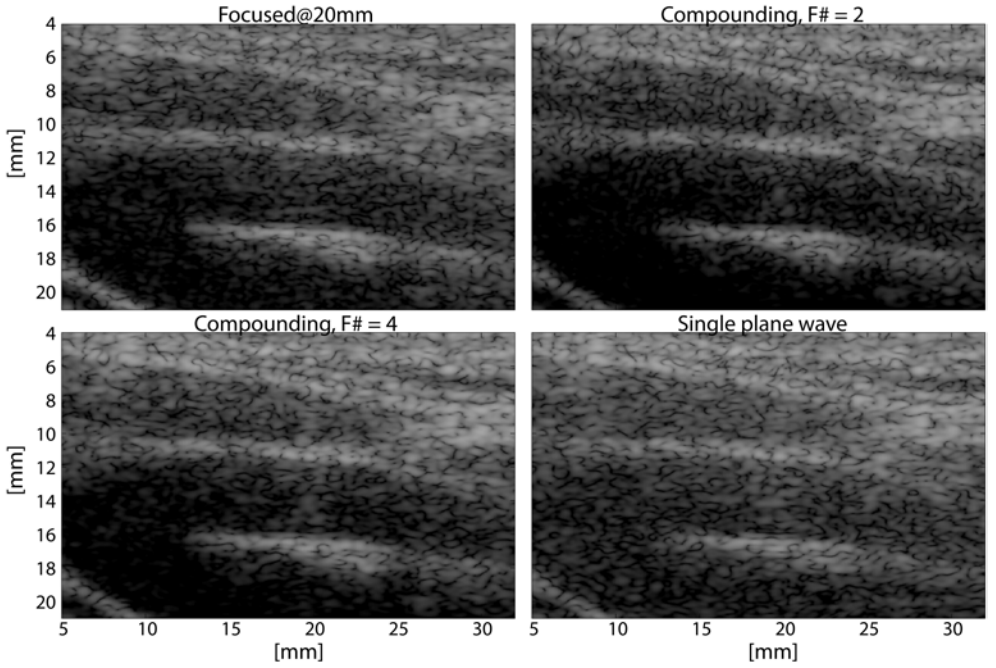

Figure 2.2: The figure shows the carotid artery bifurcation of a healthy volunteer, imaged using focused and unfocused transmit beams. *Upper left:* Focused transmit beams, $F_{tx\#} = 2$. *Upper right:* Coherent compounding corresponding to $F_{tx\#} = 2$. *Lower left:* Coherent compounding with reduced angle span and number of transmitted plane waves. *Lower right:* Single plane wave image. Dynamic range 40 dB

Are we really utilizing the Doppler shift?

Although the term Doppler imaging is used for several modalities measuring blood or tissue movement, the actual Doppler frequency shift is only used in Continuous Wave (CW) Doppler, where a single frequency is continuously emitted into the tissue by one part of the transducer aperture, while the backscattered signal is received simultaneously by a different part of the aperture. The overlap region between the two transmit and receive beams define the sample volume, resulting in a lack of range resolution, especially for closely placed transmit/receive beams. An advantage of CW Doppler, however, is that the Doppler signal is measured "continuously", which means that in practice, the technique is not limited by a maximum measurable velocity.

Two other modalities are also commonly referred to as Doppler-based, namely Pulsed Wave (PW) Doppler, and Color Doppler Imaging (often referred to as Color Flow Imaging, or CFI). These modalities are based on pulsed transmissions, where a series of ultrasound pulses are transmitted into the tissue with a certain pulse repetition frequency (PRF). Movement of scatterers through the sample volume will still cause

a shift of the emitted frequencies. However, due to frequency dependent attenuation and scattering, it is almost impossible to measure the change in frequency content of the pulse originating specifically from the Doppler effect.

Instead of estimating the Doppler shift directly, pulsed techniques for velocity estimation analyze changes in the backscattered signal between successive pulse emissions. Both the change in time-of-flight for a certain scattering signature (originating from a defined group of scatterers), and the rate of change in the phase returning from a certain sample volume may be used, but in commercial ultrasound systems the phase-shift techniques dominate due to a lower computational complexity and high robustness even in situations with low signal-to-noise ratio (SNR). The advantage of using pulsed transmissions is that by using the relation between time-of-flight, sound velocity and depth as used in regular pulse-echo imaging (2.1), range resolution is obtained. On the other hand, a limitation in the maximum measurable velocity is introduced by sampling the Doppler signal at a rate given by the pulse repetition frequency.

Sampling of the backscattered signal is normally done in two dimensions, both in the radial direction where a high sampling frequency is utilized (40–80 MHz), called *fast-time*, and between pulses in intervals given by $T_{\text{PRF}} = 1/\text{PRF}$ (typically 1–12 kHz). The signal from one depth range sampled from pulse to pulse is referred to as the *slow-time* signal. An illustration of the sampled signal from a single scatterer moving through an ultrasound beam can be found in Fig. 2.3, where the slow-time signal from one range is seen as the waveform in the lower right corner. With reference to the different receive lines from the single scatterer in Fig. 2.3, the phase shift between any pair of received signals can be estimated, enabling assessment of the velocity of the scatterer. Alternatively, the velocity can be estimated from the center frequency of the slow-time signal. Techniques for estimating the full spectral content of the slow-time signal is discussed in further detail in Chapter 3 and 4 and will not be repeated here.

A simple model for pulsed Doppler velocity estimation

A simple model for the phase change between pulse emissions can be derived by looking at the single scatterer illustrated in Fig. 2.3, moving through an ultrasound beam with velocity v, directed at an angle θ with the beam axis. A derivation provided by Jensen[5] will be reproduced here to provide some insight into velocity estimation where the true Doppler shift is not utilized.

The scatterer illustrated in Fig. 2.3 will move a distance $\Delta z = v\cos\theta\ T_{\text{PRF}} = v_z T_{\text{PRF}}$ in the radial direction between successive pulse emissions. Due to the change in position of the scatterer, the backscattered signal from two successive pulse emissions will be shifted in time by

$$\Delta t = \frac{2v_z T_{\text{PRF}}}{c}.$$

The phase change will increase as a function of pulse number, k, and assuming sinusoidal signal transmission, the received signal, $r(t,k)$ from the moving scatterer is

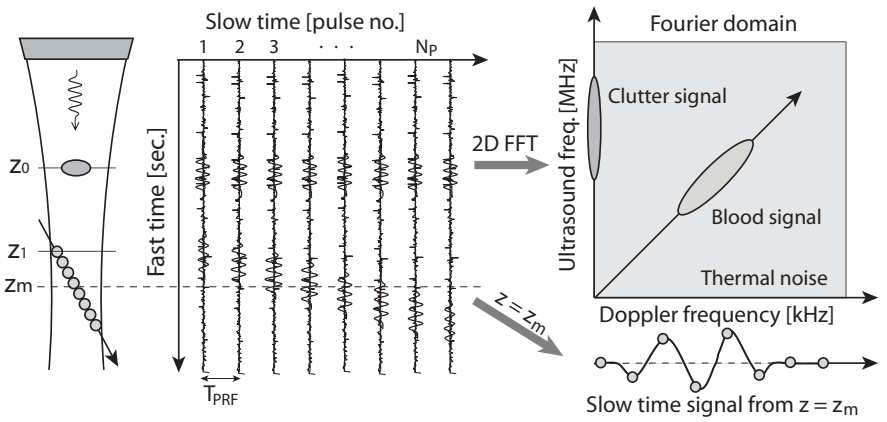

Figure 2.3: A depiction of pulsed Doppler imaging of a single scatterer moving through the ultrasound beam. A stationary scatterer is present at z_0, while the moving scatterer crosses the beam starting at depth z_1. The slow-time signal is sampled at depth z_m, resulting in the sampled waveform shown to the lower right. A typical representation of the 2D Fourier transform of the fast-time–slow-time plane is also depicted, illustrating frequency components originating from stationary scatterers (clutter), moving scatterers (blood) and thermal noise.

given by

$$r(t,k) = a\sin\left(2\pi f_0\left(t - \frac{2z_1}{c} - k\Delta t\right)\right),$$

where z_1 is the initial depth of the scatterer, and a the backscattered amplitude and t is fast time. Setting $t = t_m$ corresponds to measuring the backscattered signal at a predefined depth z_m, giving

$$\begin{aligned} r(t_m,k) &= a\sin\left(2\pi f_0\left(t_m - \frac{2z_1}{c} - k\frac{2v_z T_{\mathrm{PRF}}}{c}\right)\right) \\ &= -a\sin\left(2\pi\frac{2v_z f_0 k T_{\mathrm{PRF}}}{c} - \phi_m\right). \end{aligned}$$

$\phi_m = 2\pi f_0(t_m - (2z_1/c))$ is a constant phase factor, while the first term in the parenthesis gives the frequency of the slow time signal

$$f_r = 2f_0\frac{v_z}{c}, \tag{2.5}$$

which is similar to the equation used to interpret the true Doppler shift (2.4) and proportional to the axial blood velocity.

Fortunately, factors such as absorption and diffraction do not change much between pulses, and this consistency makes pulsed Doppler relative insensitive to

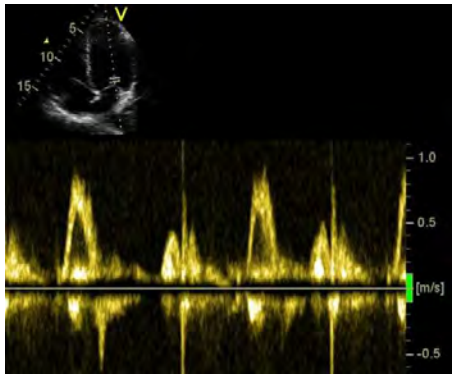

(a) PW Doppler spectrogram

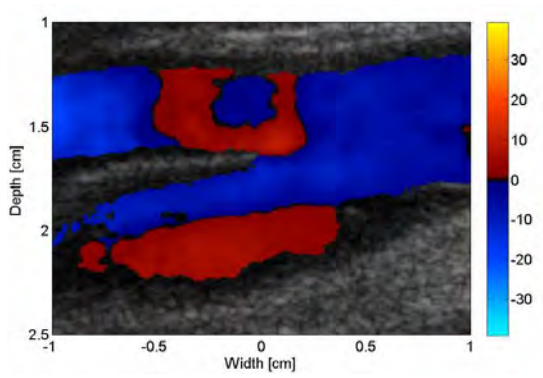

(b) Color flow image

Figure 2.4: Two pulsed Doppler techniques are demonstrated. In (a), a PW Doppler spectrogram is shown, providing velocity information from a sample volume in the heart. The sample volume is indicated by the two parallel lines in the B-mode image on top. Image (b) shows a color flow image from the carotid artery bifurcation. The axial velocities are encoded in colors, red colors indicating flow towards the transducer and blue colors indicating flow receding from the transducer. The colorbar has units in cm/s.

these confounders. However, variations and loss caused by diffraction of the beam and frequency dependent absorption affect general sensitivity.

2.2 Blood flow imaging

CW and PW Doppler techniques provide velocity spectra from a certain sample volume over time, displayed as a spectrogram. An example of a PW Doppler spectrogram is given in Fig. 2.4(a). These spectra provide valuable quantitative information on the blood velocities in the region of interest, but cannot provide an overview of the flow conditions in a larger spatial region. As it is unpractical to show spectrograms from many spatial locations simultaneously, other means of displaying velocity information in a 2D or 3D region have been developed, and a brief introduction will be given here under the collective term blood flow imaging techniques.

2.2.1 Color flow imaging

Color flow or color Doppler imaging is a modality where a dynamic display of blood velocity and relative direction (towards or away from the transducer) is provided in a 2D or 3D image region. The velocity information is encoded in colors, giving the modality its name, where red colors indicate flow towards the transducer and blue colors indicate flow away from the transducer. The velocity information is

displayed overlaid a dynamic B-mode image, and the combined information gives a good impression of the blood flow in vessels and organs such as the heart.

To be able to image the blood flow in an image region sized closer to a B-mode image than a single sample volume, rapid acquisition of mean velocity estimates from a large number of directions is needed. Development of 2D flow imaging techniques started in the 1970s and 1980s[18–24], and early attempts were based on PW Doppler from several range gates in depth and from several beam directions. However, to be accurate, these PW Doppler based techniques needed a large number of samples, and blood being quasi-stationary for only 2–10 ms made it difficult for these techniques to capture the flow dynamics in a 2D region. Estimators which could find the velocity based on 2–10 samples instead of hundreds were therefore investigated, aiming to achieve real time blood flow imaging in a larger image region.

The first successful real-time color flow imaging systems were based on the autocorrelation approach[25, 26], and emerged in the 1980s. This is a robust estimator[27], and is still the most common approach for mean velocity estimation in commercial ultrasound systems, although many alternative time-domain estimators have been suggested[28–33]. The autocorrelation technique had been described even earlier in the weather-radar community[34, 35], where it is known as the pulse pair estimator[36].

As the mean velocity derived from the autocorrelation technique is used as a basis for vector Doppler imaging in later chapters, a more thorough explanation of the estimator is given in the following.

The autocorrelation estimator

In reality, a large number of scatterers will pass trough the sample volume at all times. The combined backscattered echoes produce a received signal that can be modeled as a complex Gaussian random process, whose velocity content can be determined by the power spectrum of the slow-time signal[2]. The autocorrelation estimator is used to calculate the first spectral moments of the power spectrum; the signal power, the mean frequency and the bandwidth. Through the Wiener-Khinchin relation, the power spectrum $G(f)$ and the autocorrelation function $R(\tau)$ form a Fourier transform pair, which can be expressed using the mean Doppler frequency f_d:

$$R(\tau) = e^{i2\pi f_d \tau} \int_{-f_N}^{f_N} G(f) e^{i2\pi (f - f_d)\tau} \, \mathrm{d}f, \tag{2.6}$$

where $f_N = PRF/2$. We see that when the integral is real, the mean Doppler frequency can be found from the argument of $R(\tau)$. This implies that the imaginary part of the integral in (2.6) is zero, that is

$$R_I = \int_{-f_N}^{f_N} G(f) \sin(2\pi (f - f_d)\tau) \, \mathrm{d}f = 0. \tag{2.7}$$

As seen from (2.7), the autocorrelation estimate of f_d will be unbiased if the power spectrum is symmetric around f_d. As a consequence, white noise will not bias the

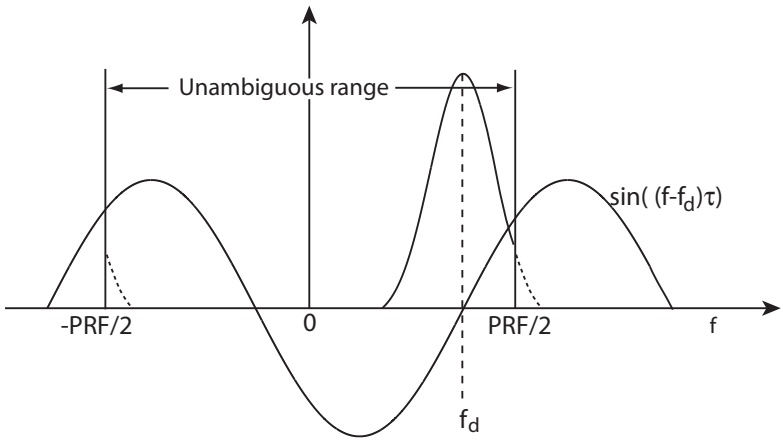

Figure 2.5: An illustration of the components of the integral in (2.7). The autocorrelation estimate of the mean Doppler frequency will not be biased by some aliased frequency components if the power spectrum is symmetric around f_d. The figure was adapted from[37]

autocorrelation estimate due to its symmetric spectrum. An *almost* unbiased estimate can be provided also for asymmetric spectra, given that the power spectrum contains frequencies only in a narrow band compared to the sampling frequency. Another advantage of the autocorrelation estimator, which is illustrated in Fig. 2.5, is that it will remain unbiased even if some frequency components of the power spectrum are aliased[37]. This is not the case for the power weighted mean Doppler frequency estimate

$$\hat{f}_d = \frac{\int_{-f_N}^{f_N} f\hat{G}(f)\,\mathrm{d}f}{\int_{-f_N}^{f_N} \hat{G}(f)\,\mathrm{d}f}, \tag{2.8}$$

where spectral components beyond the Nyquist limit ($\pm$ PRF/2) will result in a biased estimate of the mean Doppler frequency.

In practice, the autocorrelation function of lag one $R(1)$ is estimated from the complex demodulated Doppler signal from fixed spatial positions $x(k)$, as

$$\hat{R}(1) = \frac{1}{N_p}\sum_{k=0}^{N_p-1} x(k)^* x(k+1), \tag{2.9}$$

where * denotes the complex conjugate and N_p is the number of slow-time samples. The mean velocity is obtained by applying (2.5) and a frequency scaling factor $\frac{PRF}{2\pi}$ to the argument of $\hat{R}(1)$, giving

$$v_z = \frac{\angle\hat{R}(1)PRFc}{4\pi f_0} = \frac{\hat{f}_d\, c}{2\, f_0}. \tag{2.10}$$

From the Nyquist-Shannon sampling theorem, the maximum measurable Doppler frequency is equal to half the sampling frequency. By inserting $f_{d,max} = \frac{PRF}{2}$ into (2.10), the maximum measurable velocity becomes

$$v_{z,max} = \frac{c\,PRF}{4\,f_0}, \tag{2.11}$$

and the maximum measurable velocity in a pulsed Doppler scheme is therefore determined by the pulse repetition frequency and the transmit frequency.

The variance in the velocity estimates from autocorrelation decrease with an increased number of observations (an increased ensemble length). Additional variance reduction may be achieved by spatial averaging[38]. As a result, there is a trade-off between the statistical robustness of the velocity estimates and temporal and spatial resolution.

2.2.2 Clutter filtering

The backscattered signal from blood is much weaker than that from muscular tissue (40–100 dB difference), and this so-called *clutter signal* will completely dominate velocity estimates if it is not rejected. Fortunately, the velocity of blood scatterers is in many cases higher than that of slowly moving tissue, and a high pass filter may be used to separate blood and clutter signal. However, the clutter filter will also remove components of low velocity flow, limiting the minimum measurable velocity in blood flow imaging techniques. This means that in practice, the measurable velocity span is decided by properties of the clutter filter and the Nyquist velocity given in (2.11).

Clutter filters for use in blood flow imaging should have sufficient stop-band attenuation to reject the clutter component (70–80 dB is enough in most cases), and a short transition region to minimize the removal of signal from blood. As the number of signal samples acquired in conventional CFI is low (8–16), clutter filter design may be a challenging task. Several clutter filter designs have been considered in the past, including FIR filters, IIR filters and polynomial regression filters[39–41]. A short description of these filters will be given in the following.

FIR (finite impulse response) filters may be described by the convolution of an impulse response function $h(n), n = 0, 1, ..., M-1$ and the input signal $x(k), k = 0, 1, ..., N_p - 1$, as

$$y(k) = \sum_{n=0}^{M-1} h(n)x(k-n). \tag{2.12}$$

FIR filters have the advantage of being time invariant and have low computational complexity. However, some samples have to be discarded after filtering due to initialization effects. Due to the increase in variance of the autocorrelation estimate with a decreasing number of signal samples, the filter order should be kept low to avoid discarding too many.

The output of IIR (infinite impulse response) filters is dependent on both present and past input samples, as well as past output samples. IIR filters may be described using the difference equation

$$y(k) = -\sum_{n=1}^{M} a_n x(k-n) + \sum_{n=0}^{M} b_n x(k-n) \tag{2.13}$$

As the input signal in CFI is of relatively short length, the transient response of the filter becomes important, and several different techniques for reducing the transient have been considered, see for instance[41].

Polynomial regression filters calculate the best least squares fit of the signal to a set of polynomials modeling the clutter signal, and subtract this from the original signal. The output of the filter then becomes

$$\mathbf{y} = (\mathbf{I} - \sum_{n=0}^{M-1} \mathbf{b}_n \mathbf{b}_n^H)\mathbf{x}, \tag{2.14}$$

where H is the conjugate transpose, $\mathbf{I}$ is the identity matrix and $\mathbf{b}_n$ are orthonormal basis vectors spanning the M-dimensional clutter signal subspace. The Legendre polynomials form such a basis, and are typically used in polynomial regression filters[40]. The frequency response of polynomial regression filters vary both with the clutter space dimension M and the ensemble length N_p, so to obtain similar stopband attenuation for increasing ensemble lengths, the clutter space dimension must also be increased.

An advantage of the polynomial regression filters is that they have a smooth and monotonic frequency response, and for equal stopband width, they have a shorter transition region than FIR filters[42]. As no samples need to be discarded after filtering, an additional reduction in variance of the autocorrelation estimates may also be achieved[42]. A disadvantage of regression filters is that they are not time invariant, which causes frequency distortion in the transition region of the filter[40].

2.2.3 Vector velocity imaging

Once the clutter has been rejected, the Doppler signal may be further processed to find the blood velocities. Color flow imaging, CW and PW Doppler are all one-dimensional techniques, meaning that only the axial velocity component is estimated and displayed. This is a major limitation in blood flow imaging, especially as most major blood vessels run parallel to the skin surface, making the dominant direction near orthogonal to the ultrasound beam. The one-dimensional display may also lead to non-intuitive visualization of the blood flow, as the color will change abruptly in cases where the relative direction of the flow changes from towards the transducer to away from the transducer.

Several approaches have been suggested to overcome the angle dependency in color flow imaging. The two main approaches are vector Doppler imaging and speckle tracking, however, alternative techniques have also been suggested. Since the focus of

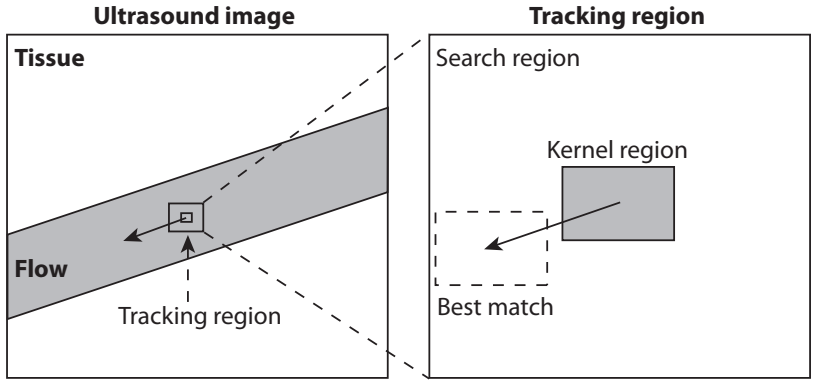

Figure 2.6: An illustration of the speckle tracking concept. The best match of a given kernel region is searched for in a larger search region of a subsequent acquisition. The velocity can be calculated based on the estimated displacement and the time between image acquisitions. The figure was adapted from[44].

two of the contributions in this work is plane wave vector Doppler, this technique will be explained in more detail than the alternatives.

Speckle tracking

Speckle tracking was proposed in the 1980s[43], and is based on tracking the interference pattern from blood, called *speckle*, between consecutive ultrasound images. Due to the computational demands of performing two- or three-dimensional cross-correlation on RF data, means to reduce the complexity have been suggested. Today, commonly used techniques include using the sum of absolute differences (SAD) or the sum of squared differences (SSD) on the signal envelope to find estimates of displacement between consecutive image frames. An illustration of the speckle tracking concept is given in Fig. 2.6.

The main challenges in speckle tracking are related to clutter filtering[42] and decorrelation of speckle pattern due to irregular flow patterns, flow gradients or out-of-plane motion. Additionally, low SNR may introduce estimation bias, as large translations become underestimated and small translations become overestimated[45].

Lateral modulation

Another approach for 2D velocity estimation was suggested by Anderson[46] (spatial quadrature) and Munk and Jensen[47] (transverse oscillation). These techniques introduce a modulation in the lateral direction of the received ultrasound field using complex apodization schemes. In the transverse oscillation technique, a lateral movement by the scatterer will, similar to phase shift estimation in the axial direction,

introduce a phase shift between parallel beams separated by a distance of $\lambda_x/4$, where λ_x is the wave length in the transverse direction of the pulse echo field[48]. Scatterers moving through the doubly oscillating field will produce a signal where two frequency components are present, related to the v_x and v_z components through

$$\begin{aligned} v_z &= \frac{c\, f_z}{2\, f_0} \\ v_x &= f_x\, \lambda_x, \end{aligned} \tag{2.15}$$

where λ_x depends on the apodization scheme applied on receive. As indicated by Anderson[46], these lateral modulation techniques are related to the dual beam/split aperture vector Doppler approach through the use of apodization on receive to create the quadrature signals. The transverse oscillation method has been validated using healthy volunteers[13, 49], and is in Europe currently available in a commercial ultrasound system from BK Medical[1].

Doppler bandwidth

A third technique is based on the bandwidth of the Doppler signal, which is dependent on inhomogeneities of the wave field, the spread of velocities and the observation time of the scatterers as they pass through the sample volume. Estimation of the velocity magnitude using the Doppler bandwidth technique has been investigated by several authors[51, 52], but due to limitations such as the requirement of a spherical sample volume if the beam-to-flow angle is unknown and because non-stationary flow will also contribute to spectral broadening, it is still in the experimental stage.

Vector Doppler imaging

Vector Doppler imaging was suggested already in the 1970s[53], using two crossed beams to find the velocity in two dimensions. A thorough review of vector Doppler imaging techniques are given by Dunmire *et al.*[54], where both single element and array systems for cross beam analysis are evaluated.

To estimate the velocity direction in vector Doppler, a triangulation approach is used, requiring the Doppler shift estimate from at least two directions. Estimates from different spatial directions may be realized both using a common transmit aperture and two separate receive apertures (Fig. 2.7(a)), or by transmitting (and receiving) tilted ultrasound beams in a (quasi) dual beam approach (Fig. 2.7(b)). The beams of different direction are not transmitted simultaneously in the dual beam approach, but rather in an interleaved scheme, hence the additional term in the parenthesis.

In the split aperture approach, the v_x and v_z components are given by

[1] http://www.bkmed.com/vector_flow_imaging_en.htm

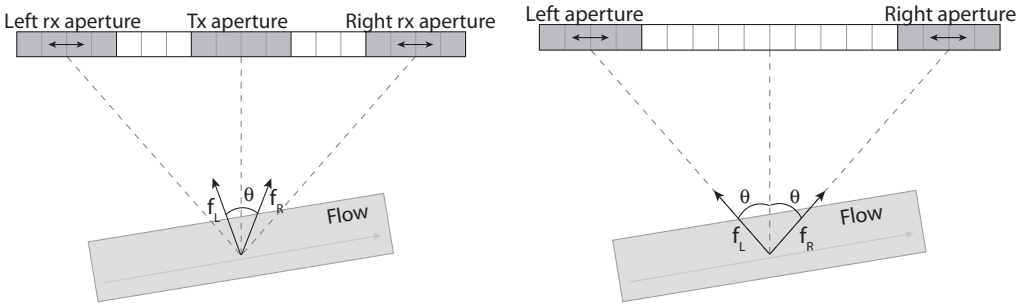

(a) Split aperture (b) Dual beam

Figure 2.7: (a): The split aperture approach with a common transmit aperture and two separate receive aperture. (b): The (quasi) dual beam approach, where two separate transmit/receive apertures are used. The arrows point in the direction of the measured Doppler shifts.

$$\begin{aligned} \hat{v}_x &= \frac{c\,(\hat{f}_l - \hat{f}_r)}{2\,f_0 \sin\theta} \\ \hat{v}_z &= \frac{c\,(\hat{f}_l + \hat{f}_r)}{2\,f_0(1+\cos\theta)}, \end{aligned} \tag{2.16}$$

whereas in the dual beam approach, the velocity components are given by

$$\begin{aligned} \hat{v}_x &= \frac{c\,(\hat{f}_l - \hat{f}_r)}{4\,f_0 \sin(\phi/2)} \\ \hat{v}_z &= \frac{c\,(\hat{f}_l + \hat{f}_r)}{4\,f_0 \cos(\phi/2)}. \end{aligned} \tag{2.17}$$

In the split aperture approach, the absolute angle between the transmit and receive direction is θ, whereas the angle between the two transmit/receive directions in the dual beam approach is ϕ ($= 2\theta$ in Fig. 2.7). c is the speed of sound, f_0 is the pulse center frequency and $\hat{f}_l$, $\hat{f}_r$ are the Doppler frequencies estimated from the left and right subaperture respectively.

An advantage of the split aperture approach is that the two directional estimates may be obtained from the same transmit events (i.e. there is no time-lag between the estimates), while an advantage of the dual beam approach is that for equal receive angle, the separation of the two directional Doppler estimates is larger than in the split aperture case, reducing the variance in the lateral velocity estimates[54]. An increased separation is achieved because the Doppler shift is measured in the direction of the vector sum of the transmit and receive unit vectors[2].

Although validated over many years and with real time solutions suggested[55, 56], there are, to the author's knowledge, currently no commercially available ultrasound systems which utilize the vector Doppler technique.

2.3 Atherosclerosis and carotid artery disease

Cardiovascular disease (CVD) is today the world's leading cause of death, with an incident rate of both coronary heart disease and stroke expected to increase due to a globally ageing population and lifestyle changes in developing countries[57]. The inflammatory disease *atherosclerosis* is the main precursor of complications in CVD, due to gradually developing plaques which can obstruct blood flow and/or give rise to hazardous emboli, as illustrated in Figs. 2.8(a) and 2.8(b). The carotid arteries are major blood vessels extending from the aorta to the brain, with the important task of supplying the face and brain with blood. The term carotid artery disease is used when blood flow through the carotid arteries is disturbed or reduced as a result of developing atherosclerotic plaques.

The healthy arterial wall consists of three layers: the intima (inner layer), media (middle layer) and the adventitia (outer layer). Additionally, one single layer of endothelial cells line the intima towards the lumen. All arteries tend to change composition and grow increasingly more fibrous with age, in a process called *arteriosclerosis*. Atherosclerosis, on the other hand, has focal manifestations which are partly modulated by blood flow patterns (Fig. 2.8(c))[61]. Atherosclerotic plaques form at sites of low density lipoprotein (LDL) accumulation and low or oscillatory wall shear stress (WSS)[60, 62], which induce an inflammatory response in the artery wall. *Fatty streaks* are early lesions which form already in childhood. If these small lesions are later invaded by macrophage foam cells, necrotic debris may accumulate underneath a fibrous cap, forming a plaque which may grow and become stenotic, rupture or erode and form a thrombus, or become calcified[61].

Blood flow patterns have a significant role both in the initiation and development of plaques. Endothelial dysfunction may be induced by disturbed flow patterns near arterial branches, bifurcations and curvatures[63], which again initiate lesion formation. Additionally, low endothelial shear stress promotes both the migration of smooth muscle cells from the media to the intima and their apoptosis, and further it promotes the transition of stable lesions to thin cap fibroatheromas, a typical precursor to rupture mediated thrombosis[60].

Atherosclerosis is generally asymptomatic until the stenosis exceeds 70–80 %, however the first symptoms may be fatal. Symptoms of the disease emerge either due to reduced flow after significant stenoses, or due to emboli caused by the rupture of unstable plaques leading to transient or permanent myocardial infarction or stroke[64]. However, due to the remodeling of the arterial wall, up to 40% of the cross sectional area of the artery may consist of lesions before the lumen becomes more narrow[58]. Because arterial wall remodeling leads to less initial narrowing of the lumen, vulnerable plaques may be less symptomatic than stable plaques. Still, frictional forces exerted by the pulsating blood flow might lead to rupture of the thin fibrous cap typically found in

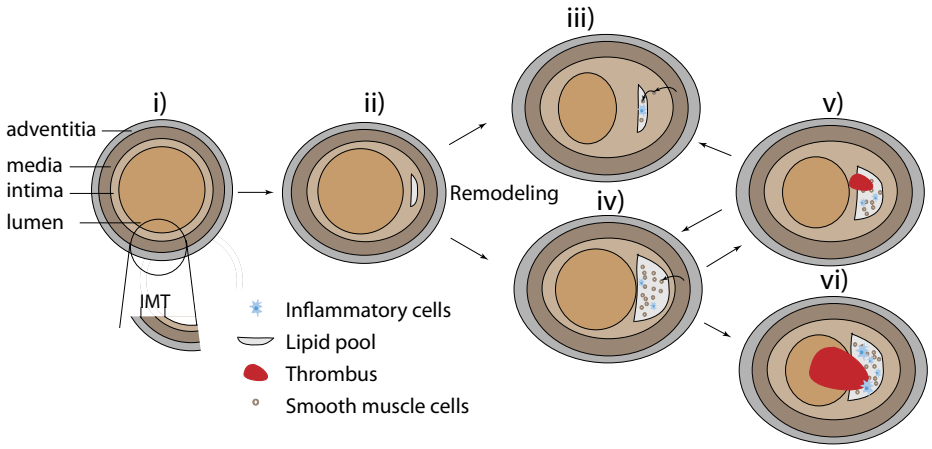

(a) Progression of atherosclerosis from normal artery (i) to the unstable plaque (iv,vi). ii) Fatty streak iii) Stable plaque with small lipid core and thick fibrous cap. iv) Vulnerable plaque with thin fibrous cap. v) Complex stabilized plaque. vi) Ruptured plaque: Transient ischemic attack or stroke

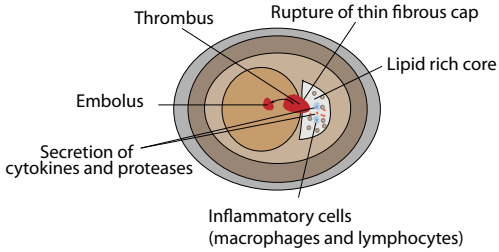

(b) The unstable plaque

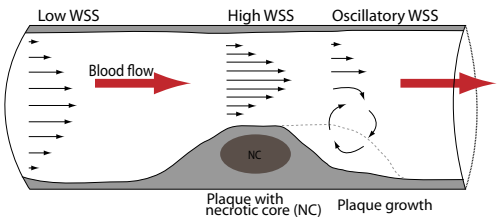

(c) Influence of blood flow patterns

Figure 2.8: (a): Progression of atherosclerosis. (b): A closer look at the unstable plaque. (c): Blood flow may modulate growth and (de)stabilization of a plaque. WSS = Wall shear stress, IMT = Intima-Media thickness. Figures adapted from[58–60].

vulnerable plaques, and the formation of a blood clot (thrombus). The plaque might stabilize again, but the thrombus might also loosen and cause occlusion in smaller arteries without preceding clinical symptoms.

Due to the widespread disease and its potential for long term disability and death, there is an increasing need for accurate and efficient non-invasive imaging techniques suitable for cardiovascular screening and diagnostics.

2.3.1 Ultrasound imaging of carotid artery disease

The gold standard for investigating stenoses in the carotid arteries has historically been X-ray angiography. However, this is a technique which is both invasive (a catheter needs to be inserted in an artery to administer the contrast agent) and makes use of ionizing radiation. Since it was found that the procedure could actually *increase* the risk of embolization and stroke[65], alternative noninvasive imaging techniques have been sought. These new techniques include Doppler ultrasound, which is safe for the patient and relatively easy to perform for a trained practician. Because the carotid arteries are situated at shallow depths without overlying spaces of air or bony structures, they are also well suited for ultrasound imaging. Several factors have made ultrasound imaging a method of choice for examining patients with carotid artery disease, amongst others the relatively high resolution compared to magnetic resonance imaging (MRI) and the ability to provide a detailed image of the arterial wall and plaque instead of the lumen only as provided by computed tomography (CT). As the examination procedure is also relatively simple, non-invasive vascular ultrasound imaging is in many cases the only imaging modality performed prior to carotid endarterectomy (carotid artery surgery)[66, 67].

Intravascular ultrasound imaging (IVUS), where an ultrasound unit is mounted on the tip of a catheter and inserted into blood vessels, is a technique that allows ultrasonic tomographic imaging of vessels. It was invented in 1972[68], and has played an important role in the development of standard care in treatment by balloon angioplasty[2] and stents[3][69]. It has been used to measure plaque progression and regression in clinical trials[70], and using additional post processing, information on plaque components may be found, for instance about plaque strain[71–74]. Still, although IVUS is a very promising technique for detecting plaque composition[75], the ideal screening technique is non-invasive.

B-mode images from non-invasive ultrasound imaging can provide information on wall morphology which changes during the course of the atherosclerotic disease. It is for instance possible to measure the thickness of the intima-media layer, which if increased is a marker of atherosclerosis[76]. The echogenicity of the plaque, or whether it appears bright (hyperechoic) or translucent (echolucent) in the B-mode image, can also be used to differentiate between soft plaques (echolucent) and fibrous plaques (hyperechoic)[77, 78].

However, the *degree of stenosis* (lumenal narrowing) is typically not determined from the geometry seen in B-mode images, but by use of Doppler ultrasound, or more specifically, by pulsed wave (PW) Doppler. PW Doppler measures which have been correlated to angiography include measurement of peak systolic velocity (PSV) in the internal carotid artery (ICA), end diastolic velocity (EDV), and ratios of ICA PSV and common carotid artery (CCA) PSV. As a guiding standard, ICA peak systolic velocity $\geq$125 cm/s is regarded as clinically significant, representing a stenosis of more than 50 %[79]. Measurements of the velocity magnitude from spectral Doppler are, however, also influenced by other factors than the actual luminal

[2] A procedure to open narrowed arteries caused by deposits of plaque
[3] A stent is a device placed within the artery to keep the vessel open

narrowing, giving large variability in measurements and thereby the management and outcome of patients with carotid artery stenosis. Variability originates from the use of different equipment[80], different laboratory practices[81], and different practitioners performing the measurements[82]. Additionally, spectral broadening[4], may cause overestimation of the peak systolic velocity, whereas the presence of collateral flow[83] or contralateral stenoses[84] might result in under- or overestimation of the severity of the disease respectively.

One factor which might reduce inaccuracies originating from intra- and interobserver variability, is automatic angle-correction of the PW Doppler spectra. Today, the velocity spectra must be manually angle-corrected with the assumption that the flow is parallel to the vessel wall. As previously mentioned, this might not be the case in stenotic regions. Additionally, if the beam-to-flow angle is close to 90°, even small variations of the correction angle will cause large variations of the measured peak systolic velocity. More consistent estimates might be obtained using automated calibration; however, this requires an estimate of the velocity direction at the measurement site. As described in Section 2.1.3, numerous techniques for estimating vector velocities have been investigated, with vector Doppler techniques[54] and speckle tracking[45] as the two main approaches. Utilizing such directional estimates in conjunction with spectral estimation could reduce the velocity measurement errors and improve categorization of carotid stenosis severity[85].

References

[1] W. McDicken, *Diagnostic Ultrasonics*. Edinburgh: Churchill Livingstone, 1991.

[2] B. Angelsen, *Ultrasound Imaging. Waves, Signals and Signal Processing*. Trondheim, Norway: Emantec, 2000.

[3] T. L. Szabo, *Diagnostic Ultrasound Imaging*. Saint Louis, MO, USA: Elsevier Academic Press, 2004.

[4] R. Cobbold, *Foundations of biomedical ultrasound*. Oxford University Press, 2007.

[5] J. Jensen, *Estimation of Blood Velocities Using Ultrasound - A Signal Processing Approach*. New York: Cambridge University Press, 1996.

[6] D. Evans and W. McDicken, *Doppler ultrasound: physics, instrumentation and clinical applications*. Chichester: John Wiley&Sons, 2000.

[7] D. Shattuck, W. M.D., S. Smith, and O. von Ramm, "Explososcan: A parallel processing technique for high speed ultrasound imaging with linear phased arrays," *J. Acoust. Soc. Amer.*, vol. 75, no. 4, pp. 1273–1282, 1984.

[8] O. von Ramm, S. Smith, and H. Pavy, "High-speed ultrasound volumetric imaging system - part II: Parallel processing and image display," *IEEE Trans Ultrason Ferroelectr Freq Control*, vol. 38, pp. 109–115, 1991.

[9] T. Hergum, T. Bjastad, K. Kristoffersen, and H. Torp, "Parallel beamforming using synthetic transmit beams," *Ultrasonics, Ferroelectrics and Frequency Control, IEEE Transactions on*, vol. 54, pp. 271 –280, february 2007.

[10] B. Delannoy, R. Torguet, C. Bruneel, E. Bridoux, J. M. Rouvaen, and H. Lasota, "Acoustical image reconstruction in parallel processing analog electronic systems," *Journal of Applied Physics*, vol. 50, pp. 3153 –3159, may 1979.

[11] M. Tanter, J. Bercoff, L. Sandrin, and M. Fink, "Ultrafast Compound Imaging for 2D Motion Vector Estimation: Application to Transient Elastography," vol. 49, no. 10, pp. 1363–1374, 2002.

[12] J. Udesen, F. Gran, K. Hansen, J. Jensen, C. Thomsen, and M. Nielsen, "High Frame-Rate Blood Vector Velocity Imaging Using Plane Waves: Simulations and Preliminary Experiments," *Ultrasonics, Ferroelectrics and Frequency Control, IEEE Transactions on*, vol. 55, no. 8, pp. 1729–1743, 2008.

[13] K. Hansen, J. Udesen, F. Gran, J. Jensen, and M. Nielsen, "In-vivo Examples of Flow Patterns With The Fast Vector Velocity Ultrasound Method," *European Journal of Ultrasound*, vol. 30, no. 5, pp. 471–477, 2009.

[14] J. Bercoff, G. Montaldo, T. Loupas, D. Savery, F. Meandzieandre, M. Fink, and M. Tanter, "Ultrafast compound doppler imaging: providing full blood flow characterization," *Ultrasonics, Ferroelectrics and Frequency Control, IEEE Transactions on*, vol. 58, pp. 134 –147, january 2011.

[15] R. Chiao, L. Thomas, and S. Silverstein, "Sparse arry imaging with spatially-encoded trasmits," in *1997 Ultrasonics Symposium*, pp. 1679–1682, 1997.

[16] S. Nikolov and J. Jensen, "In-vivo synthetic aperture flow imaging in medical ultrasound," *Ultrasonics, Ferroelectrics and Frequency Control, IEEE Transactions on*, vol. 50, pp. 848 –856, july 2003.

[17] G. Montaldo, M. Tanter, J. Bercoff, N. Benech, and M. Fink, "Coherent plane-wave compounding for very high frame rate ultrasonography and transient elastography," *Ultrasonics, Ferroelectrics and Frequency Control, IEEE Transactions on*, vol. 56, pp. 489 –506, march 2009.

[18] D. Hokanson, D. Mozersky, D. Sumner, and D. Strandness, "Ultrasonic arteriography:a new approach to arterial visualization," *Biomed. Eng.*, vol. 6, p. 420, 1971.

[19] D. Hokanson, D. Mozersky, D. Sumner, and et al., "Ultrasonic arteriography: a noninvasive method of arterial visualization," *Radiology*, vol. 102, pp. 435–436, 1972.

[20] P. Fish, V. Kakkar, T. Corrigan, and A. Nicolaides, "Arteriography using ultrasound," *The Lancet*, vol. 299, no. 7763, pp. 1269–1270, 1972.

[21] G. Curry and D. White, "Color coded ultrasonic differential velocity arterial scanner (echoflow)," *Ultrasound in Medicine & Biology*, vol. 4, no. 1, pp. 27 – 35, 1978.

[22] A. Brandestini and F. Forster, "Blood flow imaging using a discrete -time frequency meter," in *1978 Ultrasonics Symposium*, pp. 348 – 352, 1978.

[23] M. Eyer, M. Brandestini, D. Phillips, and D. Baker, "Color digital echo/doppler image presentation," *Ultrasound in Medicine & Biology*, vol. 7, no. 1, pp. 21 – 31, 1981.

[24] A. Nowicki and J. M. Reid, "An infinite gate pulse doppler," *Ultrasound in Medicine & Biology*, vol. 7, no. 1, pp. 41 – 50, 1981.

[25] K. Namekawa, C. Kasai, M. Tsukamoto, and A. Koyano, "Realtime bloodflow imaging system utilizing auto-correlation techniques," *Ultrasound in Medicine & Biology*, vol. Suppl. 2, pp. 203–208, 1983.

[26] C. Kasai, K., A. Koyano, and R. Omoto, "Real-time two-dimensional blood flow imaging using an autocorrelation technique," *IEEE Transactions on Sonics and Ultrasonics*, vol. 32, pp. 458–464, 1985.

[27] D. H. Evans, *Advances in Ultrasound Techniques and Instrumentation*, ch. 8, pp. 151–251. New York: Churchill Livingstone, 1993.

[28] K. Kristoffersen and B. Angelsen, "A comparison between mean frequency estimators for multigated doppler systems with serial signal processing," *IEEE Trans. Biomed. Eng.*, vol. 32, pp. 645–657, 1985.

[29] B. Angelsen and K. Kristoffersen, "Discrete time estimation of the mean doppler frequency in ultrasonic blood velocity measurements," *IEEE Trans. Biomed. Eng.*, vol. 30, pp. 207–214, 1983.

[30] W. Barber, J. Eberhard, and S. Karr, "A new time domain technique for velocity measurements using doppler ultrasound," *IEEE Trans. Biomed. Eng.*, vol. 32, pp. 213–229, 1985.

[31] O. Bonnefous, P. Pesque, and X. Bernard, "A new velocity estimator for color flow mapping," in *IEEE 1986 Ultrasonics Symposium*, pp. 855 – 860, 1986.

[32] K. Kristoffersen, "Time-domain estimation of the center frequency and spread of doppler spectra in diagnostic ultrasound," *IEEE Trans. Ultrason. Ferroelectr. Freq. Contr.*, vol. 35, pp. 484–497, 1988.

[33] S. Foster, P. Embree, and J. O'Brien, W.D., "Flow velocity profile via time-domain correlation: error analysis and computer simulation," *Ultrasonics, Ferroelectrics and Frequency Control, IEEE Transactions on*, vol. 37, pp. 164 –175, may 1990.

[34] K. Miller and B. Rochwarger, "A covariance approach to spectral moment estimation," *IEEE Trans. Informat. Theor.*, 1972.

[35] G. Gray, R. Serafin, D. Atlas, R. Rineheart, and J. Boyajian, "Real-time color doppler radar display," *American Meteorological Society Bulletin*, vol. 56, pp. 580–588, 1975.

[36] D. Zrnic, "Spectral moment estimates from correlated pulsed pair," *IEEE Trans. Aerosp. Electron*, vol. 13, pp. 344–354, 1977.

[37] R. Doviak and Z. D.S., *Doppler radar and weather observations*. Academic Press Inc., 2 ed., 1993.

[38] H. Torp, K. Kristoffersen, and B. Angelsen, "Autocorrelation techniques in color flow imaging: signal model and statistical properties of the autocorrelation estimates," *IEEE Transactions on Ultrasonics Ferroelectrics and Frequency Control*, vol. 41, no. 5, pp. 604–612, 1994.

[39] A. Hoeks, J. van de Vorst, A. Dabekaussen, P. Brands, and R. Reneman, "An efficient algorithm to remove low frequency doppler signals in digital doppler systems," *Ultrasonic Imaging*, vol. 13, no. 2, pp. 135 – 144, 1991.

[40] H. Torp, "Clutter Rejection Filters in Color Flow Imaging: A theoretical approach," *IEEE Transactions on Ultrasonics Ferroelectrics and Frequency Control*, vol. 44, no. 2, pp. 417–424, 1997.

[41] S. Bjaerum, H. Torp, and K. Kristoffersen, "Clutter filter design for ultrasound color flow imaging," *Ultrasonics, Ferroelectrics and Frequency Control, IEEE Transactions on*, vol. 49, pp. 204 –216, feb. 2002.

[42] S. Bjærum, *Detection and Visualization of Moving Targets in Medical Ultrasound Imaging*. PhD thesis, NTNU, 2001.

[43] G. E. Trahey, J. W. Allison, and O. T. von Ramm, "Angle independent ultrasonic detection of blood flow," *Biomedical Engineering, IEEE Transactions on*, vol. 34, no. 12, pp. 965 –967, 1987.

[44] L. Lovstakken, *Signal processing in diagnostic ultrasound: Algorithms for real-time estimation and visualization of blood flow velocity*. PhD thesis, NTNU, 2007.

[45] L. Bohs, B. Geiman, M. Anderson, S. Gebhart, and G. Trahey, "Speckle tracking for multi-dimensional flow estimation," *Ultrasonics*, vol. 38, no. 1-8, pp. 369 – 375, 2000.

[46] M. Aderson, "Multi-dimensional velocity estimation with ultrasound using spatial quadrature," *Ultrasonics, Ferroelectrics and Frequency Control, IEEE Transactions on*, vol. 45, no. 3, pp. 852 –861, 1998.

[47] J. Jensen and P. Munk, "A new method for estimation of velocity vectors," *Ultrasonics, Ferroelectrics and Frequency Control, IEEE Transactions on*, vol. 45, pp. 837 – 851, 1998.

[48] J. Udesen and J. Jensen, "Investigation of transverse oscillation method," *Ultrasonics, Ferroelectrics and Frequency Control, IEEE Transactions on*, vol. 53, pp. 959 –971, may 2006.

[49] M. M. Pedersen, M. J. Pihl, P. Haugaard, J. M. Hansen, K. L. Hansen, M. B. Nielsen, and J. A. Jensen, "Comparison of real-time in vivo spectral and vector velocity estimation," *Ultrasound in Medicine & Biology*, vol. 38, no. 1, pp. 145 – 151, 2012.

[50]

[51] V. L. Newhouse, D. Censor, T. Vontz, J. A. Cisneros, and B. B. Goldberg, "Ultrasound doppler probing of flows transverse with respect to beam axis," *Biomedical Engineering, IEEE Transactions on*, vol. BME-34, pp. 779 –789, oct. 1987.

[52] P. Tortoli, G. Guidi, L. Mantovani, and V. L. Newhouse, "Velocity magnitude estimation with linear arrays using doppler bandwidth," *Ultrasonics*, vol. 39, no. 3, pp. 157 – 161, 2001.

[53] M. Fox, "Multiple crossed-beam ultrasound doppler velocimetry," *Sonics and Ultrasonics, IEEE Transactions on*, vol. 25, pp. 281 –286, sept. 1978.

[54] B. Dunmire, K. Beach, K.-H. Labs, M. Plett, and D. S. Jr., "Cross-beam vector doppler ultrasound for angle-independent velocity measurements," *Ultrasound in Medicine & Biology*, vol. 26, no. 8, pp. 1213 – 1235, 2000.

[55] M. Scabia, M. Calzolai, L. Capineri, L. Masotti, and A. Fort, "A real-time two-dimensional pulsed-wave doppler system," *Ultrasound in Medicine & Biology*, vol. 26, no. 1, pp. 121 – 131, 2000.

[56] A. Pastorelli, G. Torricelli, M. Scabia, E. Biagi, and L. Masotti, "A real-time 2-d vector doppler system for clinical experimentation," *IEEE Transactions on Medical Imaging*, vol. 27, no. 10, pp. 1515–1524, 2008.

[57] *Atlas of cardiovascular disease*. WHO, 2011.

[58] A. Dahl, C. Lund, and D. Russel, "Aterosklerose og hjerneinfarkt," vol. 127, no. 7, pp. 892–896, 2007.

[59] H. Hansen, *Noninvasive Vascular Ultrasound Elastography*. PhD thesis, Radboud University Nijmegen, 2012.

[60] K. Koskinas, Y. Chatzizisis, A. Baker, E. Edelman, P. Stone, and C. Feldman, "The role of low endothelial shear stress in the conversion of atherosclerotic lesions from stable to unstable plaque," *Current Opinion in Cardiology*, vol. 24, no. 6, p. 580, 2009.

[61] *Hemodynamics and mechanobiology of the endothelium*. Wold Scientific, 2010.

[62] G. Hansson, A. Robertson, and C. Søderberg-Naucler, "Inflammation and atherosclerosis," 2006.

[63] R. Ross, "Atherosclerosis — an inflammatory disease," *New England Journal of Medicine*, vol. 340, no. 2, pp. 115–126, 1999.

[64] R. Ross, "The pathogenesis of atherosclerosis: a perspective for the 1990s," *Nature*, vol. 362, pp. 801–9, Apr 29 1993.

[65] E. C. for the Asymptomatic Carotid Atherosclerosis Study, "Endarterectomy for Asymptomatic Carotid Artery Stenosis," *JAMA*, vol. 273, no. 18, pp. 1421–1427, 1995.

[66] L. S. Erdoes, J. M. Marek, J. L. Mills, S. S. Berman, T. Whitehill, G. C. Hunter, W. Feinberg, and W. Krupski, "The relative contributions of carotid duplex scanning, magnetic resonance angiography, and cerebral arteriography to clinical decisionmaking: A prospective study in patients with carotid occlusive disease," *Journal of Vascular Surgery*, vol. 23, no. 5, pp. 950 – 956, 1996.

[67] J. Golledge, M. Ellis, T. Sabharwal, T. Sikdar, A. H. Davies, and R. M. Greenhalgh, "Selection of patients for carotid endarterectomy," *Journal of Vascular Surgery*, vol. 30, no. 1, pp. 122 – 130, 1999.

[68] N. Bom and C. Lancee, "Apparatur for ultrasonically examining a hollow organ." UK Patent, 1972.

[69] C. de Korte, H. H. G. Hansen, and A. F. W. van der Steen, "Vascular ultrasound for atherosclerosis imaging," *Interface Focus*, vol. 1, no. 4, pp. 565–575, 2011.

[70] S. Nicholls, M. Borgman, S. Nissen, J. Raichlen, C. Ballantyne, P. Barter, M. Chapman, R. Erbel, and P. Libby, "Impact of statins on progression of atherosclerosis: rationale and design of SATURN (Study of Coronary Atheroma by InTravascular Ultrasound: Effect of Rosuvastatin versus AtorvastatiN)," *Current Medical Research & Opinion*, vol. 27, no. 6, pp. 1119–1129, 2011.

[71] B. Shapo, J. Crowe, R. Erkamp, S. Emelianov, M. Eberle, and M. O'Donnel, "Strain imaging of coronary arteries with intraluminal ultrasound: experiments on an inhomogenous phantom," *Ultrason. Imaging*, vol. 18, pp. 173–191, 1996.

[72] C. de Korte, E. Cespedes, A. van der Dteen, and C. Lancee, "Intravascular elasticity imaging using ultrasound:feasibility studies in phantoms," *Ultrasound Med. Biol.*, vol. 23, pp. 735–746, 1997.

[73] L. Ryan and F. Foster, "Ultrasonic measurement of differential displacement and strain in a vascular model," *Ultrason. Imaging*, vol. 19, pp. 19–38, 1997.

[74] C. de Korte, R. Lopata, H. Hansen, M. Nillesen, T. Idzenga, L. Kapusta, and J. Thijssen, "Functional cardiovascular ultrasound imaging: Quantification of plaque vulnerability and cardiac function," in *Biomedical Imaging: From Nano to Macro, 2011 IEEE International Symposium on*, pp. 1610 –1613, 30 2011-april 2 2011.

[75] J. Kips, P. Segers, and L. M. van Bortel, "Identifying the vulnerable plaque: A review of invasive and non-invasive imaging modalities," *Artery Research*, vol. 2, pp. 21–34, 2008.

[76] M. Bots, A. Hofman, and D. Grobbee, "Increased common carotid intima-media thickness. Adaptive response or a reflection of atherosclerosis? Findings from the Rotterdam study.," *Stroke*, vol. 28, no. 12, pp. 2442–2447, 1997.

[77] T. Tegos, M. Sohail, M. Sabetai, P. Robless, N. Akbar, G. Pare, G. Stansby, and A. Nicolaides, "Echomorphologic and histopathologic characteristics of unstable carotid plaques.," *Am J Neuroradiol*, vol. 21, no. 10, pp. 1937–1944, 2000.

[78] J. Wilhjelm, M. Gronholdt, B. Wiebe, S. Jespersen, L. Hansen, and H. Sillesen, "Quantitative analysis of ultrasound B-mode images of carotid atherosclerotic plaques: correlation with visual classification and histological examination," *IEEE Trans Med Imaging*, vol. 17, pp. 910–922, 1998.

[79] E. Grant, C. Benson, G. Moneta, A. Alexandrov, J. Baker, E. Bluth, B. Carroll, M. Eliaziw, J. Gocke, B. Hertzberg, S. Katanick, L. Needleman, J. Pellerito, J. Polak, K. Rholl, D. Wooster, and E. Zierler, "Carotid artery stenosis: gray-scale and Doppler US diagnosis - Society of Radiologists in Ultrasound Consensus Conference," *Radiology*, vol. 229, no. 2, pp. 340–346, 2003.

[80] M. Fillinger, R. Baker, R. Zwolak, A. Musson, J. Lenz, J. Mott, F. Bech, D. Walsh, and J. Cronenwett, "Carotid duplex criteria for a 60% or greater angiographic stenosis: variation according to equipment," *Journal of Vascular Surgery*, vol. 24, no. 5, pp. 856–864, 1996.

[81] A. Alexandrov, D. Vital, D. Brodie, P. Hamilton, and J. Grotta, "Grading Carotid Stenosis With Ultrasound. An interlaboratory comparison," *Stroke*, vol. 28, pp. 1208–1210, 1997.

[82] C. Ranke and H. Trappe, "Blood flow velocity measurements for carotid stenosis estimation: interobserver variation and interequipment variability.," *VASA*, vol. 26, pp. 210–214, 1997.

[83] G.-M. von Reutern, M.-W. Goertler, N. M. Bornstein, M. D. Sette, D. H. Evans, A. Hetzel, M. kaps, F. Perren, A. Razumovky, T. Shiogai, E. Titianova, P. Traubner, N. Venketasubramanian, L. Wong, and M. Yasaka, "Grading Carotid Stenosis Using Ultrasonic Methods," *Stroke*, vol. 43, no. 3, pp. 916–921, 2012.

[84] K. van Everdingen, J. van der Grond, and L. Kapelle, "Overestimation of a stenosis in the internal carotid artery by duplex sonography caused by an increase in volume flow," *Journal of Vascular Surgery*, vol. 27, no. 3, pp. 479–485, 1998.

[85] R. Steel, K. V. Ramnarine, F. Davidson, P. J. Fish, and P. R. Hoskins, "Angle-independent estimation of maximum velocity through stenoses using vector doppler ultrasound," *Ultrasound in Medicine & Biology*, vol. 29, no. 4, pp. 575 – 584, 2003.

Chapter 3

Spectral Doppler Estimation utilizing 2D spatial information and adaptive signal processing

Ingvild Kinn Ekroll[1], Hans Torp[1], and Lasse Løvstakken[1,2]
[1] MI Lab and Dept. Circulation and Medical Imaging, NTNU
[2] St Olavs Hospital, Trondheim, Norway

The trade-off between temporal and spectral resolution in conventional PW Doppler may limit duplex/triplex quality and the depiction of rapid flow events. It is therefore desirable to reduce the required observation window (OW) of the Doppler signal while preserving the frequency resolution. This work investigates how the required observation time can be reduced by adaptive spectral estimation utilizing 2D spatial information obtained by parallel receive beamforming. Four adaptive estimation techniques were investigated, the power spectral Capon (PSC) method, the amplitude and phase estimation (APES) technique, Multiple Signal Classification (MUSIC) and a projection based version of the Capon technique. By averaging radially and laterally, the required covariance matrix could successfully be estimated without temporal averaging. Useful PW-spectra of high resolution and contrast could be generated from ensembles corresponding to those used in color flow imaging (CFI) (OW = 10). For a given OW, the frequency resolution could be increased compared to the Welch approach, however, limited to cases where the transit time was higher or comparable to the observation time. In such cases, using short or long pulses with unfocused or focused transmit, up to 4–6 times increase in temporal resolution could be obtained in *in vivo* examples. It was further shown that by using adaptive signal processing, velocity spectra may be generated without high pass filtering the Doppler signal. With the proposed approach, spectra retrospectively calculated from CFI may become feasible for unfocused as well as focused imaging. This application may provide new clinical information by inspection of velocity spectra simultaneously from several spatial locations.

3.1 Introduction

Estimation and display of blood flow velocities are essential components of cardiovascular ultrasound diagnostics. Pulsed Wave (PW) Doppler spectra provide information about blood velocities present in a certain spatial region, and are often combined with B-mode imaging and Color Flow Imaging (CFI) which visualize the surrounding anatomy and the average flow field respectively. In both CFI and PW Doppler several ultrasound pulses are transmitted in one direction at a certain pulse repetition frequency (PRF) for each velocity estimate. However, as only the mean velocity is estimated in CFI, the required number of transmissions per line in the image is low compared to what is required when estimating the full velocity spectrum. Doppler spectra are commonly estimated using the Fourier based Welch method, which has a spectral resolution inversely proportional to the number of temporal samples in a given observation window. Unless spectral resolution is compromised, this trade-off between temporal and spectral resolution in conventional PW Doppler may limit the depiction of rapid flow events, as high spectral resolution requires a long OW. When combined with other modalities, also the B-mode and CFI image quality may be compromised. To make better use of the temporal information in the Doppler signal, we would like to reduce the number of signal samples required for the velocity estimation, thus increasing the temporal resolution in the spectrum and/or maximize the frequency resolution for a given observation window. Further, we want to investigate the use of adaptive spectral estimators in a packet based acquisition context such as conventional color flow imaging, where a very limited number of continuous slow-time samples are available. A potential application would be to (retrospectively) calculate Doppler spectra from arbitrary locations in a color flow image. If successful, the approach could ease workflow and introduce new clinical information by processing data from several spatial locations simultaneously.

Attempts to improve spectrum and mean frequency estimation of short Doppler signals are many. Vaitkus and Cobbold[1, 2] considered spectral estimation methods where an assumed model was fitted to the Doppler signal. Talhami and Kitney[3] used a Kalman filter and maximum likelihood estimation to reduce the required OW, and stressed that a time window of less than 2 ms is required to resolve detailed flow structures. Herment and Giovannelli[4] proposed an spectral estimation technique to meet this criterion based on autoregressive (AR) modeling. Eigendecomposition-based methods such as Multiple signal classification (MUSIC) and related techniques have also been investigated in the past[5, 6] showing their superiority in resolution compared to the conventional Welch approach. Still, parametric methods have the disadvantage of being more computationally demanding and needing some *a priori* knowledge about the number of velocity components present in the region of interest. As the *temporal* sampling by pulse repetition in PW Doppler ultrasound is equivalent to the *spatial* sampling by array elements in direction of arrival (DOA) estimation[7], blood velocity estimation in ultrasound and DOA estimation in radar and sonar are analogous problems. This similarity allows the mentioned parametric methods, but also nonparametric high-resolution DOA methods to be applied to PW Doppler ultrasound with relative ease. Such methods include the Capon minimum variance

(MV) estimator[8, 9] and the more recent APES approach[10]. Whereas the Welch method is data independent, these two are data dependent, or *data adaptive* signal processing techniques. The adaptive property is the origin of the improved frequency resolution and lower leakage in the resulting spectra[11].

It was recently reported that the OW in PW Doppler could be reduced using two versions of these estimators; the Blood spectral Power Capon method (BPC) and the Blood spectral Amplitude and Phase EStimation (BAPES) technique[12]. It was also shown in a clinical feasibility study that the methods could work robustly for vascular imaging[13]. Continuing the investigation into these estimators, this work investigates how the observation time may be reduced further in a way that enables retrospective PW Doppler from packet based color flow imaging. Two parametric spectral estimation techniques are also considered, namely the noise subspace-based MUSIC technique and a signal subspace, projection based version of the Capon method. All the investigated spectral estimation techniques are based on the Doppler signal covariance matrix, estimated by utilizing spatial information obtained by parallel receive beamforming[14, 15], a technique that provides a substantial gain in acquisition rate for 2D imaging. Reducing or removing the need for temporal averaging allows packet acquisition schemes with extremely short ensembles to be utilized for spectral estimation.

The paper is organized as follows: In Section II the spectral estimation methods are presented. Section III presents results from *in vivo* recordings. In Section IV a discussion of the results is given, focusing on the influence of parameters such as the transmit beam, pulse length and averaging area. Concluding remarks are given in Section V.

3.2 Methods

The use of three different nonparametric spectral estimators were investigated; the averaged periodogram (with a Hamming window), the power spectral Capon estimator (PSC) and the power spectral estimate using the more recent amplitude and phase estimation (APES) approach. Two parametric approaches were also included in the comparison, the noise subspace based MUSIC, and a signal subspace projection based version of the Capon estimator.

3.2.1 The averaged periodogram

Let the slow time signal from a voxel be represented by a one-dimensional time series $x(n) = [x(0)\ x(1)\ \cdots\ x(N-1)]^T$. The discrete Fourier transform has the form

$$\hat{\alpha}_{DFT}(\omega) = \sum_{n=0}^{N-1} x(n)e^{-i\omega n} = \mathbf{a}^H(\omega)\mathbf{x},$$

where the Fourier vector $\mathbf{a}(\omega)$ is given by $\mathbf{a}(\omega) = [1\ e^{i\omega}\ \cdots\ e^{i(N-1)\omega}]^T$ and H indicates the conjugate transpose. In the periodogram approach, $\mathbf{a}(\omega)$ is the impulse

response vector of the applied bandpassfilter, which is not purposely designed to give any desired characteristics. However, by applying a predefined window function to the data, the frequency response can be tailored to some extent. Using the weights $w(n)$ to represent the window function and averaging both in the radial (r) and lateral (b) direction, the power spectral density at frequency ω is

$$\hat{P}_{WIN}(\omega) = \frac{1}{RB}\sum_{r=0}^{R-1}\sum_{b=0}^{B-1}\left|\sum_{n=0}^{N-1} w(n)x_{r,b}(n)e^{-i\omega n}\right|^2. \tag{3.1}$$

Using a rectangular window this is equivalent to

$$\hat{P}_{BOX}(\omega) = \mathbf{a}^H(\omega)\hat{\mathbf{R}}_{\mathbf{x}}\mathbf{a}(\omega), \tag{3.2}$$

where $\hat{\mathbf{R}}_{\mathbf{x}}$ is the sample covariance matrix

$$\hat{\mathbf{R}}_{\mathbf{x}} = \frac{1}{RB}\sum_{r=0}^{R-1}\sum_{b=0}^{B-1}\mathbf{x}_{r,b}\mathbf{x}_{r,b}^H. \tag{3.3}$$

Temporal averaging can be included by subdividing the signal in temporal segments before averaging both in time and space. Then, a convenient arrangement of the signal is in the form of a Hankel matrix for each (r,b) pair. Given N consecutive samples of $x(n)$, the M x L Hankel matrix for the (r,b) pair of interest is given by

$$\mathbf{Y}_{r,b} = [\mathbf{y}_{r,b}(0)\ \mathbf{y}_{r,b}(1)\ \cdots\ \mathbf{y}_{r,b}(L-1)], \tag{3.4}$$

where $L = N - M + 1$, and

$$\mathbf{y}_{r,b}(i) = [x_{r,b}(i)\ x_{r,b}(i+1)\ \cdots\ x_{r,b}(i+M-1)]^T.$$

The columns of $\mathbf{Y}_{r,b}$, $\mathbf{y}_{r,b}(i)$, are often referred to as *snapshots*. An estimate of the covariance matrix $\mathbf{R}_{\mathbf{x}}$ is thus found by averaging estimates from several sample volumes and several snapshots. Inserting this estimate into (3.2) gives a PSD estimate where spectral resolution has been traded for improved statistical robustness.

3.2.2 The Capon power spectral estimate

The Capon spectral estimator can be viewed as a matched-filterbank spectral estimator[16] where the spectrum is estimated by passing the signal through a narrowband filter with varying center frequency. The estimator can be derived by considering the design of an FIR filter with coefficients $h(k), 0 \leq k \leq M$ to be determined. If the observed data $x(n)$ is passed through the filter, the variance (and power) of the zero mean output sequence is

$$\sigma_y^2 = E[\mathbf{h}^H\mathbf{x}^*(n)\mathbf{x}^T(n)\mathbf{h}] = \mathbf{h}^H\mathbf{R}_{\mathbf{x}}\mathbf{h}. \tag{3.5}$$

By minimizing (3.5) under the constraint that at frequency ω the frequency response of the filter is normalized to unity, $\mathbf{h}^H(\omega)\mathbf{a}(\omega) = 1$, an optimized filter coefficient vector is found, [17]

$$\mathbf{h}(\omega) = \frac{\mathbf{R}_{\mathbf{x}}^{-1}\mathbf{a}(\omega)}{\mathbf{a}^H(\omega)\mathbf{R}_{\mathbf{x}}^{-1}\mathbf{a}(\omega)}. \tag{3.6}$$

The expression can be substituted into (3.5), giving the power spectral capon (PSC) estimate at the frequency ω

$$\hat{P}_{PSC}(\omega) = \frac{1}{\mathbf{a}^H(\omega)\hat{\mathbf{R}}_{\mathbf{x}}^{-1}\mathbf{a}(\omega)}, \tag{3.7}$$

where $\hat{\mathbf{R}}_{\mathbf{x}}$ is given by (3.3).

3.2.3 The APES power spectral estimate

Whereas in the PSC method the filter coefficients were chosen to minimize the *energy* of the filtered signal, the design of the APES method can be interpreted as filtering the slow time signal in a way such that the filtered signal resembles a sinusoid as closely as possible in a least squares sense. It has been shown[16] that APES outperforms the Capon estimator at true spectral peak locations. By solving the optimization problem

$$\min_{\mathbf{h}(\omega)} \left(\mathbf{h}^H(\omega)\mathbf{Q}(\omega)\mathbf{h}(\omega)\right), \tag{3.8}$$

under the same constraint as for the Capon method, noise and interference from other frequencies are minimized for each frequency of interest [12]. $\mathbf{Q}$ has been referred to as the *noise and interference covariance matrix*[16] and is the signal covariance matrix where the contribution from the frequency of interest is subtracted. An estimate of $\mathbf{Q}$ is given by

$$\hat{\mathbf{Q}} = \hat{\mathbf{R}}_{\mathbf{x}} - \sum_{r=0}^{R-1}\sum_{b=0}^{B-1} \mathbf{g}_{r,b}(\omega)\mathbf{g}_{r,b}^H(\omega),$$

where

$$\mathbf{g}(\omega) \equiv \frac{1}{L}\sum_{l=0}^{L-1} \mathbf{y}(l)e^{-i\omega l} = \frac{1}{L}\mathbf{Y}\mathbf{a}_L^*(\omega)$$

for the slow time signal from one (r,b) sample volume. $\mathbf{Y}$ is defined in (3.4) with $M = N/2$.

The optimal solution for the filter coefficients is

$$\hat{\mathbf{h}}(\omega) = \frac{\hat{\mathbf{Q}}^{-1}(\omega)\mathbf{a}_M(\omega)}{\mathbf{a}_M^H(\omega)\hat{\mathbf{Q}}^{-1}(\omega)\mathbf{a}_M(\omega)},$$

which can be used to form the final PSD estimate

$$\hat{P}_{APES}(\omega) = \frac{1}{RB}\sum_{r=0}^{R-1}\sum_{b=0}^{B-1} |\mathbf{h}^H(\omega)\mathbf{g}_{r,b}(\omega)|^2 \tag{3.9}$$

3.2.4 MUSIC and projection based Capon

An $N \times N$ covariance matrix can be decomposed into two parts residing in the noise and signal subspace using its eigenvectors[17], assuming that we are dealing with p complex exponentials in white noise. This eigendecompostion forms the basis for signal and noise subspace estimation techniques. Using the eigenvectors of the covariance matrix, $\mathbf{v}_i, i = 1, 2, ..., N$ and the corresponding eigenvalues λ_i we get

$$\mathbf{R}_x = \sum_{i=1}^{N} \lambda_i \mathbf{v}_i \mathbf{v}_i^H = \sum_{i=1}^{p} \lambda_i \mathbf{v}_i \mathbf{v}_i^H + \sum_{i=p+1}^{N} \lambda_i \mathbf{v}_i \mathbf{v}_i^H, \tag{3.10}$$

where it is assumed at the eigenvalues have been arranged in decreasing order, $\lambda_1 \geq \lambda_2 \geq ... \geq \lambda_N$. A spectral estimate based on the *noise* subspace eigenvectors

$$P(\omega) = \sum_{i=p+1}^{N} |\mathbf{a}(\omega)\mathbf{v}_i|^2, \tag{3.11}$$

will be zero at $\omega = \omega_i, i = 1, 2, ..., p$, where the signal vector is normal to the noise subspace. Thus, the estimator

$$P_{MUSIC}(\omega) = \frac{1}{\sum_{i=p+1}^{N} |\mathbf{a}(\omega)\mathbf{v}_i|^2} \tag{3.12}$$

will have peaks at these spectral locations. However, the resulting pseudospectrum does not reflect a true power estimate. Spectrograms based on the MUSIC estimators are therefore not based on estimates of the power spectral density, but rather serve as indicators of sinusoidal presence at certain frequencies.

In the projection based Capon technique, it is the *signal* subspace eigenvectors of the covariance matrix that are utilized to increase the performance of the Capon technique. Here, the optimized filter vector (3.6) is projected into the signal subspace utilizing the largest eigenvectors of the covariance matrix before the signal power is estimated using (3.5)[18]. The signal space projection of the optimized filter vector can be expressed as

$$\mathbf{h}_p(\omega) = \frac{\mathbf{V}_p \mathbf{V}_p^H \mathbf{R}_\mathbf{x}^{-1} \mathbf{a}(\omega)}{\mathbf{a}^H(\omega) \mathbf{R}_\mathbf{x}^{-1} \mathbf{a}(\omega)}, \tag{3.13}$$

where $\mathbf{V}_p$ is a $N \times p$ matrix containing the p largest eigenvectors of the $N \times N$ covariance matrix. Selection of the number of signal components is here based on a cross-spectral metric, as described in[19]. The cross-spectral metric for the ith eigenvalue indicates the amount of energy projected along the ith eigenvector of the covariance matrix. An inclusion criteria is formed by comparing the sum of the cross spectral metrics formed by the j largest eigenvalues to a factor times the total energy. The estimation procedure must be repeated for every line in the spectrogram, as the blood signal characteristics varies throughout the cardiac cycle.

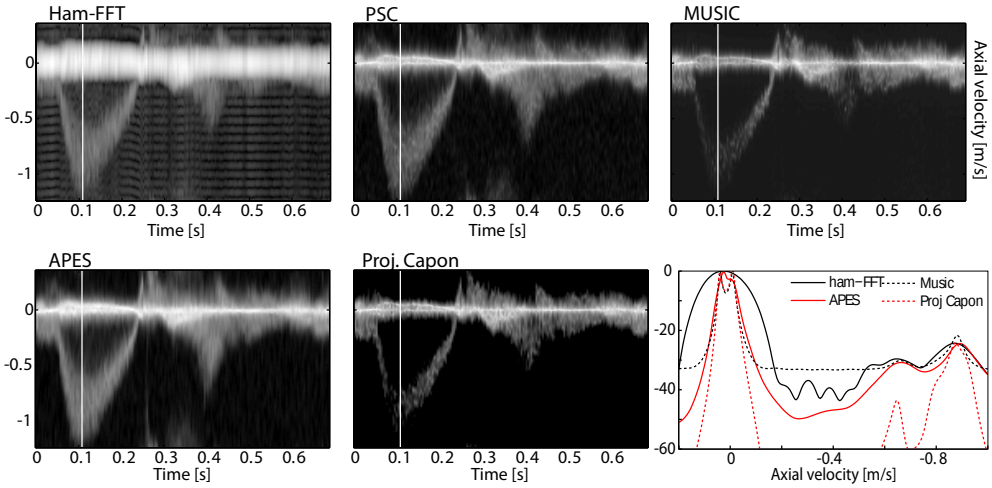

Figure 3.1: Periodograms from an OW of 20 without clutter rejection. The spectral resolution is highest when using the MUSIC, PSC or projected based Capon technique. MUSIC provides poorer contrast as compared to all the other techniques, while the projection based Capon technique displays high contrast in most frames. Comparison to ham-FFT with OW=60 in Fig. 3.2. Dynamic range 60 dB.

3.2.5 Estimation of the sample covariance matrix

All the adaptive spectral Doppler estimators require an estimate of the slow time sample covariance matrix. The estimate is normally formed by subdividing the Doppler signal in smaller temporal segments and averaging the covariance matrix estimates in time. For a given ensemble length, the spectral resolution will decrease as the length of the temporal segments decreases. If the data acquisition is continuous the segment lengths could still be adequately large, however in a packet acquisition scheme where the number of available slow time samples is limited, temporal averaging is not desirable. Thus, in this work, the covariance matrix is estimated using the Doppler signal only from a certain 2D region of interest. A small averaging area is desired as the flow pattern may be highly invariant in space. It must, however, be sufficiently large to provide a robust spectral estimate. The robustness of the spectral estimate can, however, be increased by diagonal loading of the covariance matrix before (3.6) is evaluated. This is a common approach in beamforming applications, where the technique is used to constrain the suppression level outside of the focal point, allowing reflections appearing slightly out of focus to pass through the beamformer[20]. In diagonal loading a small term is added to the diagonal of the covariance matrix prior to inversion, resulting in the modified covariance matrix $\hat{\mathbf{R}}_{\mathbf{x}}^{\delta} = \hat{\mathbf{R}}_{\mathbf{x}} + \delta\mathbf{I}$, where $\mathbf{I}$ is the identity matrix. As the loading parameter δ increases, the PSC estimator will approach the unweighted periodogram estimate, easily confirmed by allowing $\hat{\mathbf{R}}_{\mathbf{x}}^{\delta}$ to approach $\delta\mathbf{I}$ in (3.6) before evaluating the expression in (3.5).

Table 3.1: Acquisition setup

Parameter	Carotid	Cardiac 1	Cardiac 2
Probe	11L	M5S	M5S
f_0 [MHz]	6	2.5	2.5
nrCycles (nCyc)	2.5	2.5	12
SV, (nCyc*c/2*$f_{0)}$ [mm]	0.3	1	3.7
fs [MHz](baseband)	3.2	2.1	0.8
PRF [kHz]	5	5	5
F# receive	1.4	4	4

3.2.6 Data acquisition

In-phase and quadrature (IQ) data was acquired *in vivo* using a GE Vingmed Vivid E9 ultrasound system (GE Vingmed Ultrasound, Horten, Norway), and further processed off-line. A parallel receive beam setup was used to acquire PW Doppler data including both radial and lateral samples. In this work we used 16 parallel receive beams (PRB) for each transmit event, spreading the receive beams around the transmit axis according to about half the Rayleigh criterion (densely sampled). To generate a sufficiently broad transmit beam to cover a large number of PRBs, unfocused or defocused beams may be required, compromising sensitivity. In this work both focused and unfocused pulses were used to investigate sensitivity issues and the influence of transmit-receive beam misalignments caused by use of parallel receive beamforming. Two different pulse lengths (sample volumes) were compared, one longer (12 cycles @ 2.5 MHz) similar to conventional PW Doppler, and one shorter (2.5 cycles @ 2.5 MHz), more similar to what might be used in a wide-band CFI setup. Further specifications can be found in Table 3.1. To minimize artifacts due to PRB acquisition, only the minimal number of lateral samples required was used in the estimators. The number depends on the pulse length and estimator used, but turned out to be no more than about 8 for the setups and estimators investigated.

3.3 Results

3.3.1 Feasibility

Fig. 3.1 shows PW Doppler spectra of aortic flow from a healthy volunteer generated by the all estimators (OW = 20). Focused transmit beams and a small sample volume (2.5 cycles @ 2.5 MHz) was used. A spatial ROI of 4×3 mm was selected for estimation of the covariance matrix. As expected, the spectra generated by the Ham-FFT method suffer from the influence of clutter sidelobes in addition to a broad region around zero velocity being concealed due to signal from near stationary tissue. The adaptive methods, on the other hand, do not suffer from clutter sidelobes, and have

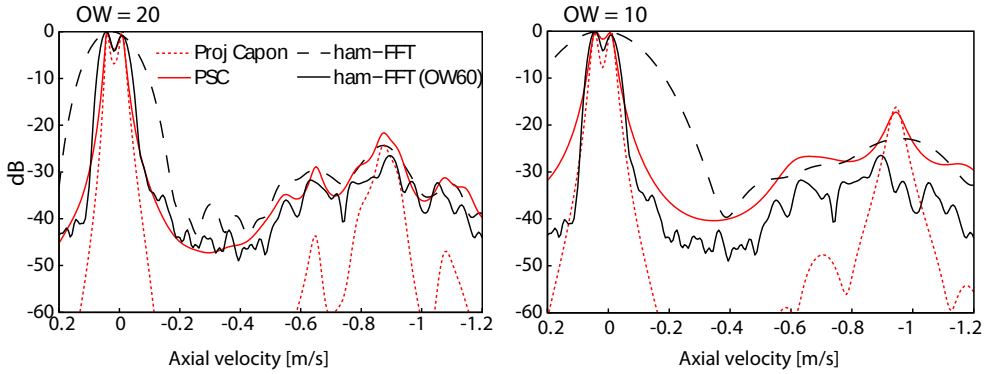

Figure 3.2: Comparison of line spectra using OW = 60 for the ham-FFT technique and reduced to 20 and 10 for the PSC and projection based Capon technique. (Frame indicated in Fig. 3.1 and 3.4.)

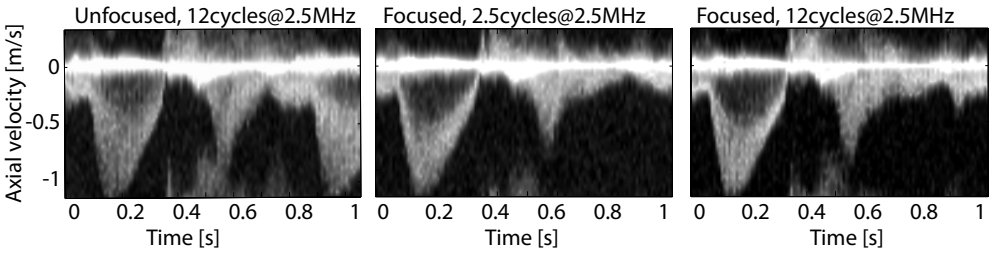

Figure 3.3: Spectrograms generated by the PSC estimator using 20 temporal samples in each frame. Unfocused transmit results in a wider spectrum, while a large sample volume results in a slightly narrower spectrum than that from a small sample volume. Dynamic range 40 dB.

also a more well defined velocity range for the clutter signal. Single frame spectra, as seen in the lower right panel of Fig. 3.1 and in the left panel of Fig. 3.2, further illustrates the improved resolution of the adaptive methods, an improvement which increased with shorter ensemble length. The separation of the near stationary and stationary clutter signal was used to compare the resolution, as this narrow-band signal component will give an upper bound for the improvement when using the adaptive estimation techniques. Fig. 3.2 shows that the resolution obtained by using 60 samples in the Welch method was comparable to that obtained by using 10 samples with the projection based Capon technique. 10 samples of the Doppler signal in an application with PRF = 5 kHz corresponds to a temporal resolution of 2 ms. As conventional spectra in cardiac imaging are based on at least 40–60 temporal samples, the temporal resolution in PW Doppler can be increased up to 4–6 times. As seen in Fig. 3.3, it was observed that focused transmit gave higher spectral quality (narrower

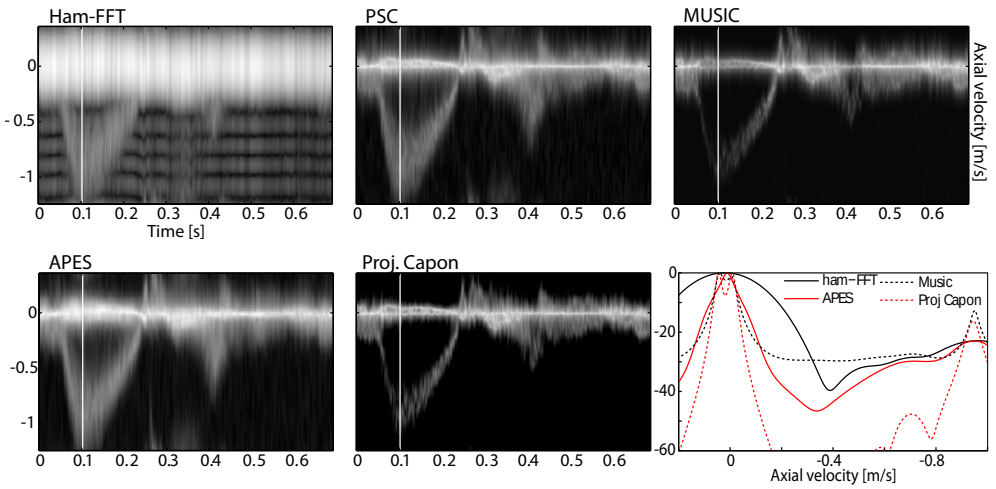

Figure 3.4: Periodograms from an OW of 10 without clutter rejection. The spectral resolution is best when using the MUSIC, PSC or projected based Capon technique which are all able to separate the stationary and slowly moving clutter components. Comparison to ham-FFT of OW=60 can be seen in Fig.3.2 Dynamic range 60 dB.

spectra and increased SNR) than unfocused transmit. A large sample volume was expected to provide the spectra of highest resolution, but in our recordings there was no clear degradation in the spectra when the smallest sample volume was used. The use of MUSIC gave a similar velocity resolution as Capon and APES, but may not be as suitable for spectrogram display due to its pseudospectral "nature" giving poorer contrast. The projection based Capon technique was on the other hand very well suited for the purpose, and also gave a substantial increase in contrast compared to the other techniques, while preserving the high resolution of the Capon spectra. Note that no clutter filters were applied before spectral estimation, and the number of estimated signal components in this frame was 6 for the parametric techniques.

The adaptive estimators were able to provide useful periodograms also for extremely short ensembles. A comparison of spectra generated by all estimation techniques (OW = 10) is given in the right panel of Fig. 3.2 and the lower right panel of Fig. 3.4. While APES is not able to separate the stationary and near stationary clutter signal, PSC, MUSIC and the projection based Capon method are all able to do so. The overall best impression is provided by the projection based Capon technique, based on both spectral resolution and contrast. In this case, four eigenvectors were estimated to span the signal subspace.

The improvement in spectral quality obtained by using the adaptive methods decreased with increasing blood velocity, as seen in Fig. 3.5, where two single frame spectra are shown. Both are nonparametric spectral estimates from the same recording (small SV, focused transmit), but at different points in time, where the blood velocity was centered around the Nyquist velocity (v_{nyq}) and $0.2 * v_{nyq}$ respectively. At v_{nyq}

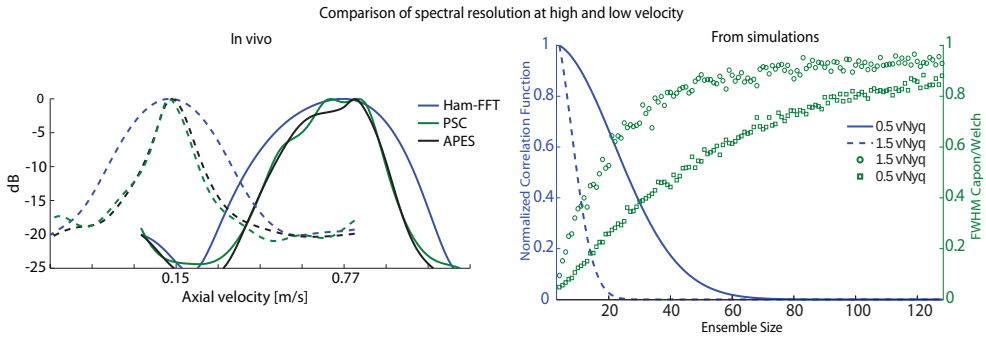

Figure 3.5: The left figure show two single frames from high (solid lines) and low (dashed lines) velocity ranges in the spectrograms of Fig. 3.4, where OW = 10. The improvement by using the adaptive methods is clearly best in the low velocity range, but present also at high velocities. The right figure shows a comparison of spectral width (FWHM) as a function of ensemble size using the PSC and Welch method on data from simulations of a complex stationary Gaussian process with two different correlation lengths, corresponding to high and low blood velocities.

the ratio of the -6 dB spectral width of the adaptive methods to that of the Ham-FFT method was approximately 0.7. At $0.2 * v_{nyq}$, the ratio was approximately 0.4. The effect was further demonstrated in simulations, assuming a gaussian correlation function in the radial and lateral direction[21], also depicted in Fig. 3.5. This figure shows in blue two correlation functions corresponding to a high ($1.5 * v_{nyq}$) and low ($0.5 * v_{nyq}$) velocity, as a function of ensemble size (for a given PRF). The velocity was then estimated using both the Welch and the PSC method. The relative FWHM of the two velocity estimates (average of 50 simulations) is plotted in green for the two situations. Similar to the *in vivo* observation, the gain from adaptive (PSC) processing was larger in the low velocity case. As the correlation approaches zero, the ratio of the spectral widths approaches 1.

3.3.2 Retrospective PW Doppler

As seen in Fig. 3.6, a CFI setup with unfocused transmit, 16 PRB and an ensemble size comparable to that of conventional color flow imaging could be used to generate PW Doppler spectra retrospectively from any region in the imaged area. In the given example, only 10 temporal samples were used to construct each line in the spectrogram. The spatial ROI was approximately 1×2 mm. As the ensemble size in conventional CFI range from 8–16, only a marginal compromise of the acquisition rate in CFI may be needed to retrospectively generate useful velocity spectra in arbitrary points in the image.

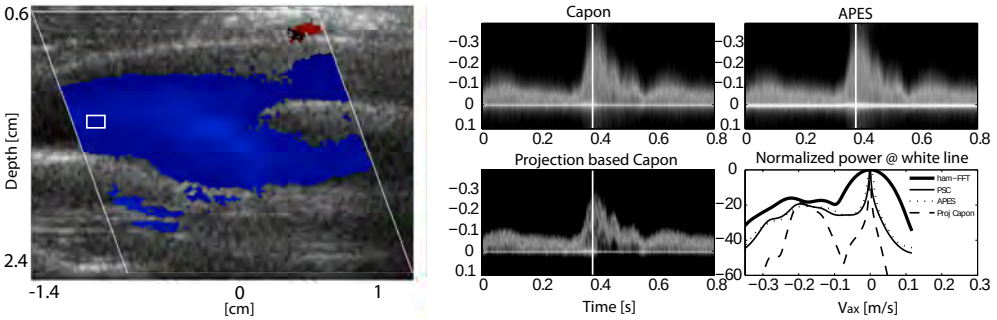

Figure 3.6: Retrospective PW Doppler using 10 temporal samples from a plane wave CFI recording of the carotid bifurcation of a healthy volunteer. No clutter filter was applied before calculation of the power spectra. Dynamic range 60 dB.

3.3.3 Averaging area

By introducing diagonal loading, situations where the PSC estimate would normally break down could be avoided, although at the cost of some decrease in spectral resolution (compared to a similar PSC spectrum estimated from a sufficiently large area). In Fig. 3.7, the rank 20 covariance matrix was estimated from a small area corresponding to only 5 equivalent independent samples[22], as estimated by using a simplified gaussian model of the correlation functions of the Doppler signal in the lateral and radial direction[21]. The PSC method without diagonal loading is unable to produce a velocity spectrum, whereas the PSC estimate with diagonal loading has a better spectral resolution than the corresponding periodogram estimate, especially for low velocities. The clutter sidelobes are also less apparent.

As seen in Fig. 3.8, some broadening of the spectrum might be induced if the transmit beam is focused and parallel receive beamforming is used. The figure shows the resulting (single frame) power spectra from two edge beams (1,16) and a middle beam (8) from a recording using focused transmit and 16 PRBs (2.5 cycles @ 2.5 MHz). As the spectrum from the left beam is biased slightly downwards in frequency, whereas the right beam is biased slightly upwards, there would be an increased spectral broadening if all beams were used in velocity spectrum estimation. The effect was, however, negligible if only a limited number of neighboring PRBs close to the transmit axis were used. As ensembles as short as 10 samples could be used to produce high resolution and high contrast spectra, the averaging region needed in estimation of the covariance matrix was small enough to avoid any spectral broadening from misaligned receive beams.

3.4 Discussion

In this work we have investigated how the required observation window in adaptive spectral Doppler estimation can be substantially reduced by utilizing 2D spatial

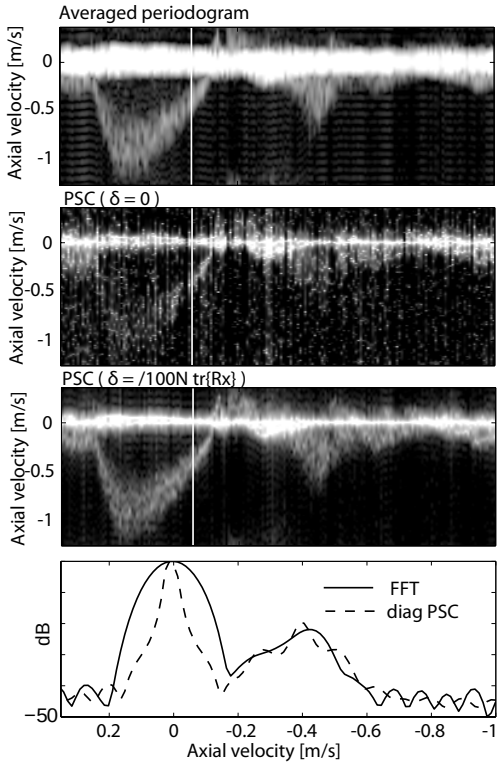

Figure 3.7: By applying diagonal loading to the estimate of the covariance matrix, the PSC method becomes more robust. Choosing δ carefully, the technique will provide a spectral estimate superior to the averaged periodogram from an averaging area that does not support the PSC method with no diagonal loading. Dynamic range 40 dB.

information obtained from parallel receive beamforming. Spectral estimators compared to the periodogram approach include the Capon method and the APES technique, due to previous works showing their robustness in general[11] and in the setting of spectral Doppler ultrasound[5, 12, 13]. Additionally, two parametric approaches were included, both based on eigendecomposition of the signal covariance matrix. These are parametric in the sense that the number of signal components needs to be estimated before spectral locations are found, adding some computational complexity to the spectral estimation. Whereas MUSIC has been considered for use in spectral Doppler estimation previously, the projection based Capon technique has not. The fundamental properties of the estimators have been thoroughly analyzed earlier[16, 23, 24], therefore this work has focus on *in vivo* examples. Other spectral estimation techniques, such as AR related approaches, have been investigated for use in spectral Doppler estimation in the past [1, 6, 7, 25–27], but were not included in the present study.

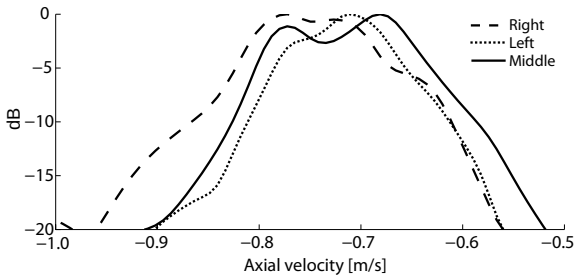

Figure 3.8: Single frame APES velocity estimates from the edge and middle beams, using focused transmit and parallel receive beamforming. The estimate from the left edge beam (#1) is biased slightly downwards, from the right edge beam (#16) it is biased slightly upwards.

Gran *et al.*[12] and Hansen *et al.*[13] have previously investigated the use of the PSC and APES estimators in PW Doppler ultrasound. Short OWs were used with good results, but temporal averaging was utilized ($M + L - 1 \geq 32$) both in the case of the Capon and APES estimator. The resulting ensembles were larger than what is provided by conventional color flow imaging. In this work, similar results as[12, 13] are shown, while using a total ensemble length shorter than 20 samples. At such small ensembles, the PSC method displayed a higher resolution than the APES method with equal averaging area. This follows from the estimator formulation; the APES estimator utilizes some temporal averaging corresponding to $M = N/2$ in the estimation of the noise and covariance matrix, while the full data window, $M = N$ was utilized for spectral estimation in the Capon formulation. The possibility of formulating the Capon spectral estimate with no temporal averaging provides an advantage in packet acquisition schemes such as CFI, where typically only 8–16 samples are available for processing. On the other hand it makes the estimator less robust than the APES formulation in respect to averaging area. It has also been shown that the Capon power estimate tends to be biased down[10, 16] as compared to the APES power estimate. The latter limitation may be more important in beamforming applications (such as[28]) than in blood velocity estimation though, where the importance is not Doppler frequency *power*, but frequency *content* (peak velocity/mean velocity), resolution and contrast. The computational burden of the APES estimator is also substantially larger than for the Capon estimator. Consequently, in a packet acquisition setting, we find the PSC estimator to be the preferred choice of the two nonparametric adaptive estimation techniques.

The parametric approaches, the signal subspace projection based Capon and the noise subspace based MUSIC, were able to provide spectrograms of a resolution only matched by the PSC technique. The contrast found in the spectral estimates of the projection based Capon technique was unmatched by any other estimator. The main disadvantage of the parametric approaches is that the dimension of the signal and noise subspace must be estimated for every new time instant in the periodogram, as the

blood signal is varying throughout the cardiac cycle, leading to higher computational load. The noise subspace based methods, here represented by MUSIC, has the additional disadvantage that only the *pseudospectrum* is estimated. Although the true power can be calculated after the p frequency locations are found, the spectrogram is formed using the pseudospectrum, which in our case provided poor contrast.

In this work the dimensions of the signal subspace were estimated using a cross spectral metric[19], however, other techniques might be more efficient or more robust. If the estimation of signal components is incorrect, the spectra can be obscured by spurious peaks (too many components) or contain only the clutter signal (too few components), a challenge which here manifests itself most clearly in the time of highest flow acceleration (highest bandwidth). This represents the more severe drawback by using the projection based Capon technique over the PSC approach, and one should beware that while noise is effectively blocked, the same could be the case for the signal if the eigenvector inclusion criterion is too strict. The investigation of an optimal component estimation is beyond the scope of this work, but might be worth looking into as the projection based Capon technique indeed showed very promising results. If the PW Doppler estimation is retrospective, one could have a variable, user set threshold value both for the eigenvector inclusion criterion and for diagonal loading, providing a robust and flexible spectral Doppler estimation technique for short ensembles.

3.4.1 Impact of some physical parameters

The quality of the spectrograms will depend on the properties of the signal to be processed. Some of the more important physical parameters and their influence on the final spectrogram are discussed here.

Tissue clutter signal

Tissue clutter signal is present in the Doppler signal due to beam sidelobes and reverberations from tissue structures. In conventional CFI and PW Doppler, the tissue clutter signal is removed by high-pass filtering the received Doppler signal. This is normally an important step before velocity estimation; in CFI to avoid a velocity bias, and in spectrum estimation to avoid clutter sidelobes obscuring the velocity spectrum. Frequency distortions can be introduced in the spectrum if clutter rejection is performed by anything else than a time-invariant filter, such as a FIR-filter[29], which will reduce the available number of samples to $N - K$, where K is the FIR filter order. The need to acquire a higher number of samples than what is utilized in the velocity estimation constrains the acquisition rate in an application such as retrospective PW Doppler. However, it was found that due to the superior resolution and interference rejection of the adaptive methods, the clutter signal did not obscure the velocity spectrum to any extent. This is a major advantage compared to the conventional periodogram approach. Thus, in a combined CFI and PW Doppler acquisition, spectrograms can be formed using all of the acquired slow time samples, whereas a clutter filter could be used to avoid velocity bias in the corresponding color

flow image, where fewer temporal samples are needed.

Averaging area

As the PSC estimate was formulated without any temporal averaging, it was less robust than the APES estimate in terms of averaging area size. Diagonal loading proved to be useful in increasing the robustness of the PSC estimate in cases where the averaging area was too small to support the temporal ensemble. This came, however, at the cost of decreased spectral resolution (gradually approaching that of the Welch method) when compared to a PSC estimate generated from a sufficiently large averaging area. For a suitable value of diagonal loading, here 1% of the estimated signal power, robust spectra with little interference from clutter sidelobes could be obtained.

Transmit beam

The Doppler shift is estimated along the vector sum of the transmit and receive beam directions. As described in[30], the curved wavefronts of a focused transmit beam will cause a changing angle with the blood flow depending on the position of the receive beam relative to the transmit axis. We therefore expected to observe a broadening of the Doppler spectrum as the velocity bias is positive on one side of the transmit beam axis and negative on the other, demonstrated in Fig. 3.8 from *in vivo* recordings of aortic flow. However, the improved SNR obtained by applying focused transmit beams is desired, especially in cardiac imaging, where the imaging depths are large and where transducer geometry and setup limits the ability to generate plane waves at relevant imaging depths. We found that when using a limited number of parallel receive beams $(5-7)$ resolution and contrast was improved as compared to spectra generated from recordings with unfocused transmit beams.

Transit time

There is a fundamental limitation in spectral resolution at short transit times, observed as an increase in spectral width at high velocities (Fig. 3.5). The signal correlation length from a certain sample volume will decrease as the blood velocity increases, limiting the number of slow time samples that contribute constructively to the velocity estimation. The shorter effective observation window at high velocities as compared to the lower velocities also influence the performance of the adaptive methods, resulting in broader spectra. As demonstrated both *in vivo* and by simulations (Fig. 3.5) the gain in spectral resolution and adaptive processing will decrease with decreasing transit time - the spectral resolution of the adaptive methods approaching that of the Welch method at high velocities.

3.4.2 Retrospective PW Doppler

Ensembles only marginally longer (OW = 10) than those found in conventional color flow imaging could be used to generate velocity spectra of high resolution and contrast. By utilizing the high acquisition rate offered by parallel receive beamforming,

simultaneous velocity spectra may then become available for comparison at arbitrary points in the region. Such a retrospective PW Doppler application would allow more careful inspection of the flow pattern in the image, ease examinations, and provide more accurate quantitative measurements. An interesting candidate application is coronary imaging, where color flow imaging is used to locate the blood vessels of interest and PW Doppler is used for quantitative measurements. The coronary arteries tend, however, to disappear from the imaging area following only small movements, which makes it hard to do the required PW Doppler measurements. An application where only the location of the vessels by CFI is needed and quantitative measurements can be extracted retrospectively could therefore be of interest. Due to the imaging depth, cardiac flow imaging might in general provide the situations where short ensemble processing remains most important. Though use of unfocused transmit beams is a very promising technique for providing both CFI and PW-Doppler simultaneously[31] - it is limited to situations where plane wave imaging gives adequate sensitivity, which is not necessarily the case for cardiac imaging depths.

3.5 Conclusion

Spatial information obtained by parallel receive beamforming was used to reduce or remove the requirement for temporal averaging in four adaptive estimation techniques; the power spectral Capon (PSC) method and the amplitude and phase estimation (APES) technique, the MUSIC technique and the projection based Capon method. The approach was tested in both vascular and cardiac imaging situations, using both focused and unfocused transmit beams. For a given observation window, the frequency resolution could be increased compared to the periodogram approach, however, limited to cases where the transit time was higher or comparable to the observation time. For narrow-band spectra, it was found that an observation window of 10 slow time samples could provide comparable spectral resolution as a window of 60 samples using the conventional approach. For these very short ensembles, the PSC and the projection based Capon technique gave the spectra of highest resolution. The latter method also provides a substantial gain in contrast, but has the drawback of depending on robust estimation of the signal subspace dimension. The investigated adaptive techniques enabled spectral estimation without high pass filtering of the Doppler signal, keeping the full ensemble available for velocity estimation. The advantages of using adaptive signal processing techniques in conjunction with spatial averaging may enable retrospective PW Doppler to be a feasible application for CFI in general.

Acknowledgment

The authors would like to thank Thomas Skaug (MD) for providing us with excellent *in vivo* ultrasound recordings and Saeed Mehdizadeh for fruitful discussions on adaptive signal processing techniques.

References

[1] P. Vaitkus and R. Cobbold, "A comparative study and assessment of Doppler ultrasound spectral estimation techniques. Part I: Estimation methods.," *Ultrasound in medicine & biology*, vol. 14, no. 8, pp. 661–672, 1988.

[2] P. Vaitkus, R. Cobbold, and K. Johnston, "A comparative study and assessment of Doppler ultrasound spectral estimation techniques. Part II: Methods and results.," *Ultrasound in medicine & biology*, vol. 14, no. 8, pp. 673–688, 1988.

[3] H. Talhami and R. Kitney, "Maximum likelihood frequency tracking of the audio pulsed doppler ultrasound signal using a Kalman filter," *Ultrasound in Med. Biol.*, vol. 14, no. 7, pp. 599–609, 1988.

[4] A. Herment and J. Giovanelli, "An adaptive approach to computing the spectrum and mean frequency of doppler signals," *Ultrasonic Imaging*, vol. 17, pp. 1–26, 1995.

[5] M. Allam and J. Greenleaf, "Isomorphism Between Pulsed-Wave Doppler Ultrasound and Direction-of-Arrival Estimation-Part II: Experimental Results," *IEEE Transactions on Ultrasonics, Ferroelectrics and Frequency Control*, vol. 43, pp. 923–935, 1996.

[6] E. D. Übeyli and I. Güler, "Comparison of eigenvector methods with classical and model-based methods in analysis of internal carotid arterial doppler signals," *Computers in Biology and Medicine*, vol. 33, no. 6, pp. 473 – 493, 2003.

[7] M. Allam and J. Greenleaf, "Isomorphism Between Pulsed-Wave Doppler Ultrasound and Direction-of-Arrival Estimation-Part I: Basic Principles," *IEEE Transactions on Ultrasonics, Ferroelectrics and Frequency Control*, vol. 43, pp. 911–922, 1996.

[8] J. Capon, "High resolution frequency-wavenumber spectrum analysis," *Proc. IEEE*, vol. 57, no. 8, pp. 1408–1418, 1969.

[9] R. Lacoss, "Data adaptive spectral analysis methods," *Geophysics*, vol. 36, p. 661, 1971.

[10] J. Li and P. Stoica, "An adaptive filtering approach to spectral estimation and SAR imaging," *IEEE Transactions on Signal Processing*, vol. 44, no. 6, pp. 1469–1484, 1996.

[11] P. Stoica and R. Moses, *Spectral Analysis of Signals*. Upper Saddle River, NJ: Prentice Hall, 2005.

[12] F. Gran, A. Jakobsson, and J. Jensen, "Adaptive spectral doppler estimation.," *IEEE transactions on ultrasonics, ferroelectrics, and frequency control*, vol. 56, no. 4, p. 700, 2009.

[13] K. Hansen, F. Gran, M. Pedersen, I. Holfort, J. Jensen, and M. Nielsen, "In-vivo validation of fast spectral velocity estimation techniques," *Ultrasonics*, 2009.

[14] D. Shattuck, W. M.D., S. Smith, and O. von Ramm, "Explososcan: A parallel processing technique for high speed ultrasound imaging with linear phased arrays," *J. Acoust. Soc. Amer.*, vol. 75, no. 4, pp. 1273–1282, 1984.

[15] O. von Ramm, S. Smith, and H. Pavy, "High-speed ultrasound volumetric imaging system - part II: Parallel processing and image display," *IEEE Trans Ultrason Ferroelectr Freq Control*, vol. 38, pp. 109–115, 1991.

[16] P. Stoica, A. Jakobsson, and J. Li, "Matched-filter bank interpretation of some spectral estimators," *Signal Processing*, vol. 66, no. 1, pp. 45–59, 1998.

[17] J. G. Proakis and D. G. Manolakis, *Digital signal processing. Principles, Algorithms and Applications*. Prentice Hall, fourth ed., 2007.

[18] D. Feldman and L. Griffiths, "A projection approach for robust adaptive beamforming," *IEEE Transactions on Signal Processing*, vol. 42, no. 4, pp. 867–876, 1994.

[19] J. Goldstein and S. Reed, "Reduced-Rank Adaptive Filtering," *IEEE Transactions on Signal Processing*, vol. 45, no. 2, pp. 492–496, 1997.

[20] J.-F. Synnevåg, A. Austeng, and S. Holm, "Adaptive Beamforming Applied to Medical Ultrasound Imaging," *IEEE Transactions on Ultrasonics Ferroelectrics and Frequency Control*, vol. 54, no. 8, pp. 1606–1613, 2007.

[21] H. Torp, K. Kristoffersen, and B. Angelsen, "Autocorrelation techniques in color flow imaging: signal model and statistical properties of the autocorrelation estimates," *IEEE Transactions on Ultrasonics Ferroelectrics and Frequency Control*, vol. 41, no. 5, pp. 604–612, 1994.

[22] A. Papoulis and S. Pillai, *Probability, random variables and stochastic processes*. McGraw-Hill, third ed.

[23] A. Jakobsson and P. Stoica, "Combining Capon and APES for estimation of spectral lines," *Circuits, Systems, and Signal Processing*, vol. 19, no. 2, pp. 159–169, 2000.

[24] D. Feldman, "An analysis of the projection method for robust adaptive beamforming," *IEEE Transactions on Antennas and Propagation*, vol. 44, no. 7, pp. 1023–1030, 1997.

[25] F. Schlindweind and D. Evans, "Selection of the order of autoregressive models for spectral analysis of Doppler ultrasound signals," *Ultrasound in Medicine & Biology*, vol. 16, no. 1, pp. 81 – 91, 1989.

[26] A. Fort, C. Manfredi, and S. Rocchi, "Adaptive SVD-based AR model order determination for time-frequency analysis of Doppler ultrasound signals," *Ultrasound in Medicine & Biology*, vol. 21, no. 6, pp. 793 –805, 1995.

[27] F. Forsberg, "On the usefulness of singular value decomposition - ARMA models in Doppler ultrasound," *Ultrasonics, Ferroelectrics and Frequency Control, IEEE Transactions on*, vol. 38, no. 5, pp. 416 –426, 1991.

[28] J.-F. Synnevåg, A. Austeng, and S. Holm, "Benefits of Minimum-Variance Beamforming in Medical Ultrasound Imaging," *IEEE Transactions on Ultrasonics Ferroelectrics and Frequency Control*, vol. 56, no. 9, pp. 1868–1879, 2009.

[29] H. Torp, "Clutter Rejection Filters in Color Flow Imaging: A theoretical approach," *IEEE Transactions on Ultrasonics Ferroelectrics and Frequency Control*, vol. 44, no. 2, pp. 417–424, 1997.

[30] T. Hergum, B. T.G., L. Løvstakken, K. Kristoffersen, and H. Torp, "Reducing Color Flow Artifacts Caused by Parallel Beamforming," *IEEE Trans Ultrason Ferroelectr Freq Control*, vol. 57, pp. 830–838, 2010.

[31] J. Bercoff, G. Montaldo, T. Loupas, D. Savery, F. Meandzieandre, M. Fink, and M. Tanter, "Ultrafast compound doppler imaging: providing full blood flow characterization," *Ultrasonics, Ferroelectrics and Frequency Control, IEEE Transactions on*, vol. 58, pp. 134 –147, january 2011.

Chapter 4

2D Tracking Doppler: A New Method to Limit Spectral Broadening in Pulsed Wave Doppler

Tonje Fredriksen[1], Ingvild Kinn Ekroll[1], Lasse Løvstakken[1], and Hans Torp[1]
[1] MI Lab and Dept. Circulation and Medical Imaging, NTNU

Transit time broadening is a major limitation in Pulsed Wave (PW) Doppler, especially when the angle between the flow direction and the ultrasound beam is large. The associated loss in frequency resolution may give severe overestimation of blood velocities, and finer details in the spectral display are lost. By using plane wave transmissions and parallel receive beamforming, multiple PW Doppler signals can be acquired simultaneously in a 2D region. This enables tracking of the moving blood scatterers over a longer spatial distance to avoid transit time broadening.
In this work, the new method was tested using *in vitro* ultrasound recordings from a flow phantom, and *in vivo* recordings from a human carotid artery. The resulting 2D Tracking Doppler spectra showed significantly reduced spectral broadening compared to Doppler spectra generated by the Welch method. The reduction in spectral broadening was four-fold when the velocity was 0.82 m/s and the beam-to-flow angle was 62°. A signal model was derived and the expected Doppler power spectra were calculated, showing good agreement with experimental data. Improved spectral resolution was shown for beam-to-flow angles between 40° and 82°.

4.1 Introduction

Pulsed Wave (PW) Doppler is an important tool in cardiovascular diagnostics, where the complete spectrum of blood or tissue velocities is estimated. It is typically displayed as a two dimensional (2D) sonogram with velocity along the y-axis and time along the x-axis. Fundamentally, the spectrum of velocities presented will broaden due

to the so-called transit time effect. Even though a uniform velocity field is present, a spectrum of velocities will be estimated and displayed. The transit time is the effective observation time of the blood scatterers in the received signal. The scatterers pass through the insonified area during a short time interval, and as the velocity increases, the transit time decreases, resulting in more severe spectral broadening for high velocities. This limitation makes it more challenging to delineate the true maximum velocities, decreasing diagnostic confidence and making quantitative analysis more challenging and less reproducible. In the context of blood velocity measurement, delineation is particular challenging when high velocity jets are present, for instance in stenotic regions. The transit time is usually limited by the pulse length. However, if the beam-to-flow angle is large, the transit time will be given by the beam width. This is illustrated in Fig. 4.1, where PW Doppler spectra from two situations are shown. The beam-to-flow angle is small and large in the left and right image panel respectively.

Attempts to improve spectrum and mean frequency estimation of Doppler signals are many, but most techniques base the spectral estimation on samples originating from one spatial position. Recent approaches to increase the spectral resolution in PW Doppler include non-parametric methods earlier used in direction-of-arrival estimation, such as the Capon minimum variance estimator[1] and the APES approach[2]. Whereas the commonly used Welch technique is data independent, these two are data dependent, or data adaptive, signal processing techniques. The adaptive property is the source of the improved frequency resolution and lower leakage in the resulting spectra[3]. It was recently reported that the observation window in PW Doppler could be reduced using two versions of these estimators; the blood spectral power Capon method (BPC) and the blood spectral amplitude and phase estimation (BAPES) technique[4]. It was also shown in a clinical feasibility study that the methods could work robustly for vascular imaging[5]. However, the transit time presents a fundamental limitation to the gain in spectral resolution when using these techniques[6]. To obtain improved delineation both in low and high velocity regions, ways to increase the observation time should be investigated.

A method for generating velocity spectra with reduced spectral broadening, called "Velocity Matched Spectrum", has previously been published[7]. By tracking the scatterers along the direction of the flow, the transit time was increased, giving a better velocity resolution in the spectrum. A similar method is the "butterfly search" technique[8], developed by Alam and Parker. In this method the complex demodulated signal is sampled on different delay trajectories (butterfly lines) in the slow-time–fast-time space. If the delay trajectory matches the scatterer movement, all the data samples will have similar values and their variance will be low. To estimate the velocity, the butterfly lines on which the variance is minimum is searched for. Both of these methods are limited to track along the direction of the beam, and have shown improved performance only for small beam-to-flow angles.

We have now extended the "Velocity Matched Spectrum" method to allow for tracking in a 2D space. An enabling technology for 2D tracking is parallel receive beamforming, a technique now implemented in most high-end ultrasound imaging systems. This technology allows for the instantaneous acquisition of multiple image

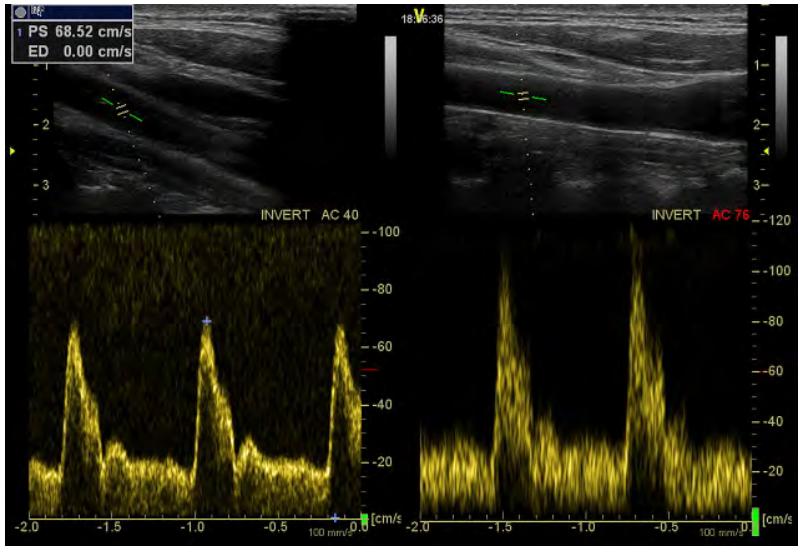

Figure 4.1: Two screenshots from a high end ultrasound scanner, Vivid E9 (GE Vingmed Ultrasound, Norway). B-mode images of a carotid artery are shown at the top. PW Doppler spectra are shown at the bottom. The beam-to-flow angle was 40° for the recording to the left, and 76° for the recording to the right. The spectral broadening is prominent in the recording with the largest beam-to-flow angle.

lines in 2D, without affecting the desired pulse repetition frequency (PRF), by using plane wave transmissions. Using this scheme we can acquire data that makes it possible to follow blood or tissue scatterers in 2D space over time. While conventional PW Doppler algorithms sample the scatterer movement over time from a fixed position, the proposed algorithm sample at varying positions in space, resulting in an increased observation time and decreased spectral broadening.

A related approach has been described by J. Jensen *et al.*[9], where directional beamforming was done for multiple angles in order to find the direction of flow, and a cross-correlation technique was used to estimate the flow velocity. The method is based on synthetic aperture where defocused emissions are used, and it therefore suffers from low signal-to-noise ratio (SNR). Further, the approach only includes estimation of the mean velocity and does not include spectral velocity estimation as in 2D Tracking Doppler.

In this work, plane wave transmissions and parallel receive beams are used to track the blood scatterers from pulse to pulse and to construct a Doppler spectrum display with reduced spectral broadening. The method is tested both *in vitro* and *in vivo*. The 2D Tracking Doppler algorithm is described in Section 4.2.1. The signal model presented in Section 4.2.2 is used for simulating the expected velocity spectra. In Section 4.3 the experimental work is described. The results are presented in Section 4.4 and discussed in Section 4.5.

4.2 Methods

The following terminology is used throughout this and subsequent sections: The *fast time* has time steps given by the sampling rate in the range direction, and is indexed with t. The *slow-time* has time steps given by the pulse repetition time (PRT) and is indexed with k. *M-mode* refers to a plane spanned by a line in space and the slow-time. x and z are spatial coordinates in azimuth and axial (range) direction respectively.

The new method is based on the properties of the 2D Fast Fourier Transform (FFT). Flow estimation based on the 2DFFT has been discussed by many authors[10–12]. Velocity spectra can be generated by taking the 2DFFT of the signal, in the fast- and slow-time directions, and integrating along lines of differing slope that pass through the origin[10]. The slope of each line corresponds to one particular velocity and is given by the relation between the Doppler frequency, f_D, and the transmitted frequency, f_z:

$$f_D = \frac{2 f_z v_z}{c} \ ,$$

where v_z is the velocity component of the scatterers in the axial direction and c is the speed of sound. If the flow contains one single velocity, the spectral content of the signal will extend along a line with angle $\phi = \arctan^{-1}(\frac{c}{2v_z})$, as illustrated in Fig. 4.2(a).

It has previously been shown[7] that integration along lines of differing slope in the 2DFFT is equivalent to summation along lines of differing slope in the fast-time – slow-time domain. Signal from scatterers with constant velocity that moves along the ultrasonic beam will make skewed lines in the fast-time – slow-time domain. When the integration is done along such a line, a peak in the velocity spectrum is observed. Shortened transit time and broadening of the spectrum will occur when the flow is not in the direction of the beam. By following the movement of the scatterers between parallel beams instead of just along one ultrasonic beam, the method is suited for situations with any beam-to-flow angle. In the Fourier domain this is equivalent to summation along lines in the $f_\theta f_D$ domain, where f_θ is the frequency axis in the direction of the flow.

In Fig. 4.3, tracking of the scatterers using a single ultrasonic beam is compared to tracking of the scatterers using several parallel beams (multi beam approach) when the beam-to-flow angle is 62°. Using the multi beam approach, the signal can be extracted from a line that follows the direction of the flow. The signal forms lines in the multi beam M-mode image that are much thinner and extend further than in the single beam M-mode image, making it better suited for tracking. The multi beam 2DFFT image shows a signal that is concentrated along a skewed line. In the single beam approach the shortened transit time makes the signal more dispersed. Also, signal from low velocity scatterers near the walls contributes to low Doppler frequencies in the single beam 2DFFT image.

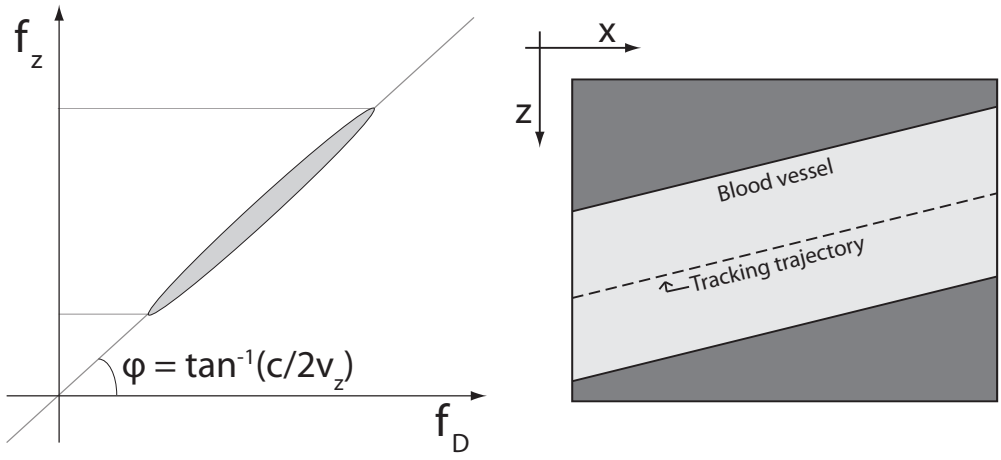

(a) (b)

Figure 4.2: (a): Velocity spectra can be generated by integrating along skewed lines in the 2DFFT of the signal. If only one velocity is present, the spectral content will extend along a line with angle ϕ. (b): Sketch of the imaging plane. The tracking trajectory was chosen to follow the direction of the blood flow in the middle of the vessel.

4.2.1 The Algorithm

The 2D Tracking Doppler spectra can be calculated from the complex pre-envelope signal, $u(x, z, k)$, or from the complex demodulated (IQ) signal, $u_{IQ}(x, z, k)$. The signal samples are extracted, using 2D spline interpolation, along a user defined straight line following the direction of the flow, as shown in Fig. 4.2(b). The data is further processed using a previously published method, "Velocity Matched Spectrum"[7], to obtain a velocity spectrum.

The signal is processed in two steps:

1. Generating the M-mode matrix:

   Data samples are selected along a straight line in space for all k. For a specific beam-to-flow angle, θ, the signal can be written as

   $$u_\theta(r, k) = u(r \sin\theta, r \cos\theta, k) \ ,$$
   $$u_{IQ,\theta}(r, k) = u_{IQ}(r \sin\theta, r \cos\theta, k) \ ,$$

   where r is the distance along the straight line.

2. Generating the velocity spectrum $\hat{p}(v)$:

   Summation is done along straight lines in the M-mode matrix. The slope of each line corresponds to a particular velocity, and the sum along the line contributes

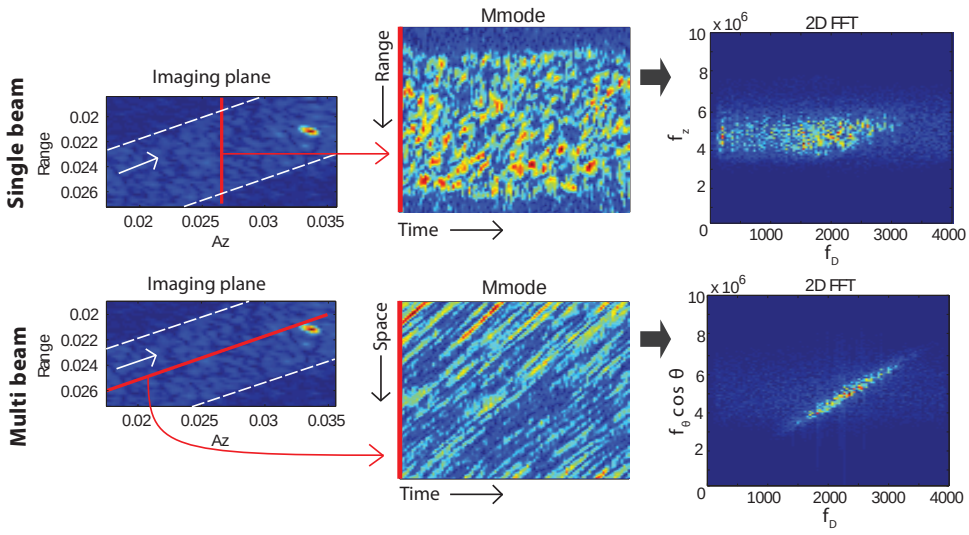

Figure 4.3: Tracking of the scatterers using a single ultrasonic beam is compared to tracking of the scatterers using several parallel beams. The beam-to-flow angle is 62°. The images to the left show the imaging plane. The flow is in the direction of the white arrow. The red line illustrates the tracking trajectory. In the images in the middle the signal is displayed in a plane spanned by the red line and the slow-time (M-mode image). The signal lines in the multi beam M-mode image are much thinner and extend further than in the single beam M-mode image. In the images to the right the complex pre-envelope signal is displayed in the 2D Fourier domain. They show a signal that is more concentrated along a skewed line in the multi beam approach compared to the single beam approach.

to the power in one velocity cell in the velocity power spectrum. Since u_{IQ} is complex demodulated, a phase correction factor must be included to account for the axial motion. A sliding-window approach is applied in the slow-time direction using a smooth window to reduce sidelobes.

$$\begin{aligned}\hat{p}(v) &= \left|\sum_k w(k) u_\theta(r_0 + kvT, k_0 + k)\right|^2 \\ &= \left|\sum_k w(k) u_{IQ,\theta}(r_0 + kvT, k_0 + k) e^{i\omega_d k \Delta t}\right|^2 ,\end{aligned}$$

$$\Delta t = \frac{2vT\cos\theta}{c} ,$$

where w is the window function with length N and defined for $k \in [-N/2, N/2]$, v is a velocity, r_0 and k_0 are the center positions in range and time, ω_d is the angular demodulation frequency and T is the pulse repetition time.

The corresponding expression for a conventional velocity spectrum is given by

$$\begin{aligned}\hat{p}_{conv}(v) &= \left|\sum_k w(k)u_\theta(r_0, k_0+k)e^{i\omega_0 k\Delta t}\right|^2 \\ &= \left|\sum_k w(k)u_{IQ,\theta}(r_0, k_0+k)e^{i\omega_0 k\Delta t}\right|^2 ,\end{aligned}$$

where ω_0 is the received center frequency.

4.2.2 Signal Model

The method was investigated by simulating the expected Doppler power spectra using an extended version of the signal model presented in[13] and[7]. The following derivations will add thermal noise, clutter filtering and tracking of the scatterers between parallel beams to the model. When deriving the expressions for the expected Doppler power spectra it is convenient to use the complex pre-envelope of the received signal, but the same calculations apply to the IQ signal.

The constructed complex pre-envelope signal, $s(x, z, k)$, is sampled along a line with angle θ, with respect to the z-axis. This can be described as a multiplication of the signal with a delta function:

$$s_\theta(r, k) = s(x, z, k) \cdot \delta(z - x\tan\theta) ,$$

where r is a continuous variable. The signal can be characterized by its autocorrelation function, defined as

$$R_{s_\theta}(\rho, m) \equiv \langle s_\theta(r, k)^* s_\theta(r+\rho, k+m)\rangle ,$$

where $*$ denotes the complex conjugate and $\langle\rangle$ is the expectation value operator. By including a noise term, $n(r, k)$, the thermal noise in the signal is accounted for, giving a combined signal

$$s_n(r, k) = s_\theta(r, k) + n(r, k) .$$

and its autocorrelation function

$$R_{s_n}(\rho, m) = R_{s_\theta}(\rho, m) + N_0\delta(\rho)\delta(m) , \tag{4.1}$$

where N_0 is the noise power.

Clutter filtering is done in slow-time, with a high pass filter with impulse response $h(k)$. Bandpass filtering is done with a filter $b(r)$ to match the bandwidth of the sampled signal. The filtered signal and its autocorrelation function is given by

$$\begin{aligned}s_f(r, k) &= s_n(r, k) \otimes_r b(r) \otimes_k h(k) , \\ R_{s_f}(\rho, m) &= R_{s_n}(\rho, m) \otimes_\rho b_2(\rho) \otimes_m h_2(m) ,\end{aligned} \tag{4.2}$$

where $\otimes$ means convolution and the subscript $_2$ indicates short notation for the autocorrelator operator. Inserting (4.1) into (4.2) and utilizing that $s_\theta(r,k)$ and $b(r)$ has the same bandwidth we get

$$\begin{aligned} R_{s_f}(\rho,m) &= R_{s_\theta}(\rho,m) \otimes_\rho b_2(\rho) \otimes_m h_2(m) \\ &\quad + N_0 b_2(\rho) \otimes_\rho \delta(\rho) \cdot h_2(m) \otimes_m \delta(m) \\ &= R_{s_\theta}(\rho,m) \otimes_m h_2(m) + N_0 b_2(\rho) \cdot h_2(m) \ . \end{aligned} \tag{4.3}$$

The velocity spectrum is then given by

$$\begin{aligned} \hat{p}(v) &= \left| \sum_k w(k) s_f(r_0 + kvT, k_0 + k) \right|^2 \\ &= \sum_{k_1,k_2} w^*(k_1) w(k_2) \\ &\quad \cdot s_f^*(r_0 + k_1 vT, k_0 + k_1) s_f(r_0 + k_2 vT, k_0 + k_2) \ , \end{aligned}$$

and its expectation value is

$$\begin{aligned} \langle \hat{p}(v) \rangle &= \sum_{k_1,k_2} w^*(k_1) w(k_2) \\ &\quad \cdot \langle s_f^*(r_0 + k_1 vT, k_0 + k_1) s_f(r_0 + k_2 vT, k_0 + k_2) \rangle \\ &= \sum_k w_2(k) R_{s_f}(kvT, k) \ , \end{aligned} \tag{4.4}$$

where $k = k_2 - k_1$. Inserting (4.3) into (4.4) we get

$$\begin{aligned} \langle \hat{p}(v) \rangle &= \sum_k w_2(k) (R_{s_\theta}(kvT, k) \otimes_k h_2(k) \\ &\quad + N_0 b_2(kvT) h_2(k)) \\ &= \sum_{k,n} w_2(k) R_{s_\theta}(kvT, k-n) h_2(n) \\ &\quad + \sum_k w_2(k) N_0 b_2(kvT) h_2(k) \ . \end{aligned} \tag{4.5}$$

If the blood field is stationary and has a uniform velocity v_0 in the direction θ, the autocorrelation function can be written in terms of the pulse-echo response, g(r):

$$R_{s_\theta}(\rho, m; v_0) = g_2(\rho - m v_0 T) \ . \tag{4.6}$$

Inserting (4.6) into (4.5) we obtain the expected power spectrum for the 2D Tracking Doppler method:

$$\begin{aligned}\langle \hat{p}(v \mid v_0) \rangle &= \sum_{k,n} w_2(k) g_2(kvT - (k-n)v_0T) h_2(n) \\ &+ \sum_{k} w_2(k) N_0 b_2(kvT) h_2(k) \ . \end{aligned} \tag{4.7}$$

Using the same signal model, but only considering samples originating from a fixed position in space, we can calculate the expected power spectrum for the conventional PW Doppler method:

$$\begin{aligned}\langle \hat{p}_{conv}(v) \rangle &= \sum_{k} w_2(k) R_{s_f}(0,k) e^{-i\omega_0 k\Delta t} \\ &= \sum_{k,n} w_2(k) R_{s_\theta}(0,k-n) h_2(n) e^{-i\omega_0 k\Delta t} \\ &+ \sum_{k} w_2(k) N_0 b_2(0) h_2(k) e^{-i\omega_0 k\Delta t} \ , \end{aligned} \tag{4.8}$$

where ω_0 is the received center frequency. Inserting (4.6) into (4.8) we get

$$\begin{aligned}\langle \hat{p}_{conv}(v \mid v_0) \rangle &= \sum_{k,n} w_2(k) g_2(-(k-n)v_0T) h_2(n) e^{-i\omega_0 k\Delta t} \\ &+ \sum_{k} w_2(k) N_0 b_2(0) h_2(k) e^{-i\omega_0 k\Delta t} \ . \end{aligned} \tag{4.9}$$

The final expressions of the expected Doppler power spectra include the autocorrelation of the pulse-echo response, g_2. In order to calculate g_2 the spectral density function, $G(f_x, f_z)$, of the received signal needs to be modeled. This can be done using the principles of the Fraunhofer approximation, which states that the lateral variation of the ultrasound field at the focal depth can be approximated as the Fourier transform of the product of the aperture and apodization functions [14]. The Fourier transform of this ultrasound field is thus a scaled version of the aperture and the apodization function. In fast time, the frequencies are centered on $2f_0/c$, where f_0 is the center frequency of the received signal[15].

The sampling of the signal along a line with angle θ is described above by a multiplication of the signal with a delta function, $\delta(z - x\tan\theta)$. In the spatial Fourier domain this corresponds to a convolution of the spectral density function with another delta function:

$$G_\theta(f_\theta) = G(f_x, f_z) \otimes \delta(f_z - f_x \tan(\theta + 90°)) \big|_{(f_\theta \sin\theta, f_\theta \cos\theta)} \ ,$$

where G_θ is the spectral density function along the axis f_θ which has an angle θ with respect to the f_z axis. As illustrated in Fig. 4.4, the convolution can be described as

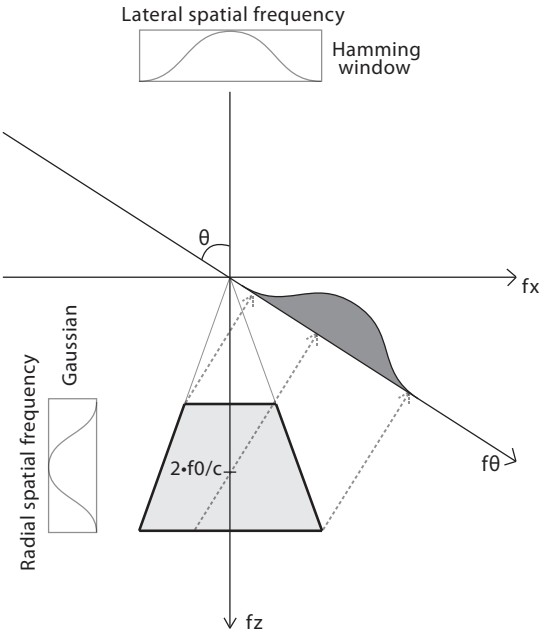

Figure 4.4: Sketch of the signal in the Fourier domain. Sampling the signal along a straight line in space is the same as projecting the signal to a line with the same angle in the Fourier domain. The beam-to-flow angle is θ, the radial distribution of frequencies is assumed to be Gaussian and the lateral distribution is given by the apodization function, which is a Hamming window.

a projection of the spectral content of the signal to a line with angle θ which extend through the origin. $\mathbf{G}_\theta$ can be found numerically by summing the spectral contribution from each radial frequency:

$$\mathbf{G}_\theta = \sum_{f_z} w_a \left(\frac{\mathbf{f}_\theta - f_z \cos\theta}{0.5\, B_x(f_z) \sin\theta} \right) G_z(f_z) \ ,$$

where w_a is the apodization function, B_x is the bandwidth and G_z is the spectral density function along the f_z axis.

The Wiener-Khinchin theorem states that the power spectral density of a wide-sense-stationary random process is the Fourier transform of the corresponding autocorrelation function[16]. $\mathbf{g_2}$ can hence be found by taking the inverse Fourier transform of $\mathbf{G}_\theta$.

$$\mathbf{g_2} = \mathcal{F}^{-1}(\mathbf{G}_\theta) \ .$$

4.3 Experiments

The 2D Tracking Doppler method was tested both *in vitro* and *in vivo*, and compared with a conventional PW Doppler method. Recordings were done using a SonixMDP ultrasound scanner with a 5 MHz linear probe and a SonixDAQ for channel data acquisition (Ultrasonix, Richmond, BC, Canada). The acquisition consisted of continuous plane wave transmissions with a PRF of 4 kHz. The RF channel data was IQ-demodulated and low-pass filtered to reduce the noise bandwidth, and beamformed using a Hamming window over the active receive aperture. The acquisition setup and the post processing parameters are listed in Table 4.1.

Table 4.1: Parameters

Acquisition Setup		Post Processing Parameters	
Parameter	Value	Parameter	Value
Tx center frequency	5 MHz	Tracking length	1.5 cm
Pulse periods	2.5	Window	Hamming
PRF	4 kHz	Window length	32 samples
F-number	1.4	HP-filter	FIR, order 50
		HP-filter cutoff	32 Hz

The conventional PW Doppler spectrum was generated from a range of approximately 2 mm in the middle of the vessel or tube, using the Welch technique. The slow-time window length was 32 samples for both methods. At the highest velocities, the tracking length was approximately 1.5 cm for the 2D Tracking Doppler method. Further, the 2D Tracking Doppler spectra were averaged in the direction of the flow. The SNR was high both *in vitro* and *in vivo*. White noise was therefore added in the post processing of the data to mimic a more realistic clinical situation with moderate SNR. The same amount of noise was added both in the conventional method and the 2D Tracking Doppler method.

4.3.1 In Vitro Recordings

In vitro flow studies give a controlled situation of the flow and are easily repeatable. Therefore, to investigate the performance of the new method, recordings were done using a flow phantom representing a carotid artery. A sketch of the experimental setup is shown in Fig. 4.5. The flow phantom consisted of a tube with an inner diameter of 6 mm that was coupled to a flow loop. A pulsatile flow was achieved using the PhysioPulse 100 Flow System (Shelley medical image technologies). The phantom was filled with a blood mimicking fluid that has been tested and described by Ramnarine *et. al.*[17]. The fluid exhibited characteristics very similar to those of blood, but produced stronger backscattered echoes. Two scan angles were applied giving beam-to-flow angles of 62° and 82°.

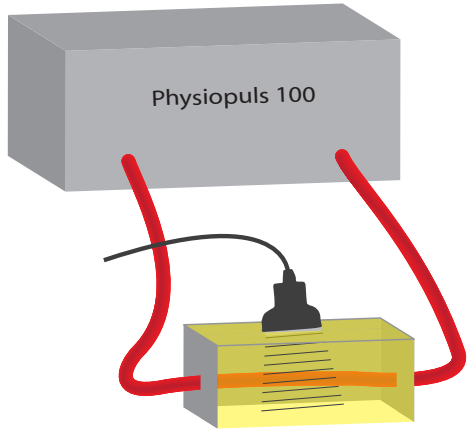

Figure 4.5: The experimental setup. The flow phantom consisted of a tube with an inner diameter of 6 mm that was coupled to a flow loop. A pulsatile flow was achieved using the PhysioPulse 100 Flow System. The phantom was filled with a blood mimicking fluid.

4.3.2 In Vivo Recordings

The method was tested on an *in vivo* recording of a carotid artery in a healthy volunteer. The region of interest (ROI) was placed in the common carotid artery, where the blood flow angle was unidirectional. The beam to flow angle was 70°.

4.4 Results

The expected 2D Tracking Doppler power spectra and the expected conventional PW Doppler power spectra were simulated, using equation (4.7) and (4.9), with a constant velocity of 0.82 m/s and beam-to-flow angles of 62° and 82°. The results are shown in Fig. 4.6. They show a noise floor that is approximately 7 dB lower for the 2D Tracking Doppler spectrum compared to the conventional PW Doppler spectrum. The simulations with a beam-to-flow angle of 62° show a main lobe resolution at -3 dB of approximately 0.1 m/s for the 2D Tracking Doppler spectrum and 0.4 m/s for the conventional PW Doppler spectrum. The simulations with a beam-to-flow angle of 82° show a main lobe resolution at -3 dB of approximately 0.2 m/s for the 2D Tracking Doppler spectrum and 1.2 m/s for the conventional PW Doppler spectrum.

In Fig. 4.7 the main lobe resolution at -3 dB is plotted with respect to the beam-to-flow angle. The results show improved velocity resolution for beam-to-flow angles between 40° and 82°.

Fig. 4.8 shows conventional PW Doppler spectra and 2D Tracking Doppler spectra generated from *in vitro* ultrasound recordings of pulsatile flow in a straight tube. In the upper panel spectra the beam-to-flow angle was 62°. For this beam-to-flow angle

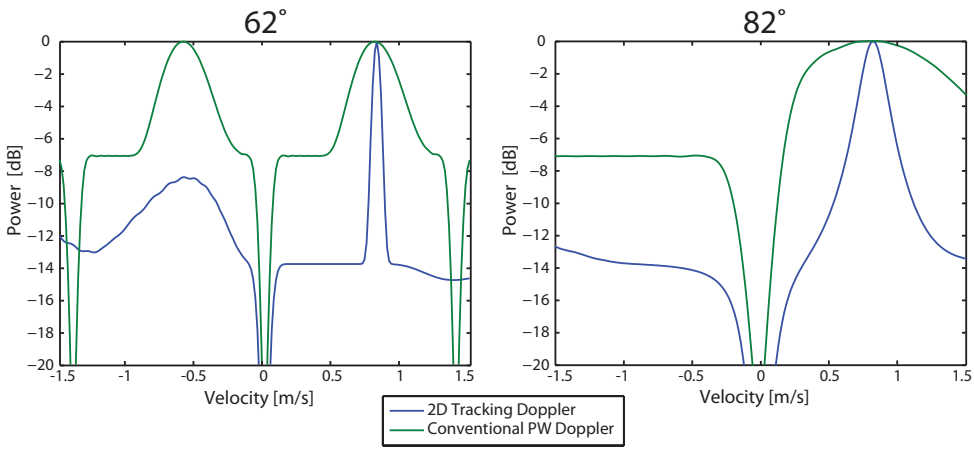

Figure 4.6: Simulations of the expected Doppler power spectra. The expected conventional Doppler power spectra are shown in green and the expected 2D Tracking Doppler power spectra are shown in blue. The spectra in the left and right panel were simulated with a beam-to-flow angle of 62° and 82° respectively. The simulations were done using a constant velocity of 0.82 m/s. The signal model includes white noise and clutter filtering.

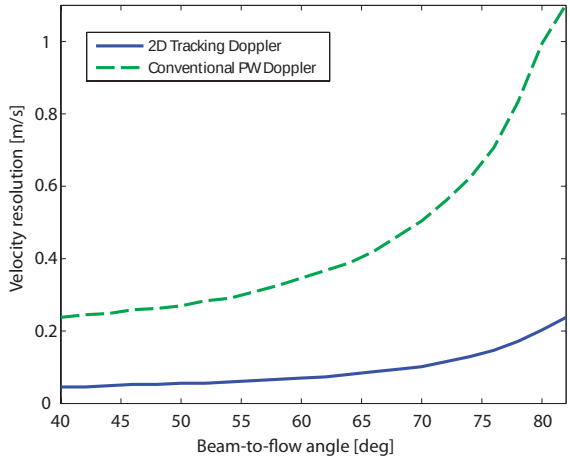

Figure 4.7: The velocity resolution of the simulated Doppler power spectra at -3 dB for beam-to-flow angles between 40° and 82°. The expected velocity resolution for the conventional Doppler power spectra is shown in green and the expected velocity resolution for the 2D Tracking Doppler power spectra is shown in blue. The simulations were done using a constant velocity of 0.82 m/s.

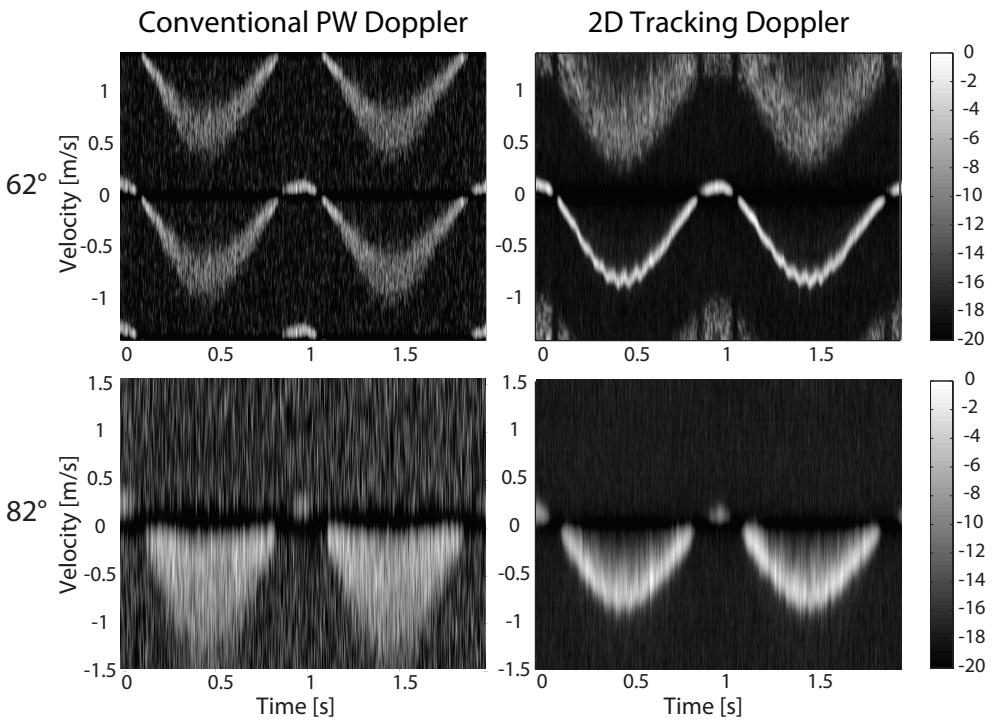

Figure 4.8: Doppler spectra generated from *in vitro* recordings of pulsatile flow in a straight tube. The spectra were generated using a conventional PW Doppler method and the 2D Tracking Doppler method. The dynamic range in decibel (dB) is given by the colorbar. The large beam-to-flow angles gave excessive spectral broadening for the highest velocities in the spectra generated by the conventional method. For the 2D Tracking Doppler spectra the spectral broadening has been reduced.

an approximately four-fold decrease in the spectral broadening can be observed for the largest velocities in the 2D Tracking Doppler spectrum compared to the conventional PW Doppler spectrum. A ripple effect in the velocity-time waveform can be observed in the 2D Tracking Doppler spectrum. These oscillations indicate that the flow pump was not running evenly. Due to the spectral broadening they are not visible in the conventional approach. In the lower panel spectra the beam-to-flow angle was 82°. For this beam-to-flow angle the velocities in the conventional PW Doppler spectrum are significantly smeared, whereas the velocities in the 2D Tracking Doppler spectrum can still be resolved.

Fig. 4.9 shows a conventional PW Doppler spectrum and a 2D Tracking Doppler spectrum generated from an *in vivo* ultrasound recording from the carotid artery of a healthy volunteer. The beam-to-flow angle was 70°. An increased velocity resolution can be observed in the 2D Tracking Doppler spectrum compared with the conventional

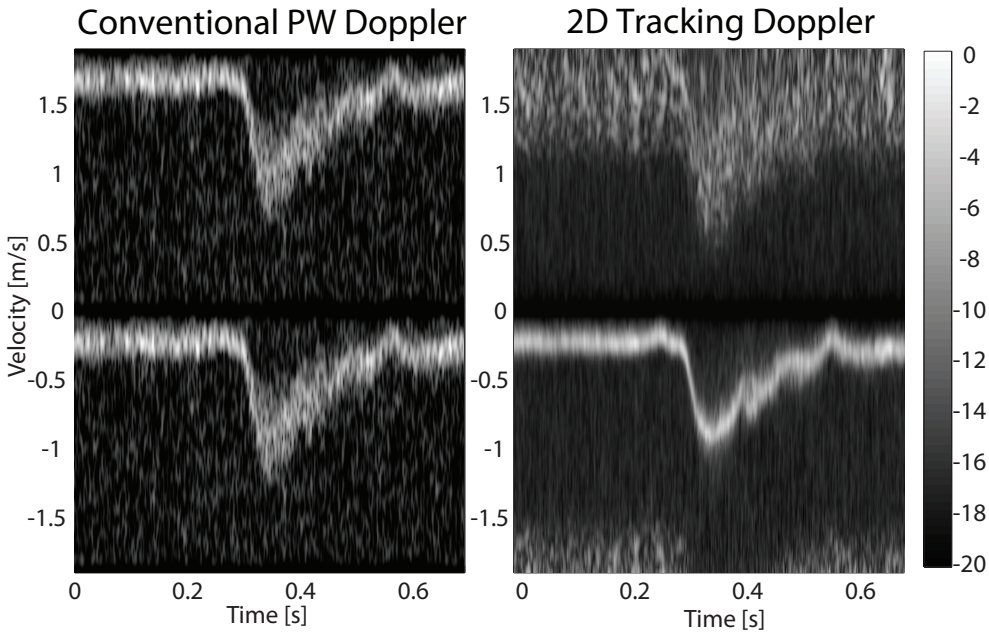

Figure 4.9: Doppler spectra generated from an *in vivo* recording of a carotid artery. The spectra were generated by a conventional PW Doppler method and the 2D Tracking Doppler method. The dynamic range in dB is given by the colorbar. The angle between the flow and the ultrasound beam was 70°, giving excessive spectral broadening for the highest velocities in the conventional spectrum. In the 2D Tracking Doppler spectrum the spectral broadening has been reduced.

PW Doppler spectrum, indicating that the method is applicable for *in vivo* imaging.

In Fig. 4.10 velocity spectra generated by the 2D Tracking Doppler method and the conventional PW Doppler method are compared to their corresponding simulated velocity spectra. The *in vitro* spectra were generated from a part of the dataset containing an approximately constant velocity of 0.82 m/s. The beam-to-flow angle was 62°. The spectra were averaged using 68 time samples. The simulated velocity spectra were generated using (4.7) and (4.9) and by inserting the same parameters as used in the *in vitro* experiment.

4.5 Discussion

The results show that spectral broadening can be considerably reduced when applying the 2D Tracking Doppler method compared with a conventional PW Doppler method. This can be explained by the increased transit time that is achieved when following the scatterers in space. An increased velocity resolution can be observed in the spectra

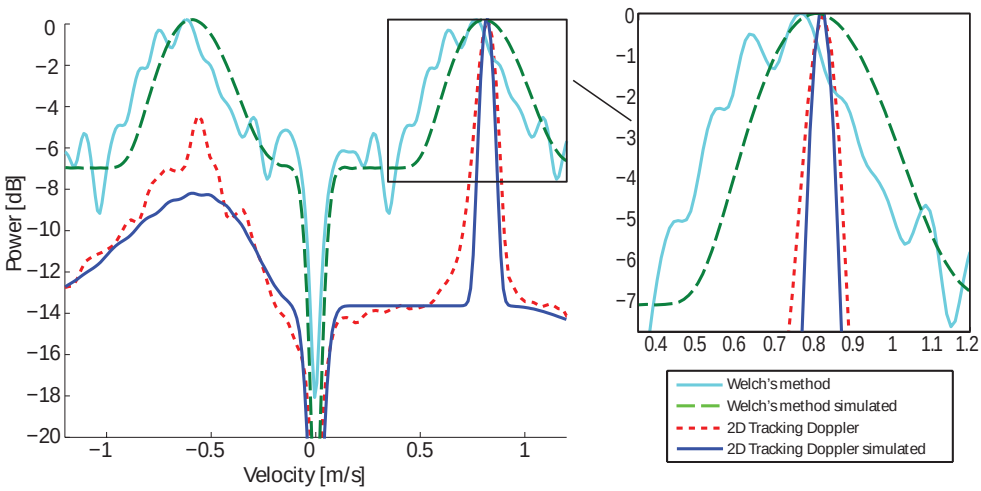

Figure 4.10: Doppler power spectra generated by the 2D Tracking Doppler method and the conventional PW Doppler method. Spectra generated from an *in vitro* recording are compared with their corresponding simulated spectra. The flow had a velocity of 0.82 m/s at an angle of 62° compared to the ultrasound beam.

generated from both the *in vitro* and *in vivo* ultrasound recordings. The simulation results also show a significant increase in velocity resolution for a wide range of beam-to-flow angles.

The 2D Tracking Doppler method is based on a plane wave acquisition. It is well known that the lack of transmit focusing results in reduced penetration depth. Reduced penetration can cause low SNR in situations where the region of interest is situated at large depths. However, in our experiments the penetration was sufficiently high. Also, the properties of the 2D Tracking Doppler method increase the SNR in the velocity spectra. Flow in cylindrical geometries, such as the straight tube and the carotid artery, has a constant velocity profile in the direction of the flow. By selecting data samples from a line in the middle of the cylinder, the scatterers have approximately equal velocity. The signal will therefore match in phase when summed in the 2D Tracking Doppler algorithm. This results in a better SNR in the 2D Tracking Doppler spectra compared with the conventional PW spectra, which is evident in both the *in vitro* and *in vivo* results.

Simulations of the expected Doppler power spectra were performed using an extended version of the signal model used in[7], including thermal noise and clutter filtering. Out-of-plane movement was not taken into account. The simulated spectra therefore describe an ideal situation where the flow direction is in the imaging plane and the beam-to-flow angle is measured precisely. Any out-of-plane movement or incorrect positioning of the tracking line would broaden the main lobe in the power spectrum. However, the simulated spectra corresponded well with the spectra generated from the *in vitro* recordings, showing 4 times increase in spectral resolution,

and 7 dB increase in spectral SNR (see Fig. 4.10). This may give new opportunities in blood flow imaging when it is desired to place the probe in an angle that is not parallel with the flow.

The 2D Tracking Doppler approach may have several advantages clinically. First of all, it may increase quantitative accuracy and reproducibility when tracing the envelope of the Doppler spectrum, due to the estimation and display of spectra with an increased accuracy and resolution. This is especially the case for high velocity blood flow that we often see in relation to pathology. It may also in general increase diagnostic confidence during visual assessment of Doppler spectra. The 2D approach to velocity estimation also provides opportunities for resolving the ambiguity problem when the maximum velocity is beyond the Nyquist limit. This has earlier been shown for blood flow direction along the ultrasound beam[7].

The use of parallel receive beamforming allows for PW Doppler based on a 2D or 3D acquisition scheme such as color-Doppler imaging. Using this approach it is possible to calculate and display multiple simultaneous velocity spectra from arbitrary spatial positions in the image region. This can be useful when quantifying valve leakages or vessel stenosis, and the approach may also help to improve workflow when both color-Doppler imaging and PW Doppler measurements are part of the protocol. The acquisition setup for color-Doppler is typically different from that of PW Doppler. For instance, the beam and pulse characteristics are chosen such that an increased spectral broadening is expected in the calculated sonograms when based on color-Doppler acquisition. The color-Doppler setup is on the other hand well suited for tracking purposes (shorter pulses and lower F-number), and by combining retrospective PW Doppler with the tracking technique it is possible to compensate for the decreased transit time in a combined acquisition mode.

An important challenge for the 2D Tracking Doppler method to work in practice is to extract data along the correct trajectory through a 3D (2D tracking + time) data set, following the movement of the blood scatterers. In this work the trajectory was determined from a B-mode image of the artery or tube and chosen as a straight line. This approach may not be suitable for more complex flow fields. Curved flow fields, accelerated flow and turbulent flow were not considered in this work. To avoid broadening of the velocity spectrum, the flow has to be constant for a length corresponding to the tracking length. In this work the maximum tracking length was 1.5 cm, which could be too long in the situations described above. One solution could be increasing the PRF which would decrease the required tracking length. Still, high velocity flow fields that change rapidly in space, such as jet flows, could be a challenge to estimate accurately. Additionally, steady-state flow conditions are assumed, which is true for short time intervals (10 ms[18]) similar to the observation time applied in this work.

4.6 Conclusion

A new method to limit spectral broadening in PW Doppler has been presented. By sampling the in-plane scatterer movement in the direction of flow an increased transit

time was achieved. This was feasible without compromising the pulse repetition frequency, as plane wave transmission and parallel receive beamforming were utilized. The velocity spectra generated by the 2D Tracking Doppler method had significantly reduced spectral broadening compared to spectra generated by a conventional PW Doppler method. Increased quantitative accuracy and reproducibility when tracing the envelope of the Doppler spectrum is expected, due to the estimation and display of spectra with increased accuracy and resolution.

References

[1] J. Capon, "High-Resolution Frequency-Wavenumber Spectrum Analysis," vol. 57, no. 8, pp. 1408–1418, 1969.

[2] J. Li and P. Stoica, "An Adaptive Filtering Approach to Spectral Estimation and SAR Imaging," *IEEE transactions on signal processing*, vol. 44, no. 6, pp. 1469–1484, 1996.

[3] P. Stoica and R. Moses, *Spectral analysis of signals*. Prentice Hall, Upper Saddle River, 2005.

[4] F. Gran, A. Jakobsson, and J. A. Jensen, "Adaptive spectral doppler estimation.," *IEEE transactions on ultrasonics, ferroelectrics, and frequency control*, vol. 56, pp. 700–14, Apr. 2009.

[5] K. L. Hansen, F. Gran, M. M. Pedersen, I. K. Holfort, J. A. Jensen, and M. B. Nielsen, "In-vivo validation of fast spectral velocity estimation techniques.," *Ultrasonics*, vol. 50, pp. 52–9, Jan. 2010.

[6] I. K. Ekroll, H. Torp, and L. Løvstakken, "Spectral Doppler estimation utilizing 2-D spatial information and adaptive signal processing.," *IEEE transactions on ultrasonics, ferroelectrics, and frequency control*, vol. 59, pp. 1182–92, June 2012.

[7] H. Torp and K. Kristoffersen, "Velocity matched spectrum analysis: A new method for suppressing velocity ambiguity in pulsed-wave Doppler," *Ultrasound in medicine & biology*, vol. 21, no. 7, pp. 937–944, 1995.

[8] S. Alam and K. Parker, "The butterfly search technique for estimation of blood velocity," *Ultrasound in medicine & biology*, vol. 21, no. 5, pp. 657–670, 1995.

[9] J. A. Jensen and N. Oddershede, "Estimation of velocity vectors in synthetic aperture ultrasound imaging," *Imaging, IEEE Transactions on*, vol. 25, no. 12, pp. 1637–1644, 2006.

[10] L. Wilson, "Description of broad-band pulsed Doppler ultrasound processing using the two-dimensional Fourier transform," *Ultrasonic imaging*, vol. 315, pp. 301–315, 1991.

[11] W. Mayo, "Two dimensional processing of pulsed Doppler signals," *US Patent 4,930,513*, 1990.

[12] T. Loupas and R. W. Gill, "Multifrequency Doppler : Improving the Quality of Spectral Estimation by Making Full Use of the Information Present in the Backscattered RF Echoes," *IEEE transactions on ultrasonics, ferroelectrics, and frequency control*, vol. 41, no. 4, pp. 522–531, 1994.

[13] H. Torp, K. Kristoffersen, and B. A. J. Angelsen, "Autocorrelation Techniques in Color Flow Imaging : Signal Model and Statistical Properties of the Autocorrelation Estimates," *IEEE transactions on ultrasonics, ferroelectrics, and frequency control*, vol. 41, no. 5, p. 9, 1994.

[14] R. S. C. Cobbold, *Foundations of Biomedical Ultrasound.* Oxford University Press, Inc., 2007.

[15] T. Hergum, S. Langeland, E. W. Remme, and H. Torp, "Fast ultrasound imaging simulation in K-space.," *IEEE transactions on ultrasonics, ferroelectrics, and frequency control*, vol. 56, pp. 1159–67, June 2009.

[16] J. G. Proakis and D. G. Manolakis, *Digital Signal Processing. Principles, Algorithms, and Applications.* Pearson Education, Inc., fourth ed., 2007.

[17] K. V. Ramnarine, D. K. Nassiri, P. R. Hoskins, and J. Lubbers, "Validation of a new blood-mimicking fluid for use in doppler flow test objects," vol. 24, no. 3, pp. 451–459, 1998.

[18] P. Vaitkus and R. Cobbold, "A comparative study and assessment of Doppler ultrasound spectral estimation techniques part I: Estimation methods," *Ultrasound in medicine & biology*, vol. 14, no. 8, pp. 661–672, 1988.

Chapter 5

Simultaneous Quantification of Flow and Tissue Velocities Based on Multi-Angle Plane Wave Imaging

Ingvild Kinn Ekroll[1], Abigail Swillens[2], Patrick Segers[2], Torbjørn Dahl[1,3], Hans Torp[1], and Lasse Løvstakken[1]
[1] MI Lab and Dept. Circulation and Medical Imaging, NTNU
[2] IBiTech-bioMMeda, Ghent University, Belgium
[3] St. Olavs Hospital, Trondheim, Norway

A quantitative angle independent 2D modality for flow and tissue imaging based on multi-angle plane wave acquisition was evaluated. Simulations of realistic flow in a carotid artery bifurcation were used to assess the accuracy of the vector Doppler (VD) technique. Reduction in root mean square deviation from 27 cm/s to 6 cm/s and 7 cm/s to 2 cm/s was found for the lateral (v_x) and axial (v_z) velocity components respectively when the ensemble size was increased from 8 to 50. Simulations of a Couette flow phantom (v_{max} = 2.7 cm/s) gave promising results for imaging of slowly moving tissue, with root mean square deviation of 4.4 mm/s and 1.6 mm/s for the x- and z-components respectively. A packet acquisition scheme providing both B-mode and vector Doppler RF data was implemented on a research scanner, and beamforming and further post processing was done offline. *In vivo* results of healthy volunteers were in accordance with simulations and gave promising results for flow and tissue vector velocity imaging. The technique was also tested in patients with carotid artery disease. Using the high ensemble vector Doppler technique, blood flow through stenoses and secondary flow patterns were better visualized than in ordinary color Doppler. Additionally the full velocity spectrum could be obtained retrospectively for arbitrary points in the image.

5.1 Introduction

Stroke is a major cause of disability and the second leading cause of death worldwide[1], and plaques in the precerebral arteries are responsible for as much as 20% of all strokes of thromboembolic origin[2, 3]. In this respect, there is a need for improved non-invasive diagnostic tools to assess developing cardiovascular disease in the carotid arteries. Ultrasound has been used to assess the degree of carotid stenosis due to atherosclerosis since the early days of Doppler sonography[4]. However, there is no general agreement to the reliability of the result of a Doppler ultrasound examination, as the degree of stenosis cannot be described by any universally accepted set of criteria[5]. Moreover, the degree of stenosis does not contain information about the vulnerability of the plaque.

A common and world-wide accepted method for assessing the degree of carotid stenosis using ultrasound is estimating the peak systolic velocity (PSV) in the stenosed region[6]. However, these estimates are also influenced by other factors than the actual diameter reduction, giving large variability in the outcome. Both patient variability, for instance whether collateral flow is present (which will lower the intrastenotic velocity), and variability in angle of insonation or the manually set correction angle[5, 7] influence the estimate of the degree of stenosis.

In addition to morphology and measurements of normal and abnormal flow in the stenosed carotid arteries, vessel wall stiffness, wall shear stress and plaque deformation are all important parameters in the pathophysiology and development of atherosclerosis. Ultrasound applications assessing these parameters require an angle independent and accurate quantification of blood and tissue velocities which so far has been lacking. Current color flow imaging (CFI) based methods are only of limited use for quantitative measurements, essentially due to three factors: 1) CFI has a limited measurable velocity span due to wall filtering and aliasing. 2) The velocity measured and displayed is dependent on the beam-to-flow angle. 3) Conventional line-by-line acquisition is time consuming, limiting the frame rate and/or image quality. The latter is especially true for duplex or triplex modalities.

Cross-beam vector Doppler has been one of the main approaches to two-dimensional flow imaging since the onset of the idea in the 1970s. Using triangulation, the 1D velocity estimates from two different angles of insonation can be used to reconstruct a 2D velocity vector[8]. Speckle tracking, where the interference pattern from flowing blood is tracked between consecutive ultrasound images[9] and other approaches such as the Doppler bandwidth method[10, 11], the spatial quadrature approach[12] and the transverse oscillation technique[13–15] are also able to reproduce 2D velocity fields. Although extensive research has been done in the field of 2D blood flow imaging[8, 16], it has not yet reached clinical practice. This may be due to lack of robustness, giving limited practical applicability, as well as limitations in the acquisition, giving low frame rates.

Given advances in parallel beamforming, a quantitative 2D flow imaging modality can be approached using plane waves on transmit and parallel beamforming on receive. The substantial gain in acquisition rates may be used for near instantaneous snapshots of flow and tissue movement, and the technique has been utilized for elastography[17],

simultaneous imaging of artery-wall strain and blood flow[18] and more recently for ultrafast compound Doppler imaging[19] and vector velocity imaging[20, 21]. The latter work utilized coded excitation and speckle tracking to obtain robust vector velocity estimates.

The high acquisition rate could also be used to increase the robustness and span of the estimated velocities, by increasing the ensemble length beyond the normal range of 8–16 transmissions. An increase in both pulse repetition frequency (PRF) and slow-time ensemble length allows a low clutter filter cut-off frequency while a high Nyquist limit is retained[22]. Further, large ensemble lengths allows generation of Pulsed Wave (PW) Doppler spectra from arbitrary image positions, as demonstrated in[19] for continuous Doppler acquisition. Throughout the text, ensemble length and packet size are both used to indicate the number of slow time samples used to form the autocorrelation estimates.

In this work the aim is to evaluate a plane-wave acquisition scheme for 2D vector Doppler imaging, used in a duplex setting to maintain sufficient B-mode image quality. We investigate whether both arterial flow and tissue velocities can be estimated with sufficient accuracy from the same acquisition. Further, the feasibility of retrospective PW Doppler will be demonstrated. All together, the investigated acquisition scheme is a single modality for vascular imaging that could allow for simultaneous examination of both flow field, wall velocities and peak systolic velocity. As the true vector velocity field is unknown *in vivo*, a simulation environment developed by Swillens *et al.*[23] was used to assess the accuracy of blood velocity estimates derived from the vector Doppler acquisition scheme. After implementing the acquisition in a research ultrasound system, the technique was also tested on healthy volunteers and patients with carotid artery disease.

5.2 Methods

5.2.1 Simulation study

The 2D vector Doppler technique was simulated using the Field II[24] simulation software, where blood is modeled as a collection of random point scatterers. The number of point scatterers was sufficient to ensure a normally distributed RF signal, approximately 10 per resolution cell. The size of the resolution cell was calculated based on the receive F-number, transmit frequency and pulse length. A scatterer phantom derived from computational fluid dynamic (CFD) simulations of flow in a carotid artery bifurcation was used to mimic realistic scatterer displacement in complex blood flow conditions. The CFD model was constructed based on MRI-scans of a healthy volunteer, in which an eccentric plaque was artificially added in the internal branch. The applied boundary conditions were a velocity profile at the common carotid, measured with PW Doppler in a healthy volunteer, and a 45-55% externa-interna flow division. An illustration of the imaging setup and the carotid bifurcation phantom can be found in Fig. 5.1. Swillens *et al.*[23] have previously presented the method and the bifurcation phantom used in the present simulation study, where the output of CFD is coupled with Field II. For each emitted beam, the

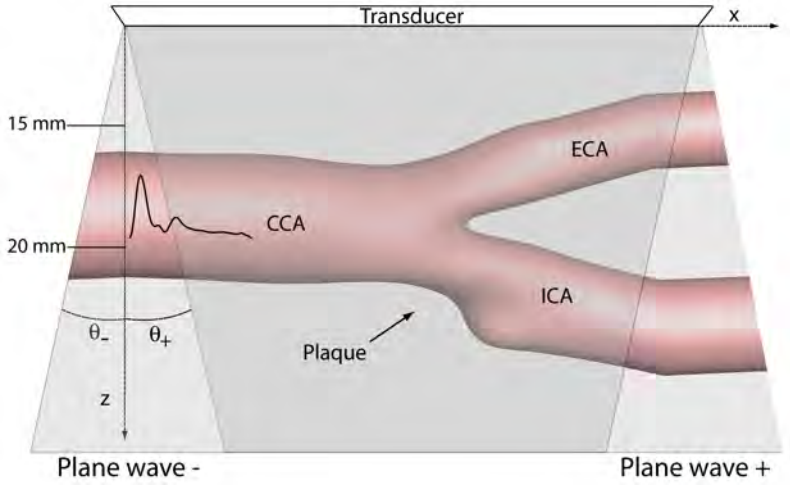

Figure 5.1: An illustration of the vector Doppler imaging setup with the carotid bifurcation phantom used in simulations. Two plane waves of opposite steering angle were transmitted and full parallel beamforming was used on receive, giving a large image sector. The common, internal and external carotid arteries are indicated as CCA, ICA and ECA respectively, whereas θ is the steering angle. The curve depicted within the CCA illustrates the time-varying boundary velocity profile.

scatterer position is updated based on the CFD velocity fields, utilizing both temporal and spatial interpolation to match the ultrasound timescale and to ensure random scatterer placement. Further details on the CFD-US coupling can be found in[23].

A simpler cylindrical phantom with analytical Couette flow was also included. The maximum measurable velocity was only 2.7 cm/s. The rotating flow provides a range of velocities at all possible angles with the transmitted beam. This was done to mimic an imaging situation with slowly moving vessel walls, where the beam-to-movement angle may change completely throughout the cardiac cycle. Moving scatterers were present in the region where $0.25\,\text{cm} \leq r \leq 1\,\text{cm}$, and the phantom was placed at a depth of 2 cm, similar to the carotid phantom.

White noise was added to give a signal-to-noise ratio (SNR) of 30 dB in both simulation cases. The accuracy of the velocity estimates was assessed by calculation of the root mean square (RMS) deviation between estimates and the ground truth from CFD simulations.

The plane wave acquisition consisted in both cases of equal transmit and receive angles in an interleaved scheme with two plane waves of opposite steering angle. A 10° steering angle gave a 3 cm wide overlap at 2.5 cm depth. Ensembles of 50 Doppler samples were simulated with an imaging PRF of 8 kHz to achieve a slow time Doppler PRF of 4 kHz in each direction. Polynomial regression filters were used to include clutter filter effects in the simulations of carotid flow, while no clutter filter was applied in the analysis of the tissue mimicking phantom. Parallel beamforming was used on

Table 5.1: Simulation parameters

Parameter	Value
Probe type	192 element linear array
Elements used on transmit	192
Pitch [μm]	250
Center frequency f_0 [MHz]	5
PRF [kHz]	8
Ensemble lengths	8→50
Cycles @ f_0	2.5
Transmit angle [deg]	±10
Receive angle [deg]	±10
Receive $F_{\#}$	1.4
Transmit $F_{\#}$	∞

receive to generate a full image per emitted plane wave, using a receive F-number of 1.4. Further specifications on the ultrasound simulations can be found in Table 5.1.

In order to provide a comparison between focused and unfocused Doppler imaging, a simulation of stationary parabolic flow in a straight tube was included. In the center of the tube, the true velocity magnitude was 30 cm/s. The carotid simulations were based on a time-varying flow profile, and was therefore not used for this purpose, as the high packet size would result in large time-lag artifacts in the focused case. The tube was placed at a depth of 2 cm and angled 30° with the horizontal direction, resulting in a beam-to-flow angle of 50° and 70° for the two transmit/receive directions. For the plane wave simulation, the imaging setup was equal to that described above. In the focused simulation, the transmit focus was set to 2 cm, and one receive beam was generated per transmit beam. The number of pointscatterers used in the flow simulations was again 10 per resolution cell. However, for illustration purposes, Fig. 5.2 gives a depiction of the phantom where the scatterer density is reduced by a factor 100. The true positions of the pointscatterers are indicated by black circles.

5.2.2 In vivo implementation

An angled plane wave setup for vector Doppler acquisition corresponding to the simulation setup was implemented on a Sonix MDP ultrasound system (Ultrasonix, Richmond, BC, Canada) using the development toolkit Texo which allows custom transmit sequences to be created. A Sonix DAQ (Ultrasonix, Richmond, BC, Canada) was used for channel data acquisition. The packet acquisition scheme consisted of a plane wave B-mode compound sequence and a vector Doppler sequence for a total of $43 + 2\times50$ transmit events per duplex frame. This gave a Doppler packet size of 50, as used in simulations. 63 duplex frames (4 GB of data) corresponded to approximately

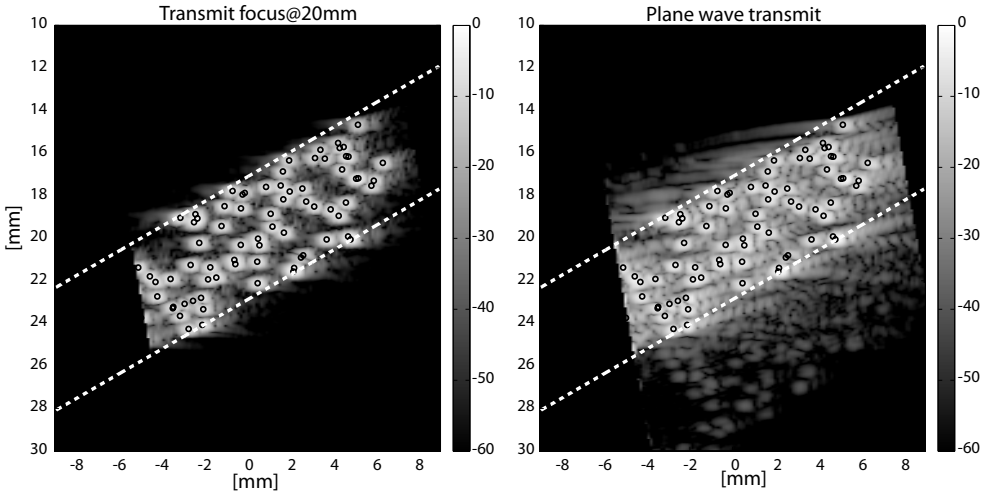

Figure 5.2: The figure shows images of a set of stationary pointscatterers, using focused and unfocused transmit for the left and right image respectively. As expected, the edge waves give a substantial degradation of the image quality.

one second with the PRFs used. The channel RF data was IQ-demodulated and low-pass filtered to reduce the noise bandwidth, and beamformed using a Hamming window over the active receive aperture. B-mode images were formed using coherent plane wave compounding[25], by beamforming echoes from 43 different transmit angles to a common grid, followed by summation of the IQ data at all grid-points. Doppler data were beamformed using a tilted receive angle equal to the transmit angle to maximize the separation angle between the Doppler shifts from the two insonations. Imaging parameters for B-mode and Doppler *in vivo* acquisition in the duplex scheme are found in Table 5.2.

Safety measurements

Both thermal and acoustical measurements were done to ensure that the transmitted pressure field satisfies the limits for *in vivo* imaging proposed by the Food and Drug Administration (FDA)[26]. The multi-angle plane wave acquisition scheme was tested using a Sonix MDP scanner with a L9-4/38 linear probe. In Table 5.3 both transmit settings and measurements can be found for two different plane wave acquisition schemes; one more suitable for Doppler and one more suitable for B-mode compound imaging.

A carotid patient feasibility study is on-going, with 12 patients included so far. The study was approved by The Regional Committee for Medical and Health Research Ethics (REC) and written consent was received from each participant. As seen in Table 5.3, surface heating was the limiting factor, leading to a compromise between penetration depth and PRF. The packet acquisition used in the *in vivo* recordings is

Table 5.2: In vivo imaging parameters

Parameter	**B-mode**	**Doppler**
Probe	L9-4/38	
Probe type	128 element linear array	
Elements used on transmit	128	
Pitch [µm]	304	
TxFrequency f_0 [MHz]	6.7	5
PRF [kHz]	12	8
Cycles @ f_0	1.5	2.5
Transmit angle [deg]	$-7.2 \rightarrow 7.2$	± 10
Receive angle [deg]	0	± 10
Δangle tx [deg]	0.34	20
Receive $F_{\#}$	1.4	1.4
Effective transmit $F_{\#}$	4	∞

Table 5.3: Safety measurements

Settings	1	2	
TxFrequency f_0	5	6.7	[MHz]
Aperture	128	128	[elements]
Cycles@f_0	2.5	1.5	
Focal depth	∞	∞	[mm]
PRF	12	15	[kHz]
Drive voltage, V_{pp}	56	68	[V]
Acoustic measurements			**FDA limit**
MI	0.4	0.3	1.9
Ispta [mW/cm^2]	124	63	720
Temperature			**FDA limit**
ΔT_{air} (measured for 30 min) [°C]	23	18.3	27
$\Delta T_{phantom}$ (measured for 30 min) [°C]	6.5	9.1	10

a duplex modality combining the two setups in Table 5.3, however with a lower PRF (8 and 12 kHz for the Doppler and B-mode respectively) than the maximally allowed from safety considerations and a drive voltage of 68 V, resulting in reduced surface heating.

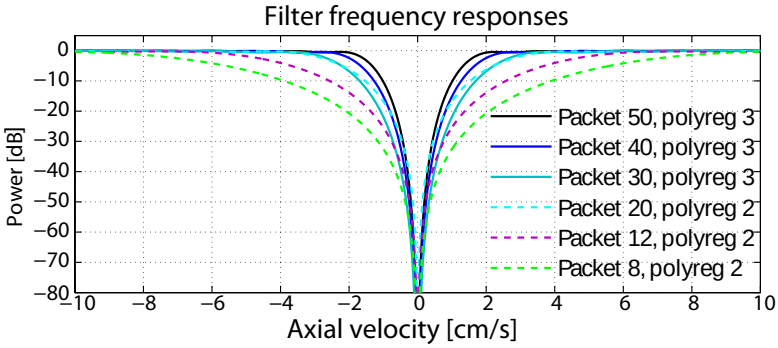

Figure 5.3: Frequency responses of the polynomial regression filters used for clutter rejection. Filter orders were chosen to give a comparable stop band attenuation for the different ensemble lengths, resulting in different characteristics in the transition band. Note: The frequency axis has been shortened.

5.2.3 Vector velocity estimation

The velocity vector components were obtained in the whole image region simultaneously by combining overlapping Doppler measurements from two directions as given in equation (5.1)[27]

$$\begin{aligned} v_x &= -\frac{c}{4\, f_0 \sin(\theta)} \left(\hat{f}_1 - \hat{f}_2\right) \\ v_z &= -\frac{c}{4\, f_0 \cos(\theta)} \left(\hat{f}_1 + \hat{f}_2\right) \end{aligned} \tag{5.1}$$

where the separation angle between the two transmit/receive directions is 2θ, c is the speed of sound, f_0 is the pulse center frequency and $\hat{f}_1$, $\hat{f}_2$ are the Doppler frequencies estimated from the IQ data based on the temporal autocorrelation function with lag one; $\hat{f} = \angle(\hat{R}(1))/2\pi \times PRF$[28, 29]. Frequency estimates at positions where the power was below a certain threshold after clutter rejection was clamped to zero for that direction. Spatial averaging of the autocorrelation estimate over an area of approximately 1×1 mm was used both in simulations and *in vivo* to further improve the estimates.

5.2.4 Clutter filtering

Clutter filtering is one of the major challenges in vector Doppler imaging as it is desirable to keep a high velocity range for blood flow, whereas the signal from moving tissue should be suppressed. A filter with good stop band attenuation and steep transition region is therefore preferable. Designing such a filter is challenging for short ensemble signals, but eases considerably when the ensemble size increases. In

order to quantify the improved accuracy in 2D vector velocity estimates for increasing ensemble lengths, regression filters with comparable stop band attenuation were chosen for the different ensembles. Polynomial regression filters were used as they have a narrower transition region for equal stopband width compared to FIR-filters[30], and as they allow the full ensemble length to be used after clutter rejection. The frequency response of polynomial regression filters varies with both ensemble length and clutter space dimension, so to make the stopband comparable, cases of longer ensembles were filtered using a higher clutter space dimension. The -3 dB cut-off velocity varied from 1.5 cm/s for ensemble length 50 and polynomial order 3, to 6.7 cm/s for ensemble length 8 and order 2. The frequency responses of the polynomial regression filters used in this work are found in Figure 5.3. In cases where the mean velocity is compared to retrospective PW Doppler spectra, the PW spectra are obtained by separate post-processing including clutter rejection by use of a FIR filter of order 8, with a -3 dB cut-off at 5.4 cm/s. This was done to avoid frequency distortions in the transition region[31].

5.2.5 Spectral estimation

Peak systolic velocity is not estimated using mean frequency estimation, but rather from the full PW Doppler spectrum. The autocorrelation estimates may have a bias due to clutter filtering or spatial averaging, so in addition to the need of velocity spectra in PSV measurements, it may be useful to compare autocorrelation estimates to velocity spectra generated retrospectively. Retrospective PW Doppler spectra from blood were obtained using a Hamming weighted periodogram approach with a window length equal to the packet size.

In the case of tissue velocity estimation, where the velocities are much lower than for blood flow, autocorrelation of lag 4 and temporal averaging was applied to reduce the variance in phase shift estimates, reducing the effective slow time PRF to 1 kHz and the ensemble length to 13. Due to poor spectral resolution at these small ensemble lengths, the periodogram approach was replaced by the power Capon spectral estimation technique[32], given by

$$\hat{P}_{PSC}(\omega) = \frac{1}{\mathbf{a}^H(\omega)\hat{\mathbf{R}}_{\mathbf{x}}^{-1}\mathbf{a}(\omega)}, \tag{5.2}$$

where $\mathbf{a}(\omega) = [1\ e^{i\omega}\ \cdots\ e^{i(N-1)\omega}]^T$ and $\hat{\mathbf{R}}_{\mathbf{x}}$ is an estimate of the signal covariance matrix, here based on an averaging area of 1×1 mm.

5.3 Results

5.3.1 Simulations

Focused vs Unfocused transmit

The simulations of flow in a straight tube showed an increased sidelobe level in the unfocused image, present at ≈ -25 dB, which resulted in poor contrast compared to that

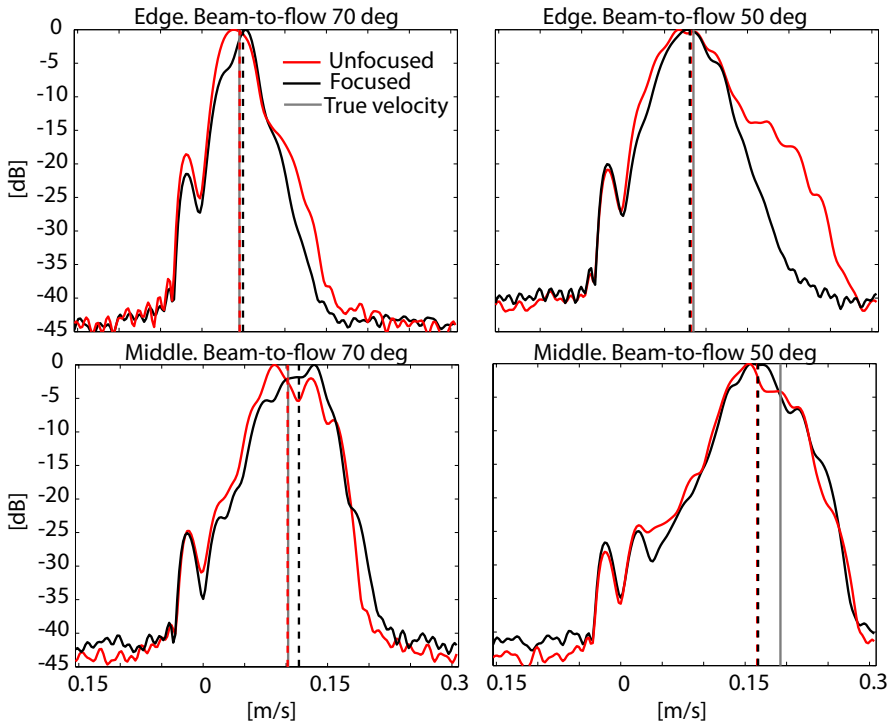

Figure 5.4: The figure shows velocity spectra and autocorrelation estimates (vertical lines) from simulations of parabolic flow in a straight tube. The two upper panels show velocity estimates from the upper edge of the tube (see Fig. 5.2), whereas the two lower panels show velocity estimates from the middle of the tube. The true axial velocity is indicated as a solid gray line for comparison.

found in the corresponding focused image. However, as shown in Fig. 5.4, the velocity estimates found from autocorrelation were almost identical in both situations. In the unfocused case, the sidelobes originating from scatterers of higher velocity contributed to an increase in the spectral width in the low velocity region close to the edge. Still, the autocorrelation estimate was not significantly affected, and the estimated velocities corresponded well to the ground truth both in the focused and the unfocused case. In the high velocity region, the autocorrelation estimates from focused and unfocused transmit were again very similar, and both underestimated the maximal velocity with approximately 15% at the lowest beam-to-flow angle.

Simulations of complex flow

The reference CFD velocity field at one instant in the cardiac cycle (systolic deceleration) is shown in the top panel of Fig. 5.5. The velocity vectors are overlaid an image of the axial velocities corresponding to those obtained from a one angle

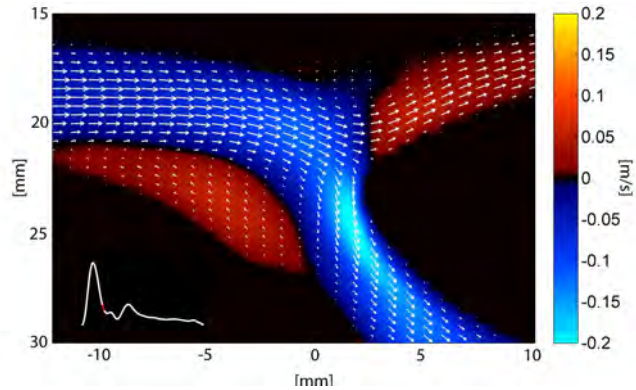

(a) Ground truth from CFD

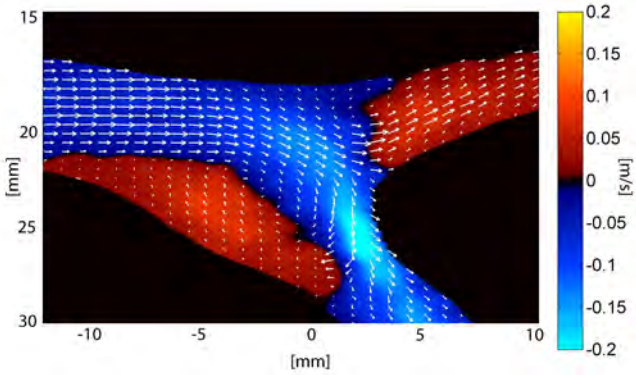

(b) Packet size 50

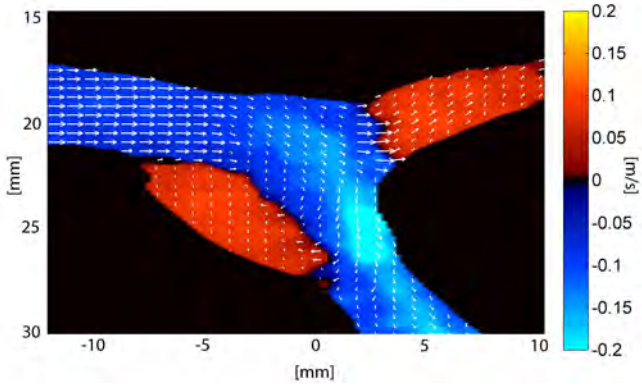

(c) Packet size 12

Figure 5.5: Results from simulations of flow in a carotid artery bifurcation, showing the increased robustness of the high ensemble vector velocity estimates. The illustrated frame is within systolic deceleration, where complex flow patterns are present, including swirling flow.

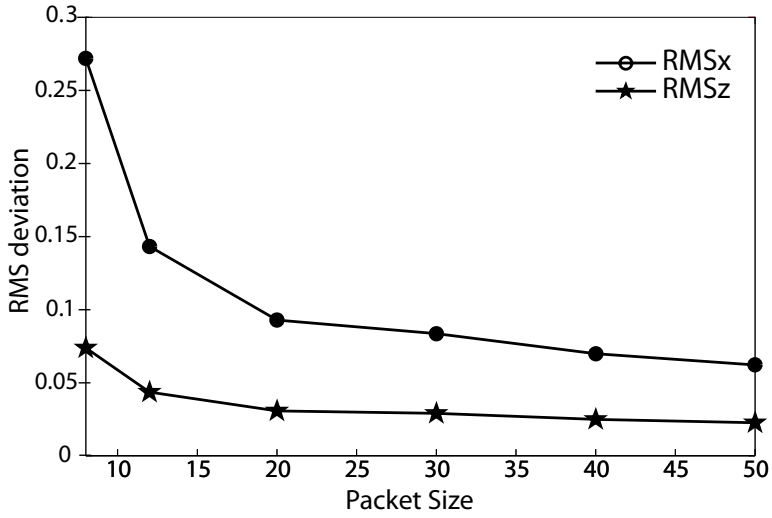

Figure 5.6: Root mean square deviation between estimated and true velocities in the carotid bifurcation simulations for different ensemble sizes. While the z-component is relatively accurate already at size 20, the x-component has a steady improvement when increasing from size 20 to 50.

(+10°) color flow image. The subsequent panels show simulated color flow images and estimated vector velocity fields using packet size 50 and 12 and clutter rejection filters of polynomial order 3 and 2 respectively. Visual inspection gives the impression that the larger ensemble acquisition provides a more correct depiction of the flow field, displaying more of the low velocities present in the swirling flow region and the bifurcation region where the beam to flow angle is near normal. Due to the slower rise of the lower order clutter filter the velocities also tend to be overestimated when small ensemble lengths are used. Scatterplots of the estimated versus the reference velocity components are found in the left panels of Fig. 5.7 for packet sizes 12 and 50. Calculation of the root mean square (RMS) deviation between the reference velocities and the velocity estimates was done for ensembles ranging from 8 to 50, with results shown in Fig. 5.6. Velocities from all spatial positions are included. A large reduction in RMS deviation is obtained by increasing the ensemble size, resulting in acceptable errors in both components. The RMS deviation drops from about 27 cm/s to 6 cm/s for v_x, and from 7 cm/s to 2 cm/s for v_z.

Slow rotating flow

The right panels of Fig. 5.7 show scatter plots of estimated versus true velocities in the slowly rotating cylindrical phantom. Velocities in the region $0.3\,\text{cm} \leq r \leq 0.9\,\text{cm}$ were included in the analysis, as well as estimates from all possible angles relative to the transmit directions (0–2π). The maximal measurable velocity was 2.7 cm/s, and

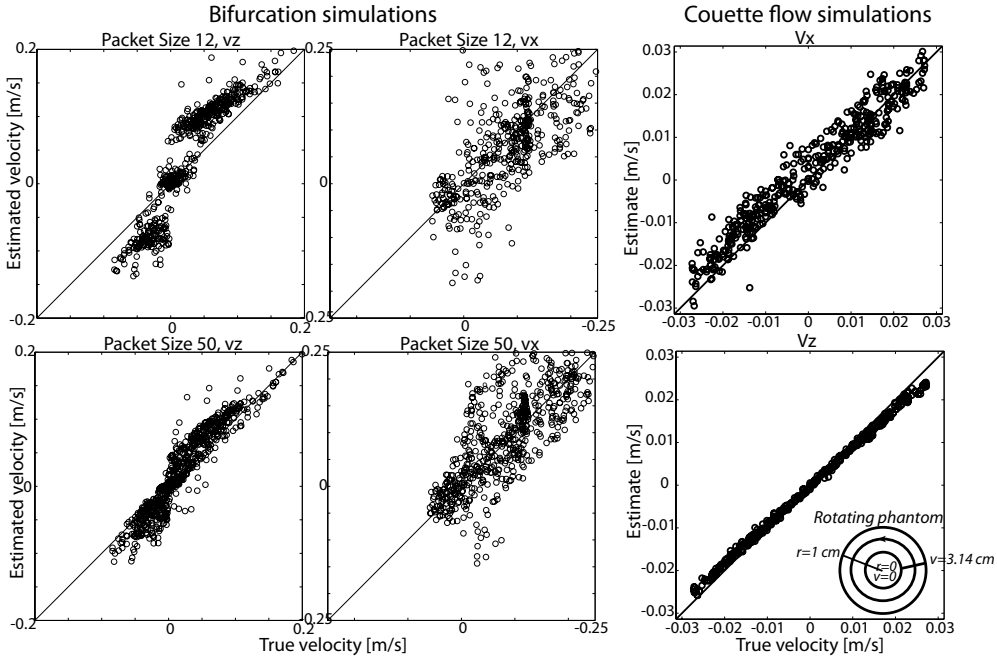

Figure 5.7: *Left:* Scatter plots showing estimated versus true velocity for packet size 12 (top) and packet size 50 (bottom). *Right:* Scatter plots showing estimated versus true velocity from slowly rotating cylinder simulations. All imaging parameters were equal in the two simulation types.

no clutter filter was applied. The RMS deviations were 4.4 mm/s and 1.6 mm/s for the x- and z-components respectively.

5.3.2 *In vivo* imaging

Vector flow imaging

Fig. 5.8(a) shows systolic flow in the carotid bifurcation of a healthy volunteer. The B-mode image is compounded from 43 angled plane waves, whereas the color flow image and the overlaid vector velocity estimates are generated from autocorrelation estimates using ensembles of 12 and 50 for the top and lower panel respectively. Although the frame is from systole with relatively high velocities, there are some dropouts close to the vessel walls and regions of erroneous velocity estimates in the small ensemble case, whereas the large ensemble case displays a higher robustness. In this example, the velocity profile in the common and external carotid is relatively flat and symmetrical without any retrograde flow during the cardiac cycle. The carotid bulb displays flow separation, with higher velocities towards the flow divider and swirling/retrograde flow on the opposite side, corresponding well with what is expected in a healthy

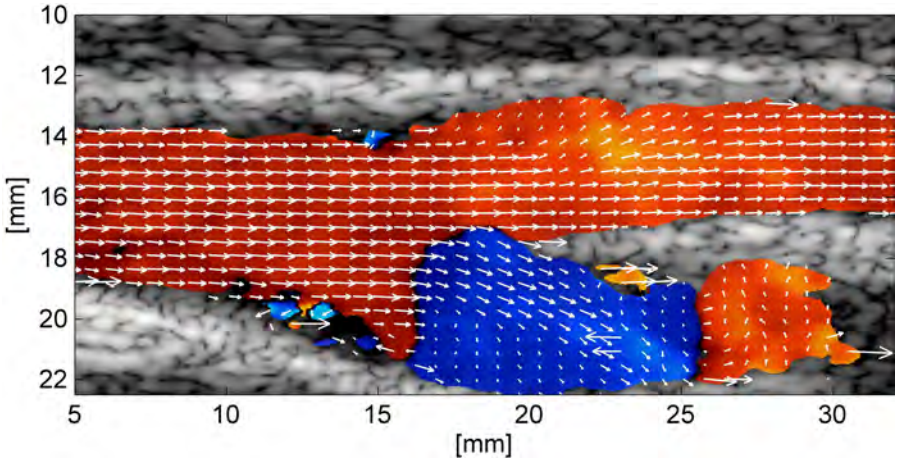

(a) Packet size 12, in systole

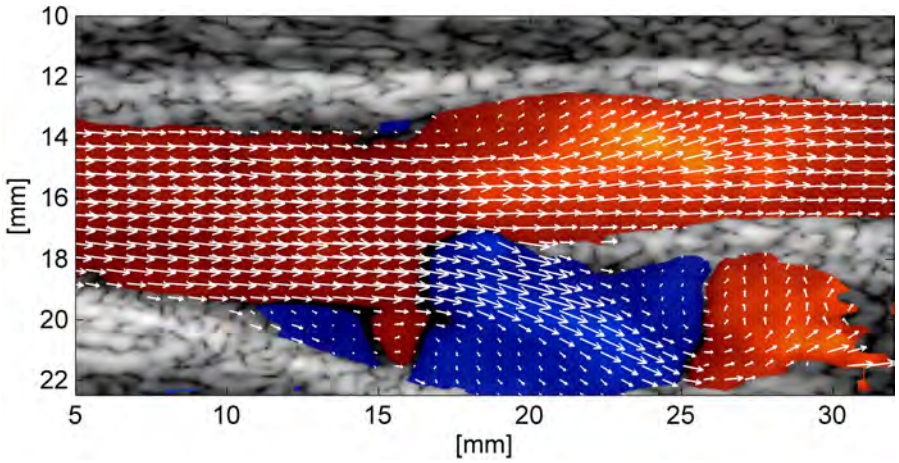

(b) Packet size 50, in systole

Figure 5.8: Blood flow in the bifurcation of a healthy volunteer in systolic acceleration. Vector velocities are overlaid the color flow image from one imaging angle.

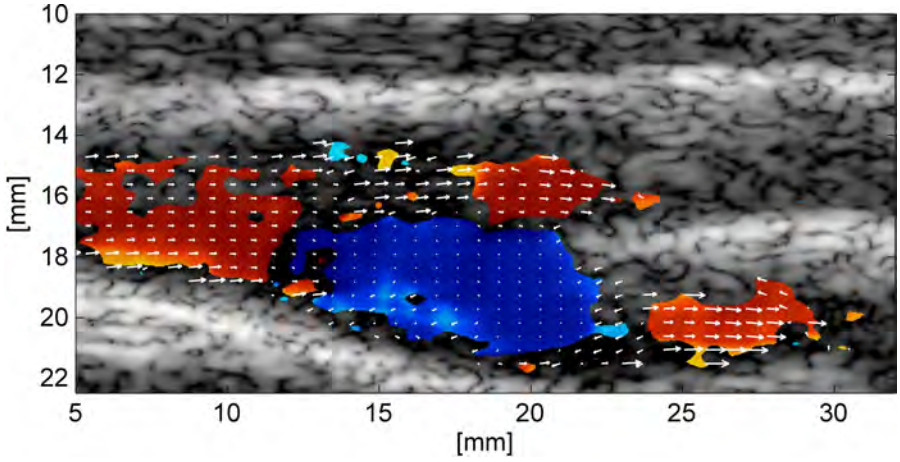

(a) Packet size 12, in diastole

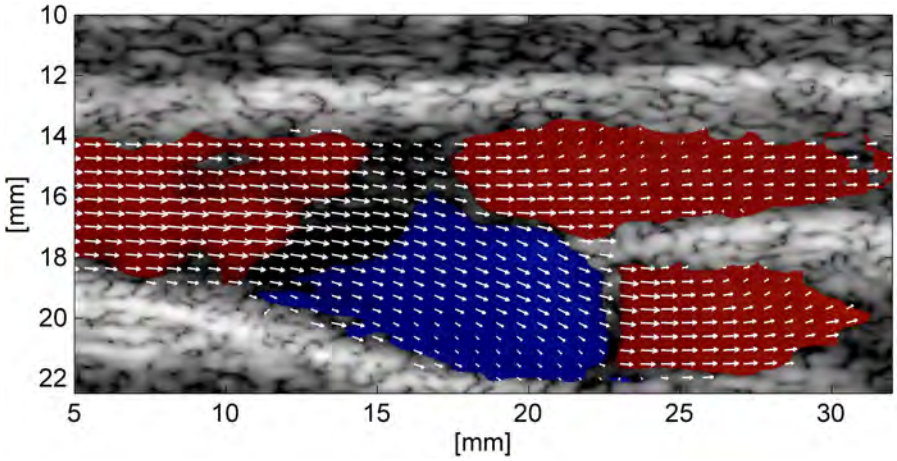

(b) Packet size 50, in diastole

Figure 5.9: Blood flow in the bifurcation of a healthy volunteer in diastole. In the short ensemble case, the low velocities cause large dropout regions and regions with highly overestimated velocities.

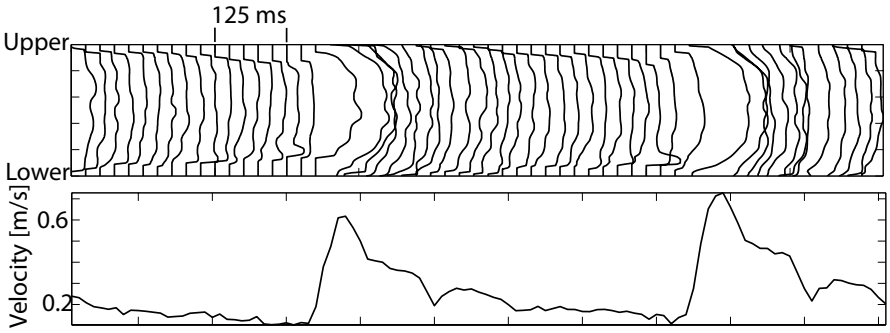

Figure 5.10: The top panel shows the temporal development of the velocity profile at the common carotid artery outlet (leftmost in Fig. 5.8 and 5.9). Also shown is the average velocity magnitude (bottom panel) at the same location.

carotid bifurcation[33]. A more illustrative depiction of the velocity profile at the outlet of the common carotid artery (the left side of the image) can be seen in the top panel of Fig. 5.10, based on an ensemble length of 50. The lower panel shows the temporal development of the mean velocity over the cross section. In diastole, (Fig. 5.9) the extended velocity range gained by using large ensemble lengths can be readily appreciated. The small ensemble case (Fig. 5.9(a)) is unable to reproduce the flow field due to the low velocities and the higher clutter filter cutoff, whereas the direction of flow is well depicted in the large ensemble case (Fig. 5.9(b)).

Patient feasibility study

In the on-going carotid patient feasibility study, the combined imaging modality under investigation is compared to a conventional focused acquisition using a high end ultrasound scanner (Vivid E9, GE Vingmed Ultrasound, Horten, Norway). In Fig. 5.11, flow in the internal carotid artery of a patient with double sided stenosis is shown alongside an image from a conventional acquisition in the same patient. In this case a slightly higher transmit frequency is used in the conventional acquisition, as well as other image enhancement techniques which gives an improved B-mode image quality over the plane wave compound image. However, it can be seen that the plane wave color flow image is comparable to the focused one, with a signal-to-noise ratio sufficiently high to produce robust vector Doppler estimates. As ensembles of length 50 is available for all points in the image at all times, retrospective PW Doppler spectra could be generated from the vector Doppler data at 63 frames per second. Fig. 5.12 shows retrospective PW Doppler from the region indicated by a yellow square, compared to regular PW Doppler using the Vivid E9 system. The spectral quality in terms of velocity resolution and contrast is comparable, but the frame rate in the retrospective example is lower than typically used in PW Doppler. For the conventional spectrogram, manual angle correction is used, while the retrospective spectrum is automatically corrected using the velocity direction estimated from vector

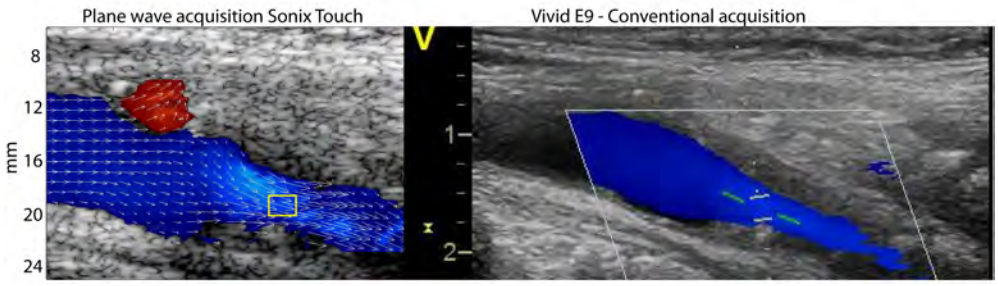

Figure 5.11: Results from a 71 year old patient (BMI 28) with double sided stenosis in the internal carotid artery. The right panel shows an image captured during the regular examination of the patient. The yellow markers indicate region of interest for PW Doppler measurement of peak systolic velocity. The left panel shows the vector velocities in a systolic frame from the same patient, using data from the acquisition scheme under investigation. The yellow rectangle indicates the region of interest for retrospective PW Doppler.

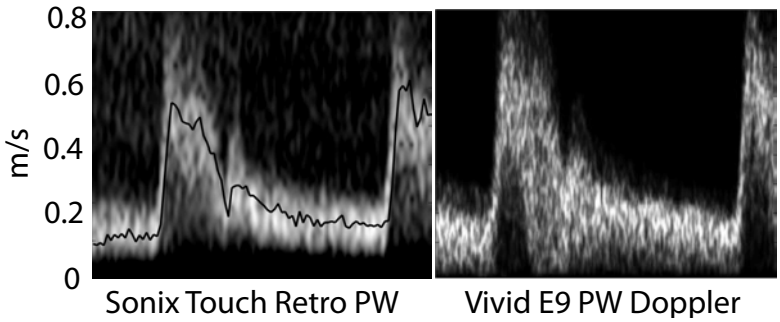

Figure 5.12: A comparison of conventional PW Doppler with manual angle correction (right) and retrospective PW Doppler with automatic angle correction (left) from the ROIs indicated in Fig.5.11. The velocity magnitude trace from vector Doppler is overlaid the spectrum in the panel to the left, showing good correspondence between the estimated velocity magnitude and the velocity spectrum.

Doppler. The estimated velocity magnitude is also shown for comparison.

Tissue vector velocity imaging

As in simulations, acquired large ensemble data could also be used to extract information about the vector velocity in the tissue. In this case no clutter filter was applied, and autocorrelation of lag 4 corresponding to a new PRF of 1 kHz was performed, giving an ensemble length of 13. Fig. 5.13 shows the tissue vector velocities at two instances in the cardiac cycle; in systolic acceleration and late diastole. In systole the velocity was mainly in the radial direction, whereas in diastole lateral

movement was clearly present. Traces of the velocity magnitude in the upper and lower wall in the middle of the bifurcation region of Fig. 5.8 are shown in the top panel of Figure 5.14, whereas the lower panel shows the estimated velocity directions in degrees relative to the transducer normal. 180° correspond to movement in a direction directly towards the transducer, 90° corresponds to horizontal movement, while 0° correspond to movement directly away from the transducer. The maximum velocity at this location was 8 mm/s, found in the upper wall. At this point in the cardiac cycle the motion was mainly in the radial direction, and the estimated velocity directions at the upper and lower wall were separated by approximately 165°. A velocity spectrum from the upper wall of the carotid bifurcation in a healthy volunteer is shown in Fig. 5.15 together with the corresponding autocorrelation estimate, confirming the accuracy of the approach for tissue velocity estimation.

5.4 Discussion

In this work the robustness of plane wave vector Doppler imaging has been investigated using both simulations, recordings of healthy volunteers, and patients with carotid artery disease. Vector velocity imaging using the autocorrelation estimator and triangulation was chosen as the technique has been shown to be robust even in cases of poor signal-to-noise ratio[34] and as it has low computational complexity. Robust velocity estimation was important as plane wave imaging suffers from decreased penetration depth and a higher side lobe level compared to focused imaging. Single plane wave imaging can provide sufficient contrast and resolution for Doppler, where the limited SNR leads to less apparent side lobe levels, but this is not the case for B-mode imaging. Based on the quality requirements in B-mode imaging, duplex acquisition was chosen.

The comparison of focused and unfocused Doppler estimates showed good correspondence between the autocorrelation estimates, although increased spectral broadening was present in the unfocused case due to larger sidelobes. The underestimation in the autocorrelation estimates in the case of high velocity and a 50° beam-to-flow angle was probably due to the misalignment between the flow direction in the tube and the sample volume. Such misalignment results in an increased influence by scatterers of lower velocity compared to the 70° case, where the sample volume and the flow direction were more parallel. The underestimation was equal in the unfocused and focused case.

Ultrasound simulations with a realistic and known velocity field from computational fluid dynamics were used to assess the accuracy of the vector velocity estimates. As expected, RMS deviation was reduced with increasing packet size. Estimates of both velocity components (v_x and v_z) were significantly improved when increasing the ensemble length from 8 to 20. However, increasing the ensemble size further mostly affected the v_x estimation, with a continued, but slow decrease in RMS deviation. From the curve in Fig. 5.6, the accuracy seems to converge in a region not far from an ensemble length of 50, indicating that there is little benefit from increasing the ensemble (or window) length even more at this PRF. After all, a packet size of 50

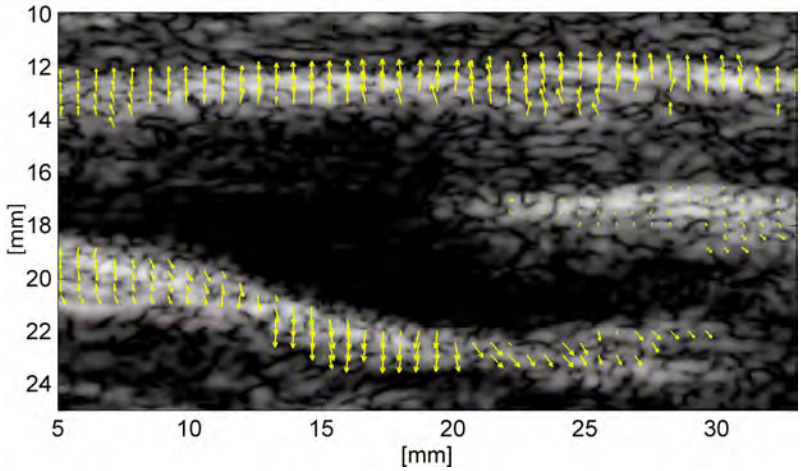

(a) In systole

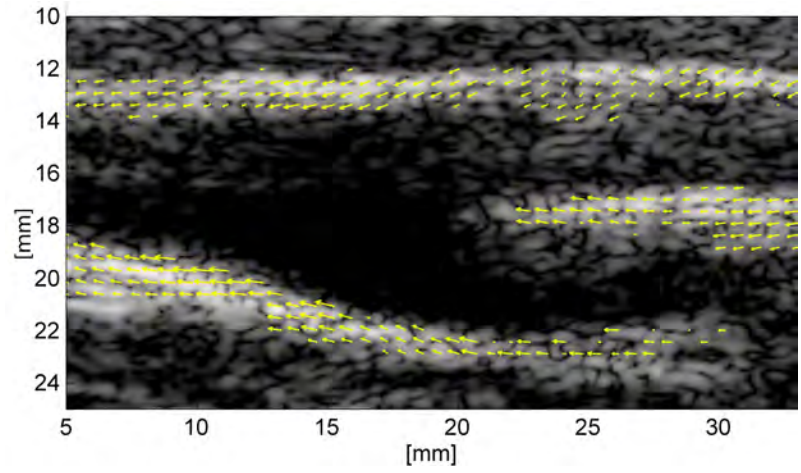

(b) In diastole

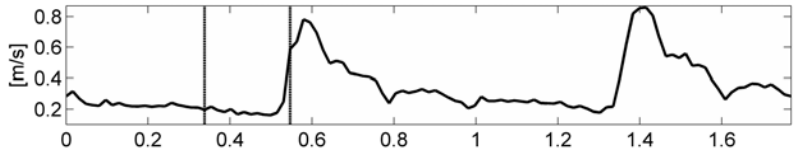

(c) Velocity trace, CCA

Figure 5.13: The upper panel shows the tissue vector velocities in the acceleration part of systole, while the middle panel shows the vector velocities in diastole. The lower panel shows the absolute blood velocity estimated using vector Doppler at the outlet of the common carotid artery, with indications of the timepoints used in the panels above.

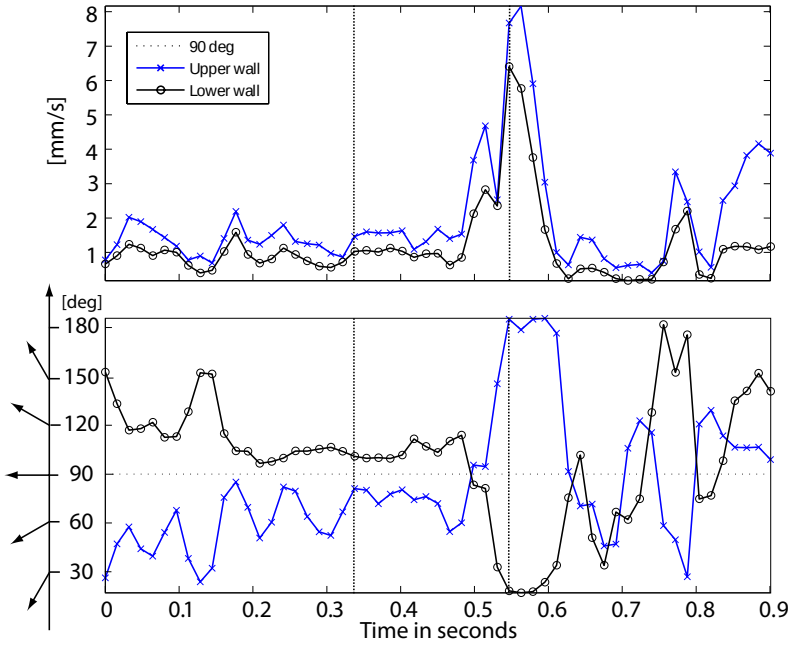

Figure 5.14: The upper panel shows the velocity magnitude in upper and lower wall of the common carotid artery depicted in Fig 5.13. The two timepoints in Fig. 5.13 are indicated with vertical lines. The lower panel shows the tissue velocity direction as the angle in degrees relative to the vertical direction (normal to the transducer surface). The direction is also indicated by arrows next to the corresponding angles.

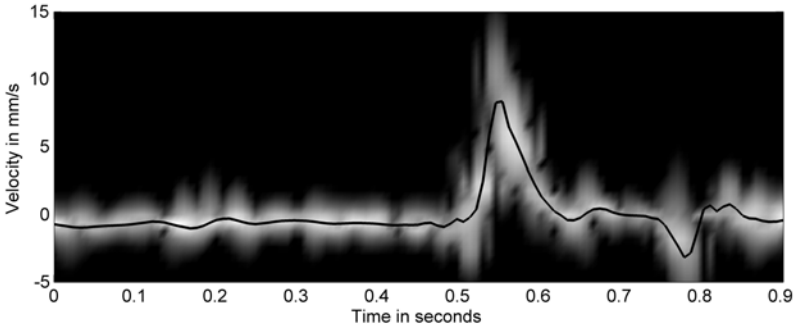

Figure 5.15: Tissue velocity spectrum from upper wall shown in Fig. 5.8 and Fig. 5.9. Velocities are not angle corrected, as the velocity direction changes throughout the cardiac cycle, shown in Fig. 5.14. The axial velocity estimate from autocorrelation is overlaid for comparison. Dynamic range 30 dB.

corresponds to 12.5 ms at a pulse repetition frequency of 4 kHz, a temporal window where the flow might change significantly.

We have demonstrated that robust vector Doppler estimates in a large region of interest could be achieved in a duplex context, with an acceptable frame rate of 63 Hz. The frame rate *in vivo* was limited due to the number of B-mode compound angles and the Doppler PRF. The maximum angle of $\pm 7.2°$ and 43 compound angles gave a spatial resolution and contrast corresponding to focused imaging with a transmit F-number of 4[25]. However, if 30 transmissions were used for B-mode at 12 kHz, and 30 transmissions were used for Doppler at 4 kHz, a modality including both B-mode, vector Doppler and retrospective PW Doppler at a frame rate of 100 Hz is achievable, where the B-mode image contrast only needs to be slightly compromised[25]. Another option is to interleave focused B-mode transmissions with plane wave Doppler transmissions on the expense of a reduced B-mode frame rate. This can provide good temporal resolution for PW- and vector Doppler imaging in addition to good spatial resolution and contrast in the B-mode image. As the movements in tissue are of a slower nature than blood flow, a lower B-mode frame rate can be accepted.

The increased robustness in vector Doppler estimates with increasing ensemble length can partly be attributed to the properties of the clutter filters, as they, depending on how much signal is removed, may introduce bias in the autocorrelation estimates. As the SNR after high pass filtering decreases, the phase estimate from autocorrelation will approach the phase estimate of high pass filtered white noise. In the context of vector Doppler, the resulting alternatives are too high velocity estimates pointing at random angles, or dropout regions due to segmentation algorithms. For diastolic flow the dropout regions may be large, as may be the case for flow close to the vessel wall. By using large ensemble imaging, desirable filter properties can be obtained by most common clutter filter designs, but an additional variance reduction is achievable when using polynomial regression filters, as more temporal samples are available for averaging. In result, angle-independent velocity estimates can be achieved with a wide measurable velocity span, including both systolic and diastolic flow velocities, and complex secondary flow patterns.

Low blood velocities perpendicular to either of the tilted beams are still a challenge. One potential application where this may apply is wall shear stress estimation, where very low velocities along the vessel wall needs to be estimated. One solution could be using more than two imaging angles. However, by increasing the number of transmit angles further, limitations from lowered PRFs or increased heating effects will be encountered. One could also increase the number of receive angles during beamforming. At some compromise in the separation angle between the estimates used in triangulation and increased computational cost per frame, the two-way Doppler angle might be varied to ensure at least two valid Doppler estimates.

One of the aims of this study was to see whether also tissue velocities could be extracted from the same vector Doppler acquisition scheme. Simulations of slowly rotating flow and recordings in healthy volunteers indicated that tissue vector Doppler was indeed possible. However, when comparing the accuracy found from simulations with velocity estimates found *in vivo*, it seems the diastolic velocities are comparable

to the RMS error. On the other hand, the tissue velocity spectra and autocorrelation estimates are convincing in their correspondence, and indicate that the velocity magnitude is correctly identified. One explanation of the seeming discrepancy could be that the obtained accuracy from simulations includes velocities from all possible angles with the transmit/receive beam direction. This will give a lower accuracy than what would be the case in a situation with a more optimal beam-to-flow angle. Another, and probably more important, difference is that the velocity in the vessel wall was more uniform than in the cylindrical phantom. Due to the large side lobes of the point spread function, neighbouring voxels will have a larger influence on the RMS error in the cylindrical phantom where a velocity gradient was present, than in the more uniform movement of the tissue *in vivo*. However, further investigations in the accuracy of tissue velocity imaging should be done using more realistic simulations of vessel wall movement through the cardiac cycle, similar to what was done in the flow simulations.

Potential applications of tissue vector velocity estimation may be angle independent strain/strain rate imaging, estimation of pulse wave velocity (PWV) and distensibility or compliance measurements, all of which quantify important parameters in developing atherosclerosis. A method for simultaneous imaging of blood flow and artery-wall strain has been suggested earlier by Hasegawa *et al.*[18], where translational motion was removed before estimation of the strain induced phase shifts. Distensibility measures can be obtained from displacement estimates, but if the regular autocorrelation technique is used with wide band pulses, the displacement estimates may be biased by shifts in the RF center frequency. In this respect, Rabben *et al.*[35] has shown that the modified autocorrelation technique[36] provides displacement estimates with improved accuracy over the conventional autocorrelation approach. An investigation of wall tracking and derivation of other measures from the acquired velocity data was not in the scope of this work, but will be a focus for further study.

The large ensemble length enabled us to compare retrospective PW spectra with automatic angle correction to that of the manually corrected conventional PW spectrum. As seen in the example of Fig. 5.12 the conventional and retrospective spectra corresponded well, and the velocity magnitude trace from the autocorrelation method indicated that also the color flow estimates had a good correspondence to the actual velocities present. In general, as some underestimation of high velocities is expected due to spatial averaging, it is beneficial to have the PW spectrum available for comparison, and also for measuring quantitative parameters such as the peak systolic velocity. In the patient case shown (Fig. 5.11), the manually set correction angle was close to that of the vector Doppler estimate (approximately 65° with the vertical direction). However, by moving slightly upstream or downstream of the stenosis, or more generally in the vicinity of bifurcations or bulbs, the flow angle changes in a manner which may not be captured by the user during a conventional examination. Small changes in the correction angle may give large variation in estimated peak velocity, and manual correction only works well if the flow is laminar and parallel to the vessel. Given that the vector Doppler estimates actually provide a better estimate than the manually suggested one, the method may improve estimates and reduce intra-observer variability of important measures in carotid patients such as

peak systolic velocity. On the other hand, retrospective PW Doppler is limited to using the plane wave steering angles, and in cases where the blood flow is near normal to either beam axis, both angles will provide relatively poor velocity spectra. This will give a varying spectral quality throughout the artery as the geometry changes and may hamper comparison at different arterial locations.

The Doppler ensemble length could be decreased to achieve a higher frame rate. A packet size of 20-30 will still improve the velocity estimation in the lateral direction substantially as compared to conventional ensemble lengths, but the shortened ensemble will impact the quality of the velocity spectrum. It may then be beneficial to use other methods than the periodogram for spectral estimation. The Capon and APES techniques have for instance been investigated for short Doppler ensembles[37, 38], where it has been demonstrated that high spectral resolution can be achieved for short ensembles due to the adaptive properties of the estimators.

A continuous acquisition could be an option where the packet size is no longer a limitation. However, there are some drawbacks to the continuous approach: One alternative is to use the same data for B-mode and Doppler. In addition to compromises in transmit frequency and pulse lengths, this will lead to a low available Doppler PRF, or too few transmits per frame to ensure sufficient contrast in the B-mode image. Another alternative is to interleave B-mode and Doppler transmits, but this may lead to problems with motion artifacts in the B-mode image as the maximum imaging PRF is limited by surface heating, and in this alternative it must be divided between B-mode and Doppler transmits. An approach where focused B-mode imaging is interleaved with plane wave Doppler imaging is also an option, either using continuous acquisition or a packet acquisition with B-mode interleave groups. Future work will study more closely how to optimize the acquisition in terms of image quality and frame rate, and how to interleave the B-mode and Doppler transmissions for an increased frame rate with acceptable B-mode image quality and vector Doppler estimates.

5.5 Conclusion

A robust vector Doppler modality could be obtained by utilizing tilted plane waves and parallel receive beamforming. This was achieved while maintaining a sufficient B-mode quality by adopting a packet based acquisition scheme with a separate setup for each modality. The high acquisition rate still allowed for large ensemble lengths (N=50) at acceptable frame rates (63 fps), resulting in improved quantitative properties over a wide velocity span. Further, the increased observation time also allowed for the simultaneous estimation of arterial tissue velocities. Simulation results showed a substantial decrease in root mean square deviation for increasing ensemble lengths, in particular for the lateral velocity component. This observation was confirmed *in vivo*, both in healthy volunteers and in patients with carotid artery disease. Retrospective PW Doppler was also demonstrated based on the proposed acquisition setup, with the benefit of automatic angle-correction from vector Doppler. All together, the proposed approach may provide more efficient clinical tools for conventional vascular imaging,

as well as quantitative information for research into new markers for cardiovascular diagnosis.

References

[1] G. A. Donnan, M. Fisher, M. Macleod, and S. M. Davis, "Stroke," *The Lancet*, vol. 371, no. 9624, pp. 1612 – 1623, 2008.

[2] S. Carr, A. Farb, W. H. Pearce, R. Virmani, and J. S. Yao, "Atherosclerotic plaque rupture in symptomatic carotid artery stenosis," *Journal of Vascular Surgery*, vol. 23, no. 5, pp. 755 – 766, 1996.

[3] J. Bamford, P. Sandercock, M. Dennis, C. Warlow, and J. Burn, "Classification and natural history of clinically identifiable subtypes of cerebral infarction," *The Lancet*, vol. 337, no. 8756, pp. 1521 – 1526, 1991.

[4] M. Spencer and J. Reid, "Quantitation of carotid stenosis with continuous-wave (C-W) Doppler ultrasound," *Stroke*, vol. 10, pp. 326–330, 1979.

[5] G.-M. von Reutern, M.-W. Goertler, N. M. Bornstein, M. D. Sette, D. H. Evans, A. Hetzel, M. kaps, F. Perren, A. Razumovky, T. Shiogai, E. Titianova, P. Traubner, N. Venketasubramanian, L. Wong, and M. Yasaka, "Grading Carotid Stenosis Using Ultrasonic Methods," *Stroke*, vol. 43, no. 3, pp. 916–921, 2012.

[6] E. Grant, C. Benson, G. Moneta, A. Alexandrov, J. Baker, E. Bluth, B. Carroll, M. Eliaziw, J. Gocke, B. Hertzberg, S. Katanick, L. Needleman, J. Pellerito, J. Polak, K. Rholl, D. Wooster, and E. Zierler, "Carotid artery stenosis: gray-scale and Doppler US diagnosis - Society of Radiologists in Ultrasound Consensus Conference," *Radiology*, vol. 229, no. 2, pp. 340–346, 2003.

[7] G.-M. von Reutern, "Measuring the degree of internal carotid artery stenosis," *Perspectives in Medicine*, 2012.

[8] B. Dunmire, K. Beach, K.-H. Labs, M. Plett, and D. S. Jr., "Cross-beam vector doppler ultrasound for angle-independent velocity measurements," *Ultrasound in Medicine & Biology*, vol. 26, no. 8, pp. 1213 – 1235, 2000.

[9] G. E. Trahey, J. W. Allison, and O. T. von Ramm, "Angle independent ultrasonic detection of blood flow," *Biomedical Engineering, IEEE Transactions on*, vol. 34, no. 12, pp. 965 –967, 1987.

[10] V. L. Newhouse, D. Censor, T. Vontz, J. A. Cisneros, and B. B. Goldberg, "Ultrasound doppler probing of flows transverse with respect to beam axis," *Biomedical Engineering, IEEE Transactions on*, vol. BME-34, no. 10, pp. 779 –789, 1987.

[11] K.-W. Yeung, "Angle-insensitive flow measurement using doppler bandwidth," *Ultrasonics, Ferroelectrics and Frequency Control, IEEE Transactions on*, vol. 45, no. 3, pp. 574 –580, 1998.

[12] M. Aderson, "Multi-dimensional velocity estimation with ultrasound using spatial quadrature," *Ultrasonics, Ferroelectrics and Frequency Control, IEEE Transactions on*, vol. 45, no. 3, pp. 852 –861, 1998.

[13] J. Jensen and P. Munk, "A new method for estimation of velocity vectors," *Ultrasonics, Ferroelectrics and Frequency Control, IEEE Transactions on*, vol. 45, pp. 837 – 851, 1998.

[14] J. Udesen and J. Jensen, "Investigation of transverse oscillation method," *Ultrasonics, Ferroelectrics and Frequency Control, IEEE Transactions on*, vol. 53, no. 5, pp. 959 –971, 2006.

[15] M. M. Pedersen, M. J. Pihl, P. Haugaard, J. M. Hansen, K. L. Hansen, M. B. Nielsen, and J. A. Jensen, "Comparison of real-time in vivo spectral and vector velocity estimation," *Ultrasound in Medicine & Biology*, vol. 38, no. 1, pp. 145 – 151, 2012.

[16] L. Bohs, B. Geiman, M. Anderson, S. Gebhart, and G. Trahey, "Speckle tracking for multi-dimensional flow estimation," *Ultrasonics*, vol. 38, no. 1-8, pp. 369 – 375, 2000.

[17] M. Tanter, J. Bercoff, L. Sandrin, and M. Fink, "Ultrafast Compound Imaging for 2D Motion Vector Estimation: Application to Transient Elastography," vol. 49, no. 10, pp. 1363–1374, 2002.

[18] H. Hasegawa and H. Kanai, "Simultaneous imaging of artery-wall strain and blood flow by high frame rate acquisition of rf signals," *Ultrasonics, Ferroelectrics and Frequency Control, IEEE Transactions on*, vol. 55, pp. 2626 –2639, december 2008.

[19] J. Bercoff, G. Montaldo, T. Loupas, D. Savery, F. Mézière, M. Fink, and M. Tanter, "Ultrafast Compound Doppler Imaging: Providing Full Blood Flow Characterization," *Ultrasonics, Ferroelectrics and Frequency Control, IEEE Transactions on*, vol. 58, no. 1, pp. 134 – 147, 2011.

[20] J. Udesen, F. Gran, K. Hansen, J. Jensen, C. Thomsen, and M. Nielsen, "High Frame-Rate Blood Vector Velocity Imaging Using Plane Waves: Simulations and Preliminary Experiments," *Ultrasonics, Ferroelectrics and Frequency Control, IEEE Transactions on*, vol. 55, no. 8, pp. 1729–1743, 2008.

[21] K. Hansen, J. Udesen, F. Gran, J. Jensen, and M. Nielsen, "In-vivo Examples of Flow Patterns With The Fast Vector Velocity Ultrasound Method," *European Journal of Ultrasound*, vol. 30, no. 5, pp. 471–477, 2009.

[22] L. Lovstakken and H. Torp, "Extended velocity range in color flow imaging using parallel receive beamforming," in *Ultrasonics Symposium (IUS), 2010 IEEE*, pp. 1198 –1201, oct. 2010.

[23] A. Swillens, L. Lovstakken, J. Kips, H. Torp, and P. Segers, "Ultrasound simulation of complex flow velocity fields based on computational fluid dynamics," *Ultrasonics, Ferroelectrics and Frequency Control, IEEE Transactions on*, vol. 56, pp. 546 –556, march 2009.

[24] J. Jensen, "Field: A program for simulating ultrasound systems," *Med.Biol.Eng.Comput.*, vol. 34, no. 5, pp. 351–352, 1996.

[25] G. Montaldo, M. Tanter, J. Bercoff, N. Benech, and M. Fink, "Coherent plane-wave compounding for very high frame rate ultrasonography and transient elastography," *Ultrasonics, Ferroelectrics and Frequency Control, IEEE Transactions on*, vol. 56, pp. 489 –506, march 2009.

[26] Food and Drug Administration - Center for Devices and Radiological Health, *Information for manufacturers seeking marketing clearance of diagnostic ultrasound systems and transducers.* US Department of Health and Human Services.

[27] O. Kripfgans, J. Rubin, A. Hall, and J. Fowlkes, "Vector Doppler imaging of a spinning disc ultrasound doppler phantom," *Ultrasound in Medicine & Biology*, vol. 32, no. 7, pp. 1037–1046, 2006.

[28] K. Namekawa, C. Kasai, M. Tsukamoto, and A. Koyano, "Realtime bloodflow imaging system utilizing auto-correlation techniques," *Ultrasound in Medicine & Biology*, vol. Suppl. 2, pp. 203–208, 1983.

[29] C. Kasai, K. Namekawa, A. Koyano, and R. Omoto, "Real-time two-dimensional blood flow imaging using an autocorrelation technique," *IEEE Transactions on Sonics and Ultrasonics*, vol. 32, pp. 458–464, 1985.

[30] S. Bjarum, H. Torp, and K. Kristoffersen, "Clutter Filter Design for Ultrasound Color Flow Imaging," *IEEE Transactions on Ultrasonics Ferroelectrics and Frequency Control*, vol. 49, no. 2, pp. 204–216, 2002.

[31] H. Torp, "Clutter Rejection Filters in Color Flow Imaging: A theoretical approach," *IEEE Transactions on Ultrasonics Ferroelectrics and Frequency Control*, vol. 44, no. 2, pp. 417–424, 1997.

[32] J. Capon, "High resolution frequency-wavenumber spectrum analysis," *Proc. IEEE*, vol. 57, no. 8, pp. 1408–1418, 1969.

[33] R. Reneman, T. van Merode, P. Hick, and A. Hoeks, "Flow velocity patterns in and distensibility of the carotid artery bulb in subjects of various ages," *Circulation*, vol. 71, no. 3, pp. 500–509, 1985.

[34] A. Swillens, P. Segers, H. Torp, and L. Lovstakken, "Two-dimensional blood velocity estimation with ultrasound: speckle tracking versus crossed-beam vector doppler based on flow simulations in a carotid bifurcation model," *Ultrasonics, Ferroelectrics and Frequency Control, IEEE Transactions on*, vol. 57, no. 2, pp. 327 –339, 2010.

[35] S. Rabben, S. Bjærum, V. Sørhus, and H. Torp, "Ultrasound-based vessel wall tracking: An auto-correlation technique with rf center frequency estimation," *Ultrasound in Med. & Biology*, vol. 44, no. 6, pp. 1332 – 1342, 1997.

[36] X. Lai, H. Torp, and K. Kristoffersen, "An extended autocorrelation method for estimation of blood velocity," *Ultrasonics, Ferroelectrics and Frequency Control, IEEE Transactions on*, vol. 44, no. 6, pp. 1332 – 1342, 1997.

[37] F. Gran, A. Jakobsson, and J. Jensen, "Adaptive spectral doppler estimation.," *IEEE transactions on ultrasonics, ferroelectrics, and frequency control*, vol. 56, no. 4, p. 700, 2009.

[38] I. Ekroll, H. Torp, and L. Lovstakken, "Spectral Doppler Estimation Utilizing 2D Spatial Information and Adaptive Signal Processing," *IEEE transactions on ultrasonics, ferroelectrics, and frequency control*, vol. 59, no. 6, pp. 1182–1192.

Chapter 6

Combined vector velocity and spectral Doppler imaging of complex blood flow in the carotid arteries

Ingvild Kinn Ekroll[1], Torbjørn Dahl[1,2], Hans Torp[1], and Lasse Løvstakken[1]
[1] MI Lab and Dept. Circulation and Medical Imaging, NTNU
[2] St. Olavs Hospital, Trondheim, Norway

Color flow imaging and Pulsed Wave Doppler are important diagnostic tools during examination of patients with carotid artery disease. However, measurement of the true peak systolic velocity is dependent on sample volume placement and the operator's ability to provide an educated guess of the flow direction. Utilizing plane wave transmissions and a duplex imaging scheme, we demonstrate an all-in-one modality which provides both vector velocity and spectral Doppler imaging, in addition to separate B-mode images of sufficient quality. The combined information was used to provide automatically calibrated (angle-corrected) PW Doppler spectra at every image point. It was also demonstrated that the combined information can be used to generate spatial maps of the peak systolic velocity, highlighting regions of high velocity and the extent of the stenotic region. The modality was tested in a small group (N=12) of patients with carotid artery disease, and successful images could be obtained from all patients, having a span in BMI of 21 to 31, and carotid depth spanning from 16 to 28 mm.

6.1 Introduction

Imaging of the carotid arteries is of special interest as they are responsible for 20% of all strokes of thromboembolic origin[1]. Situated at shallow depths, they are also well suited for ultrasound imaging. Through local manifestations of cardiovascular disease (CVD), the carotid arteries may not only provide information on developing atherosclerosis in that particular region, but also predict coronary artery disease events[2]. Nevertheless, in clinical practice, the use of ultrasound in relation to carotid

artery disease is mostly limited to grading of plaque stenosis. Utilizing B-mode and Color Flow Imaging (CFI) for navigation, the estimated peak systolic velocity (PSV) is measured from the Pulsed Wave (PW) Doppler spectrogram.

Doppler ultrasound is angle dependent, as only the velocity component parallel to the beam direction is measured. The quantitative use of CFI, where the mean velocity in a region of interest is displayed, is therefore limited, and in conventional ultrasound systems, the true velocity magnitude can only be estimated in single sample volumes using PW-Doppler and manual angle correction. Based on the maximum velocity in systole, an estimate of the degree of stenosis is found, which is further used as a selection criterion for carotid endarterectomy[3]. This estimate is highly dependent on the placement of the sample volume and the operator's ability to perform correct angle correction of the velocity spectrum. In complex geometries or stenosed regions where the stream lines differ from the vessel course, operator dependent errors may give large deviations from the actual peak velocity[4, 5], hampering patient follow-up and multi-center studies.

Vector velocity imaging, where the 2D or 3D velocity magnitude and direction is estimated, has been investigated for several years[6–9]. Such a modality could provide a more quantitative blood flow imaging technique, as the angle dependency of color Doppler is overcome. However, until recently, the robustness, frame rate and/or size of the image region have been limited, and the method has not yet reached clinical practice.

As a consequence of recent technology advances, high frame rates can be maintained while increasing the information content per ultrasound image. Using plane wave transmissions, each pulse covers a broad spatial region, and parallel beamforming[10] may be used to form multiple image lines or even a full image for every transmitted ultrasound pulse. By utilizing these techniques, vector velocity imaging may be realized with improved robustness and temporal resolution[11, 12, 17]. Available 2D velocity information could for instance be used to locate flow patterns known to enhance plaque formation[13] or to assess wall shear stress. In particular, it could be used to improve accuracy and reproducibility in grading of stenoses by providing automatic estimates of flow direction, reducing inter-observer variability in measurements of peak systolic velocity[14, 15].

Given the opportunities enabled by plane wave imaging techniques, we developed an all-in-one modality for imaging of blood flow in the carotid arteries. A duplex acquisition scheme is applied, providing 2D vector velocity blood flow images, in addition to separate B-mode images of sufficient quality. Further, PW Doppler spectra may be generated from arbitrary image points[16]. Automation of the clinical protocol with respect to measurements of the peak systolic velocity is demonstrated, utilizing vector Doppler to automatically calibrate the velocity spectra for all image points simultaneously.

Due to limitations in penetration compared to transmission of focused ultrasound beams, it is not clear whether the plane wave techniques will work robustly in a diverse patient group. Both carotid depth and surrounding tissue calcifications will vary from patient to patient, potentially providing an insufficient signal-to-noise ratio (SNR). To investigate whether plane wave imaging presents disadvantages which makes imaging

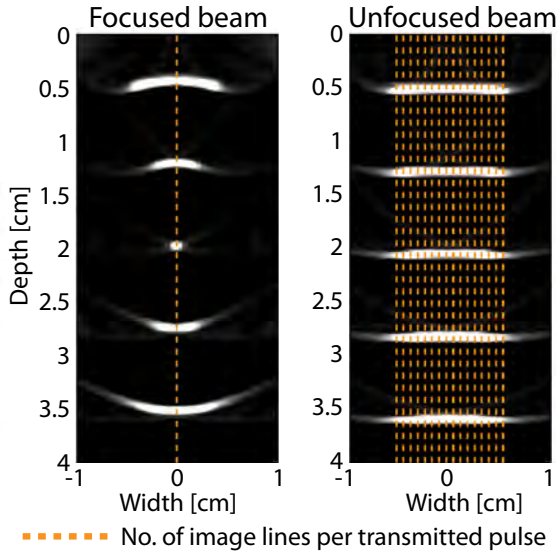

Figure 6.1: An illustration of the difference between focused and plane wave transmission. Using focused transmission, only one receive beam is normally generated per transmit beam, while multiple receive beams may be generated in the plane wave case.

of patients with carotid artery disease unfeasible in practice, the modality was applied in a small (N = 12) patient population.

6.2 Methods

Plane wave imaging

Plane wave imaging (PWI), where unfocused ultrasound beams are transmitted instead of focused beams, may be used to increase the acquisition rate in ultrasound imaging. As illustrated in Fig. 6.1, a broader region of interest is insonified for every pulse transmission, enabling several parallel beams to be generated on receive. The concept has previously been utilized both in elastography[17] and blood flow imaging[11, 16, 18]. The main disadvantage of PWI is the reduced penetration due to lack of focusing, as well as decreased contrast and lateral resolution. Although coherent compounding, where beamformed images from several plane wave transmit angles are coherently combined, has been shown to restore these properties[19], a relatively high number of transmissions are needed to provide an image quality comparable to the optimal multifocus image[19]. In Doppler imaging, however, the dynamic range is lower than in B-mode, and the side lobe level is less critical. Thus, plane wave imaging might be used directly (without compounding), to increase the frame rate and ensembles in color flow imaging. Further, these benefits may be used to improve robustness of

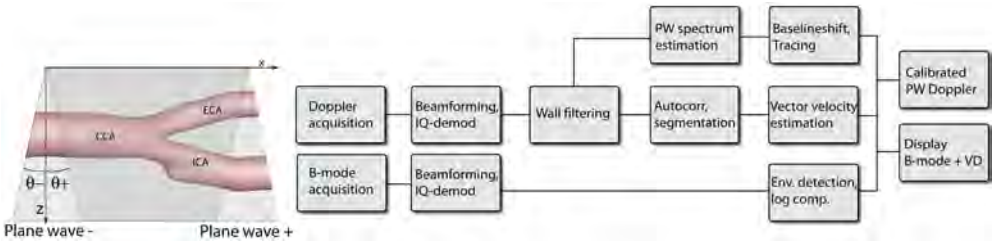

Figure 6.2: A schematic of the imaging scheme, from acquisition of B-mode and Doppler channel data through the different processing steps. At the end of the processing chain, B-mode and vector Doppler images are available, in addition to calibrated PW Doppler spectra in every image point.

existing vector Doppler techniques.

A duplex acquisition scheme was chosen, where parameters for Doppler and B-mode imaging could be optimized separately. Patients were imaged using both a high end ultrasound system (Vivid E9, GE Vingmed, Horten, Norway) and a research system (Sonix MDP, Ultrasonix, Richmond, BC, Canada), where the latter system had the all-in-one acquisition implemented (beamforming and display was done offline). One image per transmitted pulse could be acquired using the research system, while the high end system had more limited parallel receive capability. However, only one data set could be acquired per patient using the Ultrasonix system, due to a long data transfer time and the limited memory of the DAQ. The high end system was therefore included to enable comparison between regular and plane wave imaging.

Imaging schemes

Research system schemes

Two imaging schemes were implemented in the research system; one using plane wave transmissions both for B-mode and Doppler (plane wave scheme) and one using focused B-mode interleaved with plane wave Doppler (combined scheme). The acquisition setups were implemented on a Sonix MDP ultrasound system using the development toolkit Texo which allows custom transmit sequences to be created. A Sonix DAQ (Ultrasonix, Richmond, BC, Canada) was used for channel data acquisition.

The *plane wave scheme* consisted of a plane wave coherent compounding sequence for B-mode, with 41 angles in the interval $-7.4° \leq \alpha \leq 7.4°$, corresponding to a transmit F-number of 4[19], and a vector Doppler sequence using two angled plane waves of $\theta = \pm 10°$, giving in total $41 + 2{\times}50$ transmit events per duplex frame, yielding a frame rate of 63 Hz with the given imaging PRFs.

The *combined scheme* consisted of 4 B-mode interleave groups, each of 32 image lines using an $F_{\#} = 2$, interrupted by $2{\times}50$ Doppler transmissions using $\theta = \pm 10°$. In this scheme, the frame rate of vector Doppler was 66 Hz, while the duplex frame rate was 16 Hz, due to the interleaved acquisition of a full B-mode image. In both

Table 6.1: Safety measurements, research system

Settings	1	2	3	
TxFreq [MHz] f_0	5	6.7	6.7	
Nr of elements	128	128	26	
Cycles@f_0	2.5	1.5	1	
Focal depth [mm]	∞	∞	19	
PRF [kHz]	12	15	12	
Drive voltage [V_{pp}]	56	68	83	
Acoustics				**FDA**
MI	0.4	0.3	0.8	1.9
Ispta [mW/cm^2]	124	63	451	720
Temperature				**FDA**
ΔT_{air} [°C]	23	18.3	1.8	27
$\Delta T_{phantom}$ [°C]	6.5	9.1	0.8	10

schemes the channel RF data was IQ-demodulated and low-pass filtered to reduce the noise bandwidth, and beamformed using a Hamming window over the active receive aperture.

The imaging schemes applied were within the guidelines from the US Food and Drug Administration (FDA), and a summary of acoustical and thermal measurements performed using maximal PRF for a given setup is found in Table 6.1. Whereas the limits for MI and Ispta are well below FDA limits, the maximum PRF applicable for a certain pulse shape is limited by surface heating.

High end alternative schemes

The Vivid E9 system was set up (following the guidelines of FDA) to include imaging schemes utilizing plane wave transmission and 16 parallel receive beams. The limited number of parallel receive beams meant that several transmissions were needed to cover a full image sector. The ensemble length in the color flow applications was 12. Imaging was performed using 1) Conventional B-mode and conventional CFI, 2) Conventional B-mode and plane wave CFI, 3) Plane wave B-mode and plane wave CFI. The alternative imaging schemes included in the Vivid E9 enabled direct comparison of different acquisition schemes from one imaging plane in the same patient.

6.2.1 Vector Doppler estimation

The velocity vector components were obtained in the whole image region simultaneously by combining overlapping Doppler measurements from two directions as given in (1) [20]

$$
\begin{aligned}
v_x &= -\frac{c}{4\, f_0 \sin(\theta)}\,(\hat{f}_1 - \hat{f}_2) \\
v_z &= -\frac{c}{4\, f_0 \cos(\theta)}\,(\hat{f}_1 + \hat{f}_2),
\end{aligned}
\tag{6.1}
$$

where the separation angle between the two transmit/receive directions is 2θ, c is the speed of sound, f_0 is the pulse center frequency and $\hat{f}_1$, $\hat{f}_2$ are the Doppler frequencies estimated from the IQ data based on the temporal autocorrelation function with lag one; $\hat{f} = \angle(\hat{R}(1))/2\pi \times PRF$ [21, 22]. Spatial averaging of the autocorrelation estimate over an area of approximately 1×1 mm was used to further improve the estimates.

Blood pool segmentation was done based on the signal power after wall filtering and the B-mode image intensity. Using ensembles of 50, a 3. order polynomial regression filter was used, giving a -3 dB cutoff at 1.5 cm/s. Similar stop-band characteristics achieved for smaller ensembles of length 16, gave a -3 dB cutoff at 3.3 cm/s.

Based on user preference, color flow images or velocity magnitude could be shown in supplement to the vector velocity arrows. Examples of both visualization techniques will be provided.

6.2.2 Spectral Doppler estimation and calibration

Acquiring Doppler ensembles of length 50 enabled velocity spectra to be calculated using the conventional periodogram approach. Due to the simultaneous acquisition of large ensembles in every image point, also *spatial* spectral profiles showing the variation of the velocity within a region of interest at a certain time may be produced[16]. The periodogram has the following estimate of the power at the Doppler frequency ω

$$
\hat{P}(\omega) = \frac{1}{RB} \sum_{r=0}^{R-1} \sum_{b=0}^{B-1} \left| \sum_{n=0}^{N-1} w(n) x_{r,b}(n) e^{-i\omega n} \right|^2 .
$$

$x_{r,b}(n)$ is the IQ signal from a (range,beam) pair in slow time, $w(n)$ is a smooth window function, R is the number of range samples, B is the number of receive beams and N is the ensemble length. In this work, a Hamming window was applied and spectral averaging was done in a 1×1 mm region of interest.

Adaptive spectral estimation was also used. Advantages of adaptive spectral estimation techniques include increased velocity resolution for equal observation time and increased suppression of noise. Additionally, the velocity resolution can be kept comparable to that of the conventional approach for shorter observation times [23, 24]. This latter advantage can be used to produce multiple velocity spectra per Doppler ensemble, by subdividing ensembles in shorter observation windows and estimating e.g. twice the number of timepoints as provided by the conventional approach.

The adaptive Capon technique has the following estimate of the power at the Doppler frequency ω [25]

$$
\hat{P}_{PSC}(\omega) = \frac{1}{\mathbf{a}^H(\omega) \hat{\mathbf{R}}_{\mathbf{x}}^{-1} \mathbf{a}(\omega)},
$$

where $\mathbf{a}(\omega) = [1\ e^{i\omega}\ \cdots\ e^{i(N-1)\omega}]^T$ and $\hat{\mathbf{R}}_{\mathbf{x}}$ is an estimate of the signal covariance matrix, here produced from an averaging area of 1×1 mm.

Calibration of PW Doppler spectrograms was done automatically by shifting the baseline and correcting the velocity scale according to the angle estimated from vector Doppler at the specific location. Baselineshift was performed by, based on a predefined set of possible shift values, selecting the one resulting in lowest standard deviation as calculated from the baseline-shifted spectrum. A simple algorithm was chosen to trace the spectral envelope, based on the mean and standard deviation of the baseline-shifted frequency power spectrum above a certain threshold value (-25 dB). I.e.

$$f_{max} = f_{mean} \pm 3\ f_{std}, \tag{6.2}$$

where the sign ($\pm$) is dependent on the sign of the baselineshift.

Finally, the peak systolic velocity was found automatically from the traces using an algorithm finding the maximum (or minimum) value after the sharpest rise in velocity.

6.2.3 Patient population

12 patients were recruited from the outpatient vascular clinic (median age 61, min/max 42/77; 7 men, 5 women), and imaging using the new ultrasound modality was performed after the regular patient examination. The protocol was approved by the Norwegian Regional Committee for Medical and Health Research Ethics, and written informed consent was obtained from all participants.

6.3 Results

6.3.1 Patient material

Fig. 6.3 shows duplex images acquired during patient examination using a high end ultrasound system (Vivid E9, GE Vingmed Ultrasound, Horten, Norway). The three previously described setups are compared in the figure, and a loss in contrast and resolution can be seen in the downmost B-mode image where plane wave transmission was used. However, utilizing plane wave imaging resulted in a marked increase in frame rate, illustrated by the flow velocity curves in the right part of Fig. 6.3, providing new opportunities to follow rapid flow changes.

As will be demonstrated in the following, successful vector velocity images at a frame rate of 63–66 fps could be obtained using the research scanner in patients with a BMI span of 21 to 31 (carotid depth spanning from 16 to 28 mm). The span in BMI and carotid depth indicates that a range of different patients may be imaged using plane wave transmissions.

6.3.2 Flow visualization and quantification

Fig. 6.4 shows color flow images and vector velocity estimates obtained using conventional and large ensemble length imaging. The figure illustrate the increased

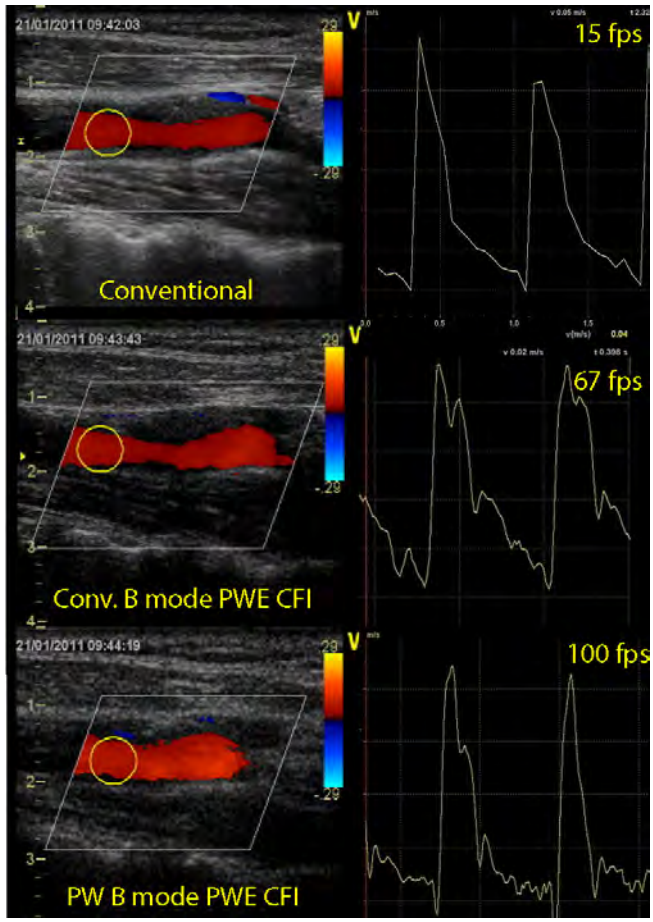

Figure 6.3: Images from the Vivid E9 scanner. The conventional carotid application is shown on top, utilizing focused B-mode (two tx foci) and focused CFI. The middle panel has single focus B-mode and plane wave CFI, whereas the lower panel has plane wave B-mode and plane wave CFI. A marked decrease in resolution and contrast is observed in the plane wave B-mode image. PWE = Plane Wave Emission.

information content obtained by using large ensemble length, plane wave vector Doppler imaging. As shown in the color flow images from conventional (top panel) and large (middle panel) ensembles, clear benefits were obtained in the large ensemble case. In diastole, the Doppler shifts from both transmission angles were very low because of near transversal and partly out-of-plane flow. However, due to the improved wall filter properties, there were no dropouts in the large ensemble case. On the other hand, when using an ensemble length of 16, the blood pool area was reduced, containing dropouts both in the middle of the vessel and in the near-wall region.

As further seen in the lower panel of Fig. 6.4, the addition of vector velocity

information to the color flow image resulted in a better understanding of the blood flow in the imaging plane. Even though this patient had no visible plaques, disturbed (non-laminar) flow was clearly present in early diastole.

Fig. 6.5 provides another example of complex flow which could not be perceived using regular color flow imaging. This patient had stenoses both in the internal and external carotid artery. Using vector Doppler, complex secondary flow could be observed after the external carotid artery stenosis. The abrupt change from a large pre-stenotic velocity magnitude to the small mid-stenotic velocity magnitude was also clearly seen from the vector velocity information, indicating that the flow direction in the mid-stenotic region was in the out-of-plane direction.

Fig. 6.6 shows images obtained from the combined acquisition, using velocity magnitude instead of the regular color flow image to indicate blood flow. As seen in the middle panel, slow and circulatory flow was present in diastole, following a small stenosis. Two spatial spectral profiles are shown in the lower right of Fig. 6.6: one parabolic from systole (indicated by dashed line in upper panel), and one showing directional change with depth from diastole (dashed line in lower image panel).

6.3.3 Temporal resolution

The flow velocity curves in Fig. 6.3 demonstrated that compared to focused flow imaging, plane wave transmission enables near instantaneous images of the flow in a large image region. Using the research system, high frame rates may be achieved with an increased velocity span (due to large ensemble lengths) and also robust vector Doppler information.

The high temporal resolution obtained in the new modality is illustrated in Fig. 6.7 and Fig. 6.8. From the vector Doppler information, it became clear that reversed flow was present in a small part of the cardiac cycle, and that during this time-window, the blood flowed from the external to the internal carotid artery. As more clearly seen in Fig. 6.8, the flow in the external carotid artery experienced a near 150° turn in diastole (region of interest indicated by a small rectangle in Fig. 6.7).

6.3.4 Automatic PW Doppler calibration

The upper panel of Fig. 6.9 shows the adaptive spectrogram from the indicated rectangular region in Fig. 6.7. Based on the directional information from vector Doppler, the spectrogram could be angle corrected automatically, and included in the figure are the calibrated traces of mean and maximum velocity. After angle correction, the spectrogram gave an estimate of the peak systolic velocity at approximately 0.6 m/s.

As seen in the middle panel of Fig. 6.9, regular spectral estimation could also be used to generate calibrated velocity spectra, however with reduced contrast (lower SNR). The wider spectral mainlobe, clearly seen in the lower panel of Fig. 6.9, also leads to higher maximum velocity estimates, here at approximately 0.85 m/s.

In Fig. 6.10 we compare a conventional PW Doppler recording (left) to regular spectral Doppler from the investigated modality (right). The conventional recording

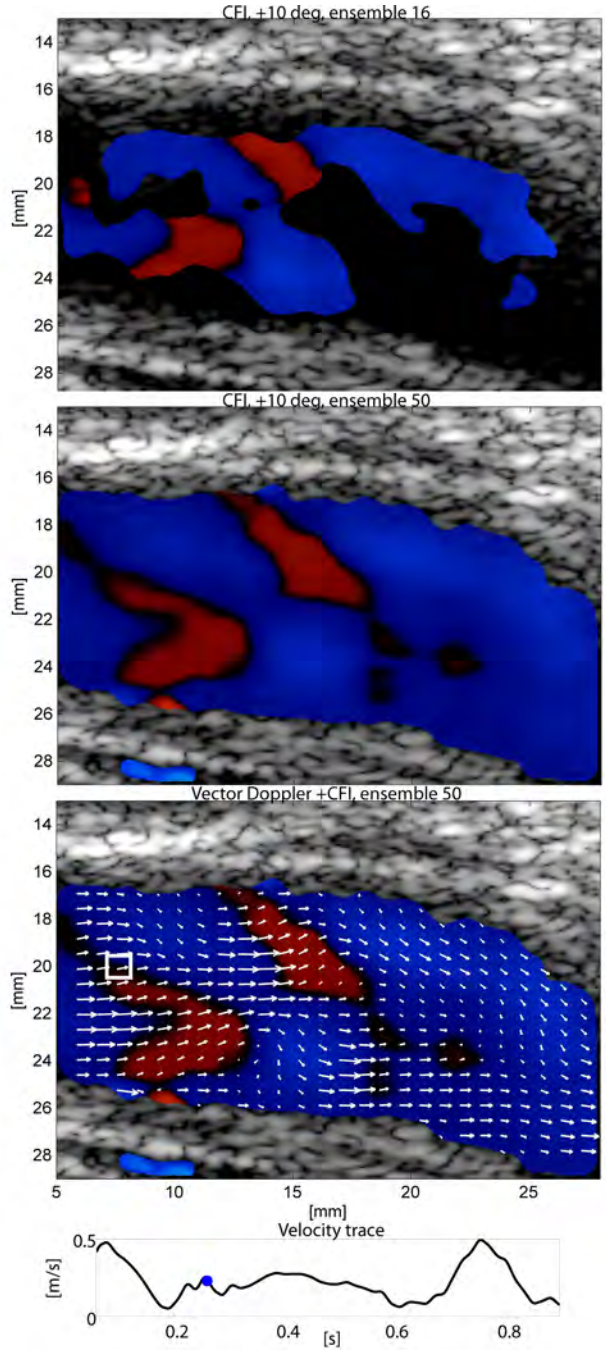

Figure 6.4: The figure shows the increased velocity span and improved visualization obtained by using high ensembles and vector Doppler imaging. The dot in the velocity trace shows the time of the depicted images.

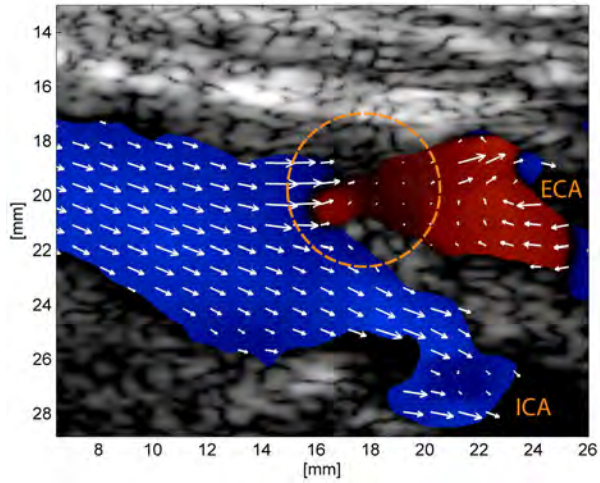

Figure 6.5: The figure shows vector velocities overlaid a color flow image form the carotid bifurcation of a patient with stenoses in both the internal and external carotid artery. After the stenosed region in the ECA, complex flow is present. The abrupt change in velocity magnitude from the pre-stenotic to the mid-stenotic region indicates that the blood flow is in the out-of-plane direction.

was done in the stenotic region of a patient with internal carotid artery stenosis, and a corresponding ROI was extracted from the plane wave recording. Whereas the conventional spectrogram was manually corrected during the examination using the assumed direction of flow, the other was automatically corrected with the direction estimated from vector Doppler. In this case, where the spectrograms originate from the mid-stenotic region, the two corrections correspond well. The spectral quality is also comparable, though with somewhat lower contrast and temporal resolution in the unfocused, retrospective case.

6.3.5 Applications of 2D spectral information

As spectrograms and information on velocity direction are available in every point of the image, angle corrected spectral estimation could be performed in all image points simultaneously. In regular color flow imaging, this is not an option, as the flow angle is generally unknown, and different regions of interest must be assessed separately, with the operator providing an educated guess of the flow direction.

By automatically calibrating and tracing the velocity spectra in every point in the image, the result may for instance be displayed as a spatial map of the peak systolic velocities. In Fig. 6.11, such a map is depicted, generated from a patient with a double sided stenosis in the internal carotid artery. Examples of velocity spectra, velocity traces and peak systolic velocity estimates are found on top, depicting the velocity content in the pre-stenotic, mid-stenotic and post-stenotic regions.

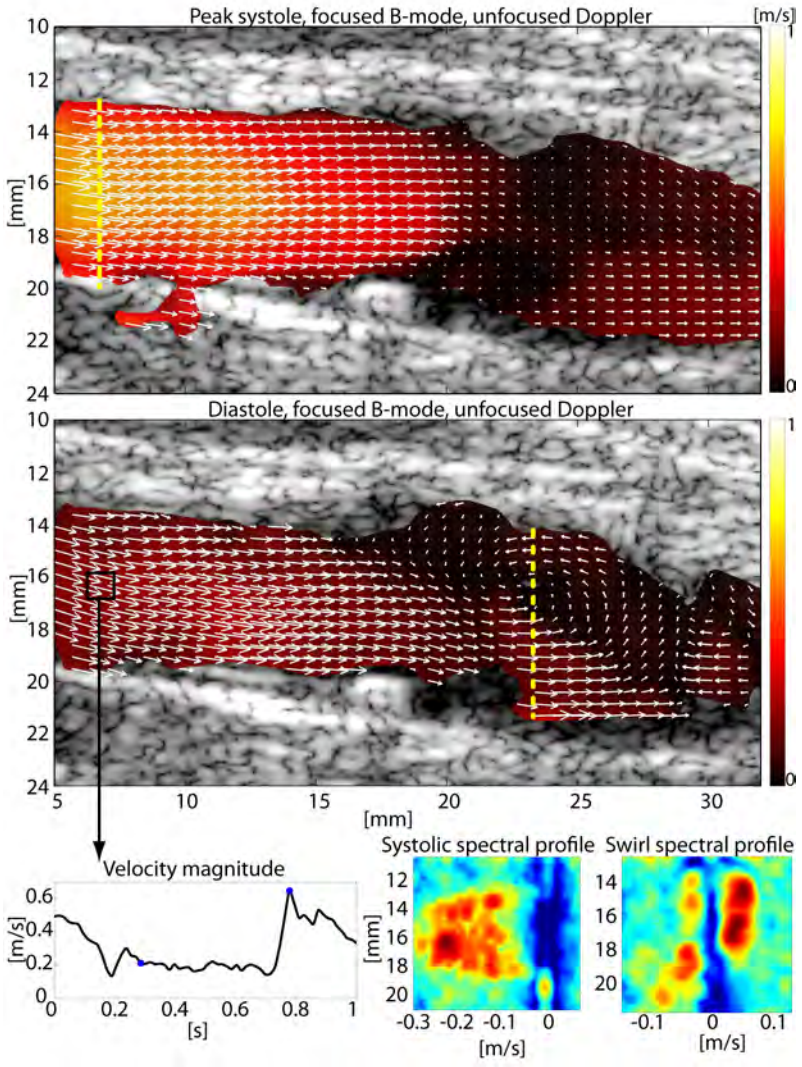

Figure 6.6: The two upper panels of the figure show vector Doppler estimates from peak systole (upper) and diastole (lower) in one of the patients using the combined acquisition scheme. The velocity magnitude trace from the leftmost part of the artery is seen in the lower left. To the lower right two spatial spectral profiles are shown. One from peak systole (left) and one from diastole (right). The regions of interest for the spectral profiles are shown as yellow dashed lines, placed to the far left in peak systole and in a region of swirling flow in diastole.

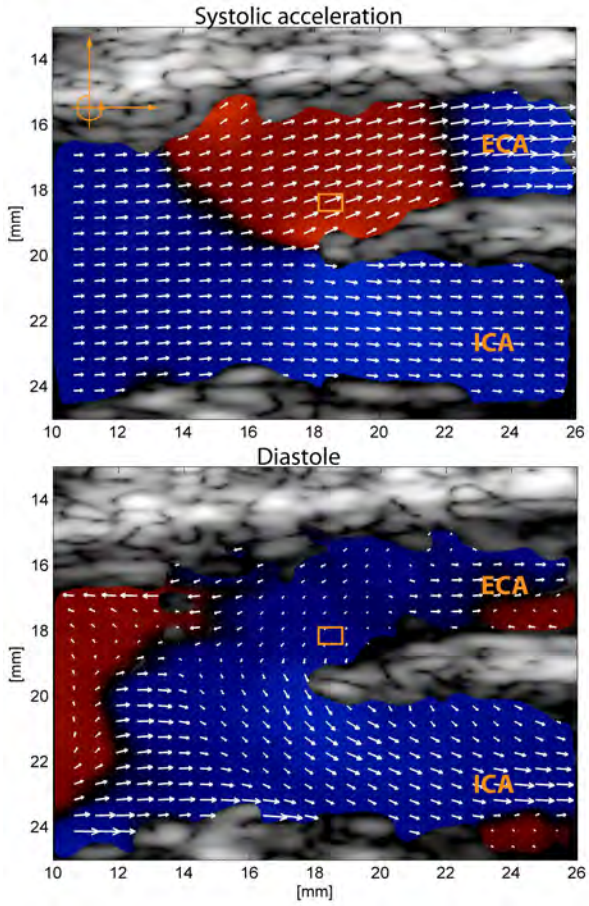

Figure 6.7: The upper panel shows blood flow in a carotid artery bifurcation during systole, whereas the lower panel depicts the situation in diastole. Here the blood flow was reversed, and flowed from the external to the internal carotid artery.

6.4 Discussion

We have presented results from an all-in-one modality utilizing plane wave imaging. The modality provides robust vector Doppler estimates, PW Doppler and separate B-mode images. Tested in a population of patients with carotid artery disease, the modality could provide successful vector Doppler images and retrospective velocity spectra from patients within a BMI-range of 21 to 31. One limitation of the study is that none of the patients had a large degree of calcifications, another that only the carotid arteries were imaged. Calcifications and the increased depth of the vertebral arteries would increase the imaging challenge, and it is still unknown whether the plane wave approach would be successful under such circumstances.

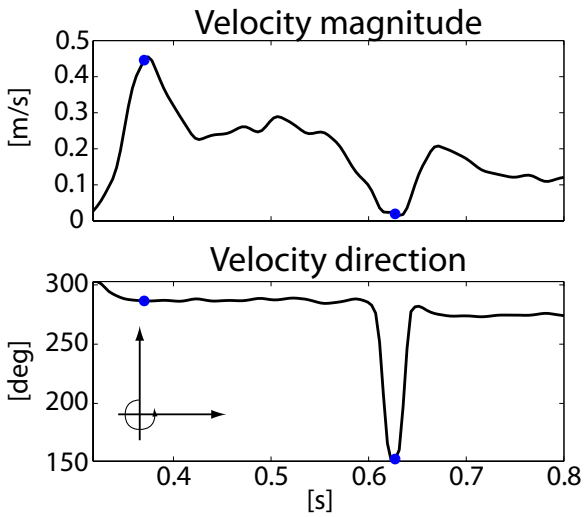

Figure 6.8: The figure shows both velocity magnitude and velocity direction curves throughout the cardiac cycle for the indicated region of interest in the patient recording illustrated in Fig. 6.7. The blue dots represent the timepoints for the frames depicted in Fig. 6.7.

A duplex scheme using separate B-mode setup hinders a continuous acquisition and processing of flow images, and also limits the overall frame rate. Separate acquisition is, however, necessary to obtain high quality B-mode images, which is considered clinically important. Still, the overall frame rate was significantly higher (>3 times) than typically available in current high end systems, and sufficiently high to capture fast variations in the flow. Duplex acquisition also enables focused B-mode imaging, with advantages including increased penetration, resolution and contrast. By utilizing an interleaved acquisition scheme, these advantages can be achieved without compromising the Doppler frame rate. The scheme applied in this work had four interleave groups, resulting in a B-mode frame rate which was only one fourth of the flow frame rate. However, when applied to carotid imaging, where the tissue movement is small compared to blood flow or myocardial contractions, such an interleaved approach is justified.

The plane wave scheme, where unfocused transmissions were used both for flow and tissue imaging, had a common frame rate for the B-mode and flow images. However, further investigation should be done to find an optimal number of imaging angles for the coherent compounding, as the span in angles chosen in our application corresponds to a transmit $F_{\#} = 4$. Reducing the number of transmitted plane waves and increasing the angle span would give an increase in the frame rate and the lateral resolution respectively, however with a reduction in contrast and SNR.

An approach to obtain both color flow and spectral Doppler simultaneously has been described by Bercoff *et al.*[16], where also coherent compounding from 3–16 angles

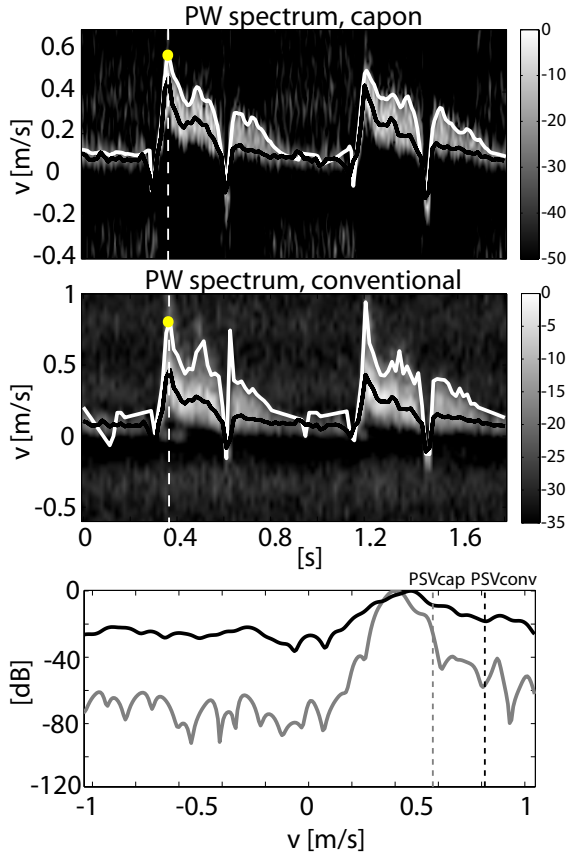

Figure 6.9: PW spectra from -10° tx/rx calibrated with angle from vector Doppler in peak systole (see Fig. 6.8). The black line is the autocorrelation estimate, whereas the white, solid line is a trace of the peak velocity. The yellow dots mark peak systolic velocity. Colorbars in dB. The lower panel depicts linespectra from peak systole, illustrating the difference in mainlobe width between the spectral estimation techniques.

was used to improve resolution and contrast in the color Doppler image. Compounding has clear benefits in regions of slow flow, where the Doppler PRF can be reduced without risking aliasing artifacts, and as a means to increase the SNR from single plane wave imaging. However, compounding in fast flow situations might induce artifacts from movement, and would also compromise the Nyquist (maximum) velocity.

To avoid excessive transducer surface heating, a compromise between penetration depth and pulse repetition frequency was encountered in our approach, thus also limiting the Nyquist velocity. Superficial vessels generally lie parallel to the skin surface and will have relatively large beam-to-flow angles. In result, most of the

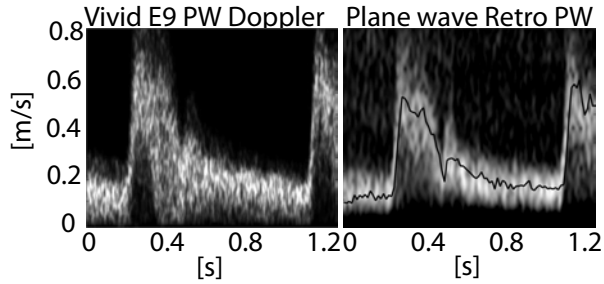

Figure 6.10: The left panel shows a conventional PW Doppler recording, manually calibrated using the assumed flow direction. The right panel shows the corresponding retrospective PW Doppler spectrum from the plane wave Doppler acquisition, automatically calibrated using the directional information from vector Doppler.

patients imaged had Doppler shifts supported by the given velocity range. However, in severely stenosed regions and in branches, aliasing could occur.

The Doppler transmissions were in this work interleaved, which means that the transmit direction changed between each pulse. However, by acquiring a full Doppler ensemble before changing transmit direction, the maximum velocity would be twice as high. On the other hand, this may lead to a significant time lag between the mean velocity estimates from the two directions.

The large Doppler ensembles used in this work (50) were motivated both by a desire to make robust velocity estimates, to give more flexible wall filtering and an increased velocity span, but also to be able to generate spectra of sufficient velocity resolution in every point of the image. As demonstrated, the plane wave packet acquisition scheme could provide spectra of sufficient temporal resolution and contrast. Both conventional and adaptive spectral estimation techniques could be used as precursors for maps of peak systolic velocities, and examples of spectra generated by both techniques were given. Increased computational time is a disadvantage of the adaptive techniques, but as the spectral estimation is retrospective in our application, the slight increase in computational complexity is tolerable when a higher spectral resolution and contrast is obtained.

Overestimation of the peak systolic velocity is a common and well known phenomenon[4, 26, 27], and the origin of error stems from many sources, including spectral broadening. As the beam-to-flow angle changes throughout the course of the vessel, spectral broadening will vary, resulting in a variable amount of overestimation in the peak systolic velocity at different locations. Adaptive spectral estimation might contribute to reduced spectral broadening and thereby a reduction in peak velocity overestimation. However, further work should investigate the differences between alternative and conventional spectral estimation techniques in a situation with a known maximum velocity.

The tracing technique applied in this work was simple, chosen as development of more advanced techniques was out of the scope of this work. Still, in our limited

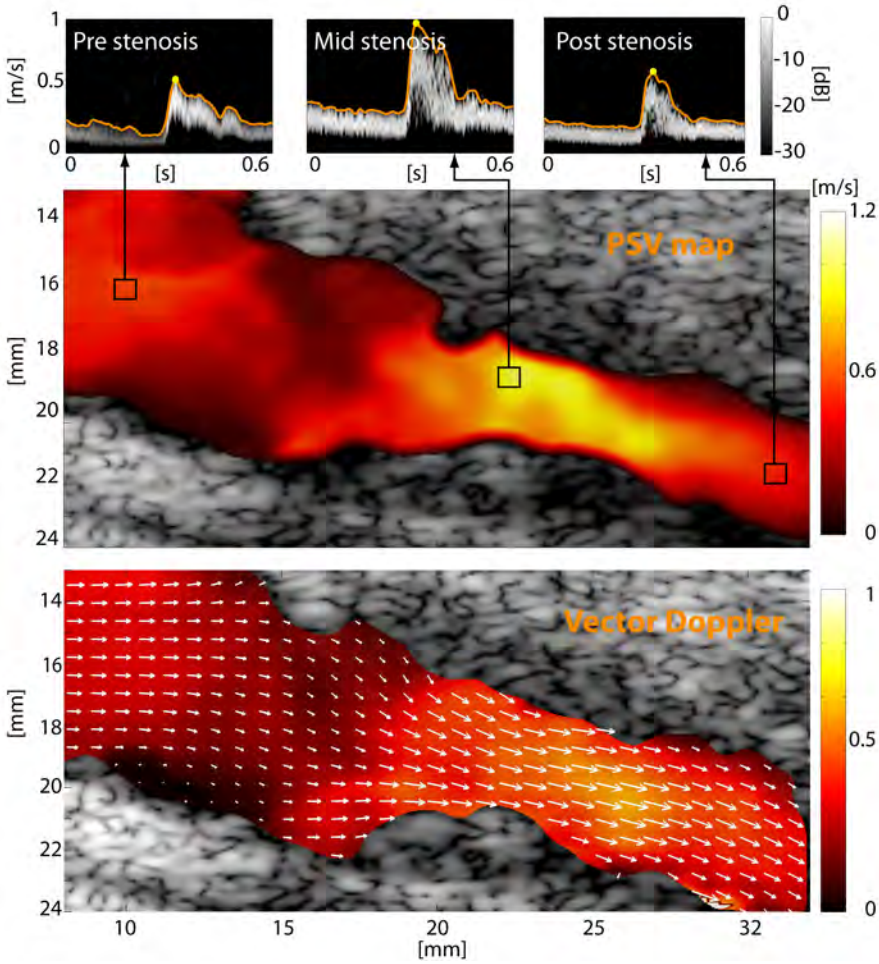

Figure 6.11: Peak systolic velocity map in a patient with carotid artery stenosis. In the bottom image, the velocity magnitude and direction is shown. Based on the flow-angle from vector-Doppler and available spectral information, a calibrated estimate of the peak systolic velocity was found automatically in every image point. The middle panel shows the resulting spatial map of the peak systolic velocities, highlighting the stenotic region. Examples of spectrograms generated from different image locations are also shown.

data material, it worked adequately. More sophisticated techniques for estimating the peak systolic velocities have been suggested[28], and especially if conventional spectral estimation is used (with only moderate SNR), the technique developed by Steinman *et al.*[29] could be useful.

It was demonstrated that vector Doppler estimates could be used to calibrate spectrograms from every image location, forming a spatial map of the peak systolic velocities. In this way, regions of high velocities are highlighted, and the patient examiner can, either during the examination or retrospectively, more easily place a sample volume in this region. The location of the spatial maximum of the peak systolic velocities may also be found automatically. Measurements of peak systolic velocity are an important part of the clinical protocol when examining a patient with carotid artery disease, and the velocity estimate is one of the selection criteria for carotid endarterectomy. In that respect, automatic angle correction of the velocities would be beneficial, as this may reduce both intra- and interobserver variability[14]. Also of importance is the extent of the stenotic region. This is visualized better in a map of the peak systolic velocities than when looking at regular color flow images, where the velocity shown is dependent on beam-to-flow angles which are changing throughout the course of the stenotic region.

Vector Doppler estimates are required for several parameters which could be of interest in relation to carotid artery disease. Wall shear stress estimation is one, where the impact of different flow patterns on the endothelium could be quantified to a larger extent than by visualizing flow patterns alone. However, very low velocity flow close to the vessel wall remains a challenge.

Volume flow estimation would also benefit from vector velocity estimates, and could provide useful diagnostic information. However, blood flow is in 3D, and some assumptions must still be made for the geometry and the flow profile when 2D imaging is used. Still, as demonstrated here, although the full velocity information is not provided by a 2D representation of the flow field, it gives increased understanding of the flow situation compared to the 1D color flow images, and might improve our understanding of the vascular physiology, both in healthy and diseased arteries.

6.5 Conclusions

An all-in-one modality for vector velocity and spectral Doppler imaging was presented, and real-life imaging feasibility was investigated using a small group of patients with carotid artery disease. The patient study gave promising results, with successful vector and spectral Doppler images generated from patients with a BMI span of 21 to 31 and carotid depth ranging from 16 to 28 mm. By combining the directional information from vector Doppler and the spectral information obtained by using large ensemble Doppler imaging, spatial maps of the peak systolic velocity could be generated. Automatic calibration of PW Doppler spectra may reduce interobserver variability, and the visualization of peak systolic velocity maps may also aid the user in placement of the sample volume, as regions of high velocity magnitude and their spatial extent are quantified and highlighted.

References

[1] J. Bamford, P. Sandercock, M. Dennis, C. Warlow, and J. Burn, "Classification and natural history of clinically identifiable subtypes of cerebral infarction," *The Lancet*, vol. 337, no. 8756, pp. 1521 – 1526, 1991.

[2] Y. Inaba, J. A. Chen, and S. R. Bergmann, "Carotid plaque, compared with carotid intima-media thickness, more accurately predicts coronary artery disease events: A meta-analysis," *Atherosclerosis*, vol. 220, no. 1, pp. 128 – 133, 2012.

[3] L. B. Goldstein, C. D. Bushnell, R. J. Adams, L. J. Appel, L. T. Braun, S. Chaturvedi, M. A. Creager, A. Culebras, R. H. Eckel, R. G. Hart, J. A. Hinchey, V. J. Howard, E. C. Jauch, S. R. Levine, J. F. Meschia, W. S. Moore, J. I. Nixon, and T. A. Pearson, "Guidelines for the primary prevention of stroke: A guideline for healthcare professionals from the american heart association/american stroke association," *Stroke*, vol. 42, no. 2, pp. 517–584, 2011.

[4] E. Y. Lui, A. H. Steinman, R. S. Cobbold, and K. W. Johnston, "Human factors as a source of error in peak doppler velocity measurement," *Journal of Vascular Surgery*, vol. 42, no. 5, pp. 972.e1 – 972.e10, 2005.

[5] G.-M. von Reutern, M.-W. Goertler, N. M. Bornstein, M. D. Sette, D. H. Evans, A. Hetzel, M. kaps, F. Perren, A. Razumovky, T. Shiogai, E. Titianova, P. Traubner, N. Venketasubramanian, L. Wong, and M. Yasaka, "Grading Carotid Stenosis Using Ultrasonic Methods," *Stroke*, vol. 43, no. 3, pp. 916–921, 2012.

[6] B. Dunmire, K. Beach, K.-H. Labs, M. Plett, and D. S. Jr., "Cross-beam vector doppler ultrasound for angle-independent velocity measurements," *Ultrasound in Medicine & Biology*, vol. 26, no. 8, pp. 1213 – 1235, 2000.

[7] L. Bohs, B. Geiman, M. Anderson, S. Gebhart, and G. Trahey, "Speckle tracking for multi-dimensional flow estimation," *Ultrasonics*, vol. 38, no. 1-8, pp. 369 – 375, 2000.

[8] J. Jensen and P. Munk, "A new method for estimation of velocity vectors," *Ultrasonics, Ferroelectrics and Frequency Control, IEEE Transactions on*, vol. 45, pp. 837 – 851, 1998.

[9] K.-W. Yeung, "Angle-insensitive flow measurement using doppler bandwidth," *Ultrasonics, Ferroelectrics and Frequency Control, IEEE Transactions on*, vol. 45, no. 3, pp. 574 –580, 1998.

[10] O. von Ramm, S. Smith, and H. Pavy, "High-speed ultrasound volumetric imaging system - part II: Parallel processing and image display," *IEEE Trans Ultrason Ferroelectr Freq Control*, vol. 38, pp. 109–115, 1991.

[11] K. Hansen, J. Udesen, F. Gran, J. Jensen, and M. Nielsen, "In-vivo Examples of Flow Patterns With The Fast Vector Velocity Ultrasound Method," *European Journal of Ultrasound*, vol. 30, no. 5, pp. 471–477, 2009.

[12] I. Ekroll, A. Swillens, P. Segers, H. Torp, and L. Lovstakken, "Simultaneous quantification of flow and tissue velocities using multi-angle plane wave imaging," *Unpublished work, PhD Thesis, Chapter 5*, 2012.

[13] K. Koskinas, Y. Chatzizisis, A. Baker, E. Edelman, P. Stone, and C. Feldman, "The role of low endothelial shear stress in the conversion of atherosclerotic lesions from stable to unstable plaque," *Current Opinion in Cardiology*, vol. 24, no. 6, p. 580, 2009.

[14] R. Steel, K. V. Ramnarine, F. Davidson, P. J. Fish, and P. R. Hoskins, "Angle-independent estimation of maximum velocity through stenoses using vector doppler ultrasound," *Ultrasound in Medicine & Biology*, vol. 29, no. 4, pp. 575 – 584, 2003.

[15] P. Hoskins, "Peak velocity estimation in arterial stenosis models using colour vector doppler," *Ultrasound in Medicine & Biology*, vol. 23, no. 6, pp. 889–897, 1997.

[16] J. Bercoff, G. Montaldo, T. Loupas, D. Savery, F. Mézière, M. Fink, and M. Tanter, "Ultrafast Compound Doppler Imaging: Providing Full Blood Flow Characterization," *Ultrasonics, Ferroelectrics and Frequency Control, IEEE Transactions on*, vol. 58, no. 1, pp. 134 – 147, 2011.

[17] M. Tanter, J. Bercoff, L. Sandrin, and M. Fink, "Ultrafast compound imaging for 2-d motion vector estimation: application to transient elastography," *Ultrasonics, Ferroelectrics and Frequency Control, IEEE Transactions on*, vol. 49, no. 10, pp. 1363 –1374, 2002.

[18] J. Udesen, F. Gran, K. Hansen, J. Jensen, C. Thomsen, and M. Nielsen, "High Frame-Rate Blood Vector Velocity Imaging Using Plane Waves: Simulations and Preliminary Experiments," *Ultrasonics, Ferroelectrics and Frequency Control, IEEE Transactions on*, vol. 55, no. 8, pp. 1729–1743, 2008.

[19] G. Montaldo, M. Tanter, J. Bercoff, N. Benech, and M. Fink, "Coherent plane-wave compounding for very high frame rate ultrasonography and transient elastography," *Ultrasonics, Ferroelectrics and Frequency Control, IEEE Transactions on*, vol. 56, pp. 489 –506, march 2009.

[20] O. Kripfgans, J. Rubin, A. Hall, and J. Fowlkes, "Vector Doppler imaging of a spinning disc ultrasound doppler phantom," *Ultrasound in Medicine & Biology*, vol. 32, no. 7, pp. 1037–1046, 2006.

[21] K. Namekawa, C. Kasai, M. Tsukamoto, and A. Koyano, "Realtime bloodflow imaging system utilizing auto-correlation techniques," *Ultrasound in Medicine & Biology*, vol. Suppl. 2, pp. 203–208, 1983.

[22] C. Kasai, K. Namekawa, A. Koyano, and R. Omoto, "Real-time two-dimensional blood flow imaging using an autocorrelation technique," *IEEE Transactions on Sonics and Ultrasonics*, vol. 32, pp. 458–464, 1985.

[23] F. Gran, A. Jakobsson, and J. Jensen, "Adaptive spectral doppler estimation.," *IEEE transactions on ultrasonics, ferroelectrics, and frequency control*, vol. 56, no. 4, p. 700, 2009.

[24] I. Ekroll, H. Torp, and L. Lovstakken, "Spectral Doppler Estimation Utilizing 2D Spatial Information and Adaptive Signal Processing," *IEEE transactions on ultrasonics, ferroelectrics, and frequency control*, vol. 59, no. 6, pp. 1182–1192, 2012.

[25] J. Capon, "High resolution frequency-wavenumber spectrum analysis," *Proc. IEEE*, vol. 57, no. 8, pp. 1408–1418, 1969.

[26] A. H. Steinman, J. Tavakkoli, J. G. M. Jr., R. S. Cobbold, and K. Johnston, "Sources of error in maximum velocity estimation using linear phased-array doppler systems with steady flow," *Ultrasound in Medicine & Biology*, vol. 27, no. 5, pp. 655 – 664, 2001.

[27] P. Hoskins, "Accuracy of maximum velocity estimates made using doppler ultrasound systems," *British Journal of Radiology*, vol. 69, pp. 172–177, 1996.

[28] L.Y.L.Mo, L. Yun, and R. Cobbold, "Comparison of four digital maximum frequency estimators for doppler ultrasound," *Ultrasound in Medicine & Biology*, vol. 14, no. 5, pp. 355 – 363, 1988.

[29] A. Steinman, J. Tavakkoli, J. Myers, J.G., R. Cobbold, and K. Johnston, "A new approach for determining maximum frequency in clinical doppler ultrasound spectral estimates," in *Engineering in Medicine and Biology Society, 2000. Proceedings of the 22nd Annual International Conference of the IEEE*, vol. 4, pp. 2640 –2643 vol.4, 2000.